Field Study of Wind Driven Rain Penetration into Vinyl Sidings and Stucco-Clad Wood-Frame
Wall Systems at Window Sill

Elsa Ngudjiharto

A Thesis

In

The Department

of

Building, Civil and Environmental Engineering

Presented in Partial Fulfillment of the Requirements
for the Degree of Master of Applied Science (Building Engineering) at
Concordia University
Montreal, Quebec, Canada

September 2015

CONCORDIA UNIVERSITY
School of Graduate Studies

This is to certify that the thesis prepared

By: Elsa Ngudjiharto

Entitled: Field Study of Wind Driven Rain Penetration into Vinyl Sidings and Stucco-Clad Wood-Frame Wall Systems at Window Sill

and submitted in partial fulfillment of the requirements for the degree of

Master of Applied Science (Building Engineering)

complies with the regulations of the University and meets the accepted standards with respect to originality and quality.

Signed by the final Examining Committee:

_____
Dr. K. Galal, Chair

_____
Dr. Y. Zhang, Examiner, external to program

_____
Dr. Hua Ge, Examiner

_____
Dr. Paul Fazio, Co-supervisor

_____
Dr. Fitsum Tariku, Co-supervisor

_____
Dr. Fariborz Haghighat, Co-supervisor

Approved by   _____
Chair of Department or Graduate Program Director

_____2015   _____
Dean of Faculty

ABSTRACT

Field Study of Wind Driven Rain Penetration into Vinyl Sidings and Stucco-Clad Wood-Frame Wall Systems at Window Sill

Elsa Ngudjiharto

According to the 1996 survey of building envelope failures in the West coast climate of British Columbia (BC), 23% of the failures were related to windows and their interface around the rough openings on the walls. Moreover, rain was found to be a significant moisture source to water penetration through wall assemblies. A study is presented here on the correlation between wind driven rain (WDR) as the moisture source and the relative proportions of water penetration at intended defects (openings) at the interface of windows and walls. In this field investigation, eight full-scale exterior wall panels with vinyl sidings and concealed barrier stucco claddings were built and installed on a field testing station, subjected to real BC climate. From November 1, 2013 – June 19, 2014, rainwater was collected and measured instantaneously from vulnerable detail locations, such as at window sill and at missing sealant defect locations, and then synchronized to the weather data to estimate the potential rain load that may contribute to a leakage into the wood framing assembly. Leakage amounts of approximately 0.5% and 1.5% of WDR were estimated from the sill corner locations of vinyl sidings and stucco-clad test walls, respectively. Although high solar exposures on these South East facing walls facilitated the drying process, the sheathing membranes on the stucco-clad walls were found to experience high amounts of moisture loads. These results are useful for fine-tuning the principal moisture load that is applied in hygrothermal performance assessment and design of exterior wall systems.

TABLE OF CONTENTS

LIST OF FIGURES

LIST OF TABLES

CHAPTER 1: INTRODUCTION

In the late 1990s, major durability problems were found at the building envelopes of many wood-framed multi-unit residential buildings in the coastal climate region of British Columbia, Canada. The building envelope failures were premature on the 1980-1990s-built, low-rise wood-framed residential buildings of up to four storeys high and required more than $10,000 in moisture damage related repair costs. These extensive water ingress issues affected the financial well-being of the homeowner and the construction industry, and were commonly referred to as the leaky-condo crisis. In response, a survey was conducted on 37 problem buildings and 9 control buildings with no moisture problems to identify the cause of the problems (Morrison Hershfield, 1996). The survey found that the moisture problems were due to exterior water penetration, in particular at interface details, such as windows, balconies, wall penetrations for wiring, vents, and structural connections of handrails and other exterior elements. Lack of protection by roof overhangs above the walls was also found to be a contributing factor to the problems. Figure 1 is an example of moisture damaged wood framing around windows at sill corners. Many of these problems were found on face sealed stucco clad walls, and although at fewer numbers, also on wood and vinyl sidings walls.

Figure 1. Sheathing board damage observed on the window sills of a wood frame wall of a garage structure in BC. Photo courtesy of David Croft (2012).

Rain screen cladding systems using vertically strapped drainage cavity have been adopted by building envelope professionals as a best practice solution to detail these vulnerable interfaces. However, as the provision of the drainage cavity shifted the plane of the cladding outwards by the additional thickness of the drainage cavity, a costly full wall cladding retrofit was usually required. One concern building professionals had was whether the building owners' resources were wasted on an over-design (Lawton, 1999). Although best practice solution was recommended, many owners could not afford this costly repairs.

Among its multiple responsibilities, the Homeowner Protection Office (HPO) was established to provide financial assistance to fund these renovations through no-interest mortgage loans and rebates of Provincial Sales Tax on repair materials. According to an assessment of future demand for this financial assistance from HPO, out of the 72,193 apartment strata units that experienced envelope failures, approximately only 42% had been repaired up to 2007, and the assistance loans estimated for the period of 2008 to 2012 were in the range of $445 million to $696 million (McClanaghan & Copas, 2007). Approximately up to 24,000 units were estimated left to repair after 2012. This assessment did not include co-operatively owned buildings, which have also experienced major envelope failures (McClanaghan & Copas, 2007). The conclusion of this assessment was that the demand for the financial assistance remains high. Furthermore, in 2009, the HPO interest-free loan program was cancelled, leaving many owners in financial strain to repair major building envelope failures (Penner, 2014).

Not all underlying defects causing the leaks found were repaired during the leaky condo crisis. In addition to the issues with the currently aging existing building envelopes on multi-unit residential buildings built in the 1980s and 1990s, a second wave of leaky-condo crisis is beginning to surface in recent years (Penner, 2014). It is clear that rainwater leakage through exterior wall assemblies is a decade-old issue that is still relevant today.

The wetting and drying of exterior wood-frame wall assemblies have been researched in the past decades. However, many are based on laboratory and field studies using simulated moisture

loading. Moreover, although many studies have showed the superiority of the rain screen wall cladding systems, which are useful for the newly constructed housing and fully retrofitted buildings with the rain screen wall claddings, there is still a need to investigate the rainwater leakage through exterior wall assemblies typically constructed at the older housing stock with face-sealed stucco cladding, as well as vinyl and wood sidings. It is also important to be able to estimate the moisture loads contributing to these leakages. Current guide on designing building envelope assemblies suitable to the climate, such as the ASHRAE Standard 160 - Criteria for Moisture Control Design Analysis in Buildings (ASHRAE Standard, 2009) requires the rain penetration as one of the moisture load source. However, the field research data on this input parameter are still lacking. Therefore, a new field experimental study was conducted to fill this research need.

1.1   RESEARCH GOAL AND OBJECTIVE

Aiming to investigate the correlation between rain and wind data to the proportion of presence of water near a particular defect location, this field experimental study is designed to measure and analyze amount of water collected through specific defects or wall interface locations and the effect of the leakage on the moisture content of the wood framing component and the relative humidity of the wood framing cavity in vinyl sidings and non-rain screen stucco clad wood-frame wall construction during fall and winter rain events in BC.

1.2   SCOPE

This field experimental study focuses on the common existing construction practice in older residential wood-frame buildings exposed to the West coast climate of British Columbia. As the climate in this area has long periods of high humidity and precipitation, any wet wood framing in wall assemblies from rain penetration leakages is at a higher risk of being prevented from drying out to safer moisture content levels for wood. While the current British Columbia Building Code only allows rain screen wall assemblies on new construction, concealed barrier stucco wall assembly and the vinyl siding wall system are still found on many existing residential buildings.

To reflect the two most common claddings used in these older residential wood-frame buildings, vinyl sidings and the concealed barrier stucco wall assemblies typical of the housing stocks built in the 1980s are selected for this study. In addition, vinyl sidings and stucco cladding with acrylic finish coat are chosen to compare the different material properties, i.e. non-absorptive vs. absorptive cladding. In the perfect barrier wall type, any joint details are particularly susceptible to water ingress damage. The acrylic finish coat is chosen for stucco cladding to reflect the most common type of finish used for stucco in BC.

This study also focuses on the defects at window and wall interfaces, in particular below the window sill. The Survey of Building Envelope Failures in the Coastal Climate of British Columbia (Morrison Hershfield, 1996) found 23% of surveyed building envelope failures occurred at window areas. Moreover, missing sealants at frame/cladding joint was one of the problems observed. To this day, water staining marks from window sill corners are easily observed on the exterior of many older residential buildings, indicating that it is a location vulnerable to rainwater ingress issues. Deficiencies simulated in this study include missing sealants between window frame and stucco cladding, as well as the lack of window head drip edge accessories at vinyl siding wall.

1.3   THESIS OUTLINE

This thesis begins with a review of existing literature regarding wind driven rain. The wall façade response to the onslaught rain and rain penetration is discussed in Chapter 2: Literature review. Discussions of hygrothermal analysis and building construction industry's attempt to limit the rainwater penetration through walls are also included in this chapter, with a focus on vinyl siding and stucco cladded walls. An overview of the research approach is discussed in Chapter 3. Chapter 4 describes the construction of the eight full-sized wood frame wall panels of 4 feet x16 feet test walls at the Building Envelope Testing Facility at the Burnaby campus of the British Columbia Institute of Technology, the measuring equipment and monitoring sensors. The data collected at

the test walls from November 1, 2013 to June 19, 2014 are then presented, analyzed, and discussed

in Chapter 5. Finally, the study is concluded in Chapter 6, with recommendations for future studies.

CHAPTER 2: LITERATURE REVIEW

The literature review section is organized into five sections based on the overall path of rainwater starting from its raindrop form to the vapour form inside the stud cavity of a typical wall assemblies, followed by the construction industry's effort in mitigating rainwater penetration issues and a summary of the overall research development. The first four sections also discuss definitions and parameters used in wind driven rain (WDR) studies.

2.1   WOOD FRAME WALL'S RESPONSE TO WIND-DRIVEN RAIN

Based on a wall's performance on managing wind driven rainwater, different wall assemblies are generally classified into the categorization as shown in Figure 2.
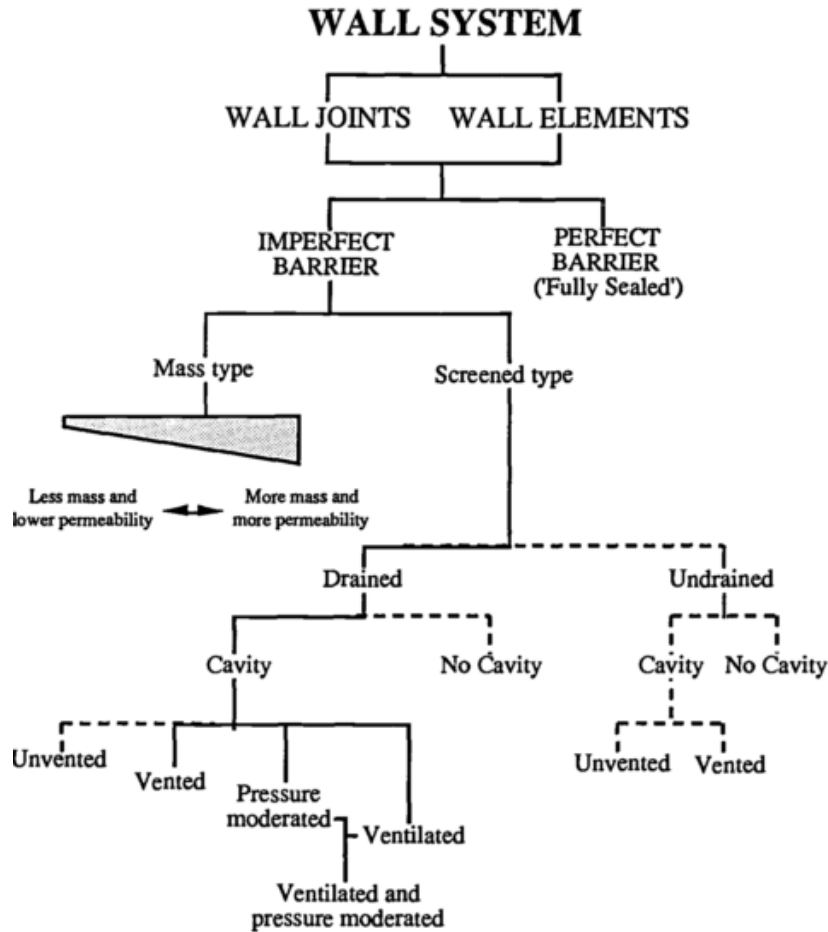
Figure 2. Classifications of wall based on the wall's performance in managing wind driven rain (Straube & Burnett, 1998).

Straube and Burnett (2005) further classified the Perfect Barrier wall into Face-Sealed and Concealed Barrier walls. In Perfect Barrier walls, by definition, all rainwater penetration is stopped at one plane; for the Face-Sealed walls, this plane is at the exterior of the cladding, while for the Concealed Barrier walls, this plane is concealed by the cladding.

According to this classification, stucco walls with two layers of building paper installed directly on wood sheathing may be classified as a Concealed Barrier wall. Compared to a concrete wall, stucco

does not have enough mass to manage the rainwater solely by absorption, while the lack of a clear gap for drainage and cavity does not categorize the stucco walls in the screened wall category. On the other hand, a wall with vinyl sidings installed directly over sheathing membrane is an example of a vented drained wall. In horizontal vinyl sidings, however, the drainage path on the sheathing membrane may be obstructed by the profile of the sidings. The air gaps behind the vinyl sidings provide vapor diffusion and some air flow. The classification of the walls assists designers in understanding the walls' responses to onslaught rainwater.

Figure 3 shows some of the phenomena experienced by a raindrop at the moment of impact on a wall. Among these phenomena, splashing, bouncing, adhesion and spreading occur instantaneously, while film forming, evaporation, and absorption last over a longer period of time, resulting in the rainwater runoff on the surface of the wall. Most rain runoff models on building facades focus on short rain events without intermittent dry periods, hence eliminating the evaporation as a factor and accounting only for the impinging wind-driven rain (WDR) and the absorption. The absorption phenomenon occurs only on mass type claddings such as stucco, concrete, and brick walls. Splashing and bouncing of raindrops affect the actual amount of WDR received by walls. Abuku, et. al. (2009b) cautioned that the amount of raindrops captured by a driving rain gauge may be more than the actual rain load on the wall as the side walls of the gauge may have additionally collected the bounced and splashed raindrops that would not have affected the wall.
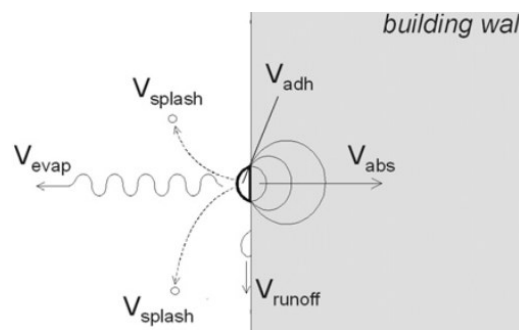
Figure 3. Response of wall to WDR and effect of a raindrop impinging on the wall (Blocken, et al., 2013).

Rain Run-offs

On non-absorbent wall surfaces, runoff occurs once gravity overtakes the surface tension that holds the raindrops onto the surfaces. On absorbent walls, runoff occurs once the surface material maximizes its absorption limit, i.e. is saturated, and rainwater forms a film on the surface.

In-depth details of the surface response to the WDR have been studied on different material types, for example, on window glass surface (Blocken & Carmeliet, 2015), on smooth ceramic brick surface (Abuku, et al., 2009b), and on hand-cut historic brick, fired and unfired bricks and lime mortar (Erkal, et al., 2012). In addition to the absorptive capacity of absorbent materials, the surface roughness of the materials also matter. Surfaces with higher roughness are found to allow for more absorption (Erkal, et al., 2012).

Studies into rain runoff on absorbent material wall facades can be found from as early as 1970s. The focus of the studies at the time was on the visual effects of weathering, primarily due to surface staining by dirt particles, on the facades (Blocken, et al., 2003; El-Shimi, et al., 1980). More recent studies on runoff also focus on runoff on glass surfaces with the aim of improving self-cleaning windows (Blocken & Carmeliet, 2015; Carmeliet, et al., 2006).

In addition to façade surface soiling and erosion, as well as rain runoff for self-cleaning glass surfaces, rain run-off contribution to the rain leakage into building envelope is also observed. Research into this aspect of rain run-off is still limited, in particular on wall facades that are not glass or masonry wall types. However, improvements to façade designs can still be learned from the observations of rain run-off and from the general recommendations to avoid façade weathering problems.

One of the observations made by Couper (1972) is that runoff occurs more commonly in streams – also known as fingering or rivulets, rather than uniformly down a building surface, in particular any vertical channel-like paths, such as the surfaces of column and the jambs of window and doors (Blocken, et al., 2013). In addition, surface tension allows the runoff films to adhere to the underside of horizontal returns, such as at the return edges of the vinyl sidings and the bottom of

horizontal stucco casing beads or stucco stops. Drip edge details are typically recommended to break this surface tension (El-Shimi, et al., 1980).

The type of rainfall from either cumuliform or the stratiform clouds also affect the cumulative amount of runoff. Cumuliform or heap clouds generate short duration showers, while stratiform or layer clouds typically generate longer duration, lighter intensity rain of less than 7.6 mm/h (Blocken & Carmeliet, 2015). In one study, the evaporation in between the showers from cumuliform clouds was found to decrease the amount of total runoff on a window by 26% (Blocken & Carmeliet, 2015).

Multiple runoff and absorption mathematical models have been developed, such as the models by Beijer (1977), El-Shimi, et al. (1980), Hall and Hoff (2011), Carmeliet and Blocken (2004) and Blocken and Carmeliet (2012). These models can be reviewed in details in Blocken, et. al. (2013) and Van Goethem (2014). Simulation of rain runoff is a complex numerical analysis problem and has not been incorporated in hygrothermal analysis models (Blocken, et al., 2013).

2.2 RAINWATER PENETRATION INTO STUD WALL CAVITY

In any water leakage through a building envelope, three factors must be present: source, force, and course (Parsons, 2004), i.e. water must be present and a force must contribute to direct that water through a path or a hole to a component of the assembly that is vulnerable to moisture damage (Garden, 1963). The types of forces that contributes to water leakage include kinetic energy, capillary action, gravity, and air pressure gradient. Depending on the size of the leakage path, either one type of force may be the primary contributing force or a combination of these forces may be the cause. To mitigate water leakage, all three factors must be controlled through the design, proper installation, and maintenance of the building assembly.

A study on the leakage paths around several different types of windows described the multiple leakage paths through the window assemblies and at the window to wall interface (RDH Building

Engineering Ltd., 2003). Leakage pathways at the moisture vulnerable areas around windows were identified (RDH Building Engineering Ltd., 2003) as shown in Figure 4 below.

Leakage Paths:

L1 - Through fixed unit to interior
(includes through fixed portion of sash)

L2 - Around operable unit to interior

L3 - Through window to wall interface to interior
(head, sill and jambs, also includes leakage at coupler mullions or corner posts between two adjacent window assemblies)

L4 - Through window assembly to adjacent wall assembly

L5 - Through window to wall interface to adjacent wall assembly
(head, sill and jambs, also includes leakage at coupler mullions or corner posts between two adjacent window assemblies)

L6 - Through window assembly to concealed compartments within window assembly
(includes frame sections that do not drain and spandrel cavities within window walls)

Figure 4. Water leakage paths at window-to-wall interfaces (RDH Building Engineering Ltd., 2003).

At location Leakage Path L5, through window to wall interface to adjacent wall assembly, several factors likely to cause the water leakage including the following:

- Sealant failure at window to water shedding surface on the wall interface

- Sealant failure at window to exterior moisture barrier on the wall interface

- Sealant failure at fasteners

- Lack of slope on head flashing and sill flashing

- No end dams on head flashing and sill flashing

- Damaged exterior moisture barrier near the window to wall interface (RDH Building Engineering Ltd., 2003).

For concealed barrier and drained walls, one source of rain penetration load is the rainwater draining on the moisture barriers, such as building paper or synthetic housewrap type of sheathing paper. The amount of the drainage water depends on the cladding type. Non-absorbent cladding, e.g. vinyl sidings, are expected to have higher surface water shedding or runoff, but less drainage water on the moisture barrier layer behind the cladding (Straube & Burnett, 2005).

In general, rain runoff or shedding on the surface of sorptive materials are reduced due to the capillary absorption of the sorptive materials (Hall & Hoff, 2011). On the contrary, smooth, impermeable and non-absorptive claddings will experience large amount of water runoff on the surface. While leakage due to WDR is less likely to occur from the field area of impermeable claddings, leakage may occur at the interfaces between these claddings and other wall components, in particular at defective joints at sills and along the jamb of vertical joints (Hall & Hoff, 2011). In the case of vinyl sidings, rain runoff is also shed by the geometry of the vinyl sidings profile. However, vinyl siding accessories, such as J-trims, function as channels that may direct rain runoff onto vulnerable joint locations.

A study on the window jamb flashing on vinyl nail-on windows follows the ASTM E2112-01 guidelines on windows installation and is one of the few research on windows installation on siding-type of claddings (Parsons, 2004). This study visually assessed the different Water Resistive Barrier (WRB), flashing membrane, and siding installation sequences for nail-on or flanged vinyl windows on clear acrylic sheets as the wall sheathing. The following are several of the findings related to vinyl sidings as concluded from that study:

- When water was dripped over the jamb of the window's nail-on fin, the water followed a direct line along the jamb. However, when the water drops hit an obstruction in their paths, the straight path became a fan dispersal pattern. When passing behind the vinyl sidings nail bands, the water flow pattern was of a dripping or dot pattern.

- On wrinkled WRB, the water flow pattern was S-like pattern, following the folds of the WRB.

- The lap joints in cedar and clapboard sidings allowed water to be directed out to the exterior of the sidings. However, in vinyl sidings, the interlocking joints between the upper and lower panels significantly reduced the direct exit path for the water, even when there were pre-drilled drain holes (Parsons, 2004).

This study concluded that depending on the rough opening WRB application and window installation sequence, the vinyl window's integral nail-on flange is adequate as a jamb flashing (Parsons, 2004). However, in areas with climates that are at high risk for rain leakage, redundancy in moisture barriers design with flashing membranes around the window rough opening should be considered.

Typical Wall Defects in Stucco Clad Walls

Guidelines to the installation of stucco cladding and the necessary lath have been outlined in ASTM C926, Standard Specification for Application of Portland Cement-Based Plaster (ASTM, 2015), and in ASTM C1063, Standard Specification for Installation of Lathing and Furring to Receive Interior and Exterior Portland Cement-Based Plaster (ASTM, 2014). As cautioned in ASTM C926, stucco should not be considered waterproof. Water may penetrate the stucco through cracks across its thickness, at stucco interface to stucco accessories, through failed or missing sealants at these interfaces, and by absorption through its mass. Field observations and studies by building envelope consultants (Cope & Horst, 2014; Nelson & Norris, 2009; Spagna & Ruggiero, 2003) have identified several common defects typically found in stucco clad walls that lead to water leakage into the wall assemblies, in particular around windows, as following:

- Cracking from corners of windows, such as at window head and sill corners.

- Sealant failure or omission between windows and stucco.

- Out of concerns of stucco cracking from the window corners, the head flashing is typically not extended beyond the jamb and end dams are usually not detailed.

- Loss of drainage plane on single WRB due to the stucco adhering to the WRB, combined with damaged WRB during stucco application, especially for housewrap-type of WRB.

- Unsealed and discontinuities of stucco casing bead flanges at window head corners and laps

- Perforated flange of casing bead when the casing bead is relied on as the flashing component

- Lack of sill pan flashing.

Similar to the vinyl J-trim used around the windows in vinyl siding cladded walls, the stucco accessories, casing beads, may also increase the likelihood of water leakage from the window to wall interface when these accessories are not installed properly.

There are two schools of thoughts regarding how non-rain screen stucco walls manage rainwater load. The first is as Nelson and Norris (2009) stated regarding these walls, that "… WRB serves as the drainage plane behind the outer cladding of stucco." The second is the notion many building science professionals hold, that the stucco mass is able to retain the rain load and the moisture will eventually dry out by evaporation; therefore, only minimal amount of water is expected to drain on the building paper.

A sheathing membrane is typically designed as the second plane of defense against liquid water. Only incipient amount of water should reach this second plane of defense as the water shedding surface should be the exterior surface of the cladding. Therefore, the non-rain screen stucco walls as a concealed barrier wall type are expected to shed most rainwater on the exterior surface of the stucco, hold the bulk of the rest of the water within the stucco materials until weather condition allows the moisture to evaporate, and drains only small amount of water on the sheathing membrane. This is the reasoning behind the second school of thought.

Following this line of reasoning, commonly used acrylic stucco finish which are less permeable than stucco are typically used under the misconception that the function of the finishing coat of the stucco is to protect stucco from rain penetration (Pazera & Bomberg, 2010). Properly designed stucco cladded walls should have layers that are more permeable towards the outside to increase the evaporation of the high moisture load from the stucco mass (Pazera & Bomberg, 2010).

The absorptive nature of stucco cladding on non-rain screen stucco walls means that a moisture load is held close to the WRB for longer period of time, while relying on the capillary moisture transport to drain this moisture load away from the assembly. However, drainage by capillary moisture transport is substantially slower than gravity drainage (Leslie, 2007). In this high moisture load condition, stucco walls with perforated housewraps are the most vulnerable for leakage. For this reason, double layers of building paper are better for concealed barrier stucco assemblies, as one layer is considered the sacrificial layer, while the other provides wrinkled surfaces that allows for partial gravity drainage (Leslie, 2007).

In addition to the typical installation defects at stucco wall penetrations, such as windows and doors, the absorptive nature of the stucco mass, the type of the finish coat and the sheathing membrane types used in the assembly may be additional factors that contribute to the vulnerability of the stucco walls to rainwater leakage.

2.3   ESTIMATING WIND-DRIVEN RAIN INTENSITY

During a typical rain event with wind speeds greater than zero, raindrops fall in oblique direction as wind provides a horizontal force component to vertical falling drops that are primarily governed by gravity. Therefore, the oblique rain intensity can be considered a vector (Figure 5). The nomenclature for the rain intensity with respect to the impinging rain on a vertical building façade is as follows. The vertical downwards rain intensity is referred to as the horizontal rain intensity, R_h – a reference to the measurement method of collecting the rain over a known horizontal area. In

the studies of rain on vertical building facades, the horizontal component of the rain intensity vector

is referred to as the wind driven rain intensity, R_{wdr}.
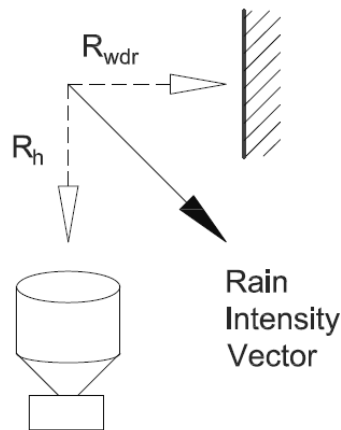
Figure 5. Rain intensity vector definitions and its vector components.

The following theoretical formula was one of the first mathematical expression describing the Wind

Driven Rain intensity.

$$R_{wdr} = R_h \times \frac{U}{V_t}$$

Equation 1

R_{wdr} = WDR intensity through the imaginary vertical surface [mm/hr.m^2]

R_h = unobstructed horizontal rainfall intensity [mm/hr]

U = wind speed [m/s]

V_t = raindrop terminal velocity [m/s]

Equation 1 assumes a singular raindrops size and a uniform and steady wind speed. To reflect more

realistic rain events, more comprehensive expressions have been developed through multiple

investigation methods to account for the multiple factors that influence the flow of raindrops onto

the building façade, including wind speed, wind direction, horizontal rain intensity, distribution of

raindrop size – also known as raindrop spectra, building geometry, and topography.

2.3.1 Raindrop Spectra

The raindrop spectrum is the relative probability distribution of raindrop size that depends on the rainfall intensity. Many other factors influence raindrop size distribution, including position relative to the center of rainstorm and type of rain (e.g. orographic, thunderstorm, convective). However these factors are also accounted for by the rainfall intensity. The relationship between the raindrop size and rainfall intensity most commonly used now was based on the work by Best (1950a) who reviewed experimental studies on raindrop spectra from 1904 to 1948. Two methods typically used to study raindrops distribution were as follows (Best, 1950a):

1) Filter paper method, where a sheet of absorbent, powder dye-treated, filter paper was exposed to the rain for a short period of time, resulting in stains of drop sizes which are then counted and measured.

2) Pans of sifted flour method, where the raindrops that fall into the flour result in dough pellets and are then baked and passed through graded sieves to be separated into the different sizes.

2.3.2 Terminal Velocity of Raindrops

For a raindrop, the terminal velocity depends on the raindrop diameter or the sphere of its equivalent volume if the drop is deformed, as well as on the density and viscosity of the air in the atmosphere. For the WDR studies, it is appropriate to consider the standard atmosphere condition, in which the density and viscosity are dependent on the height. Based on this principle, Best (1950b) developed the terminal velocity formulae for large or 0.3 to 6.0 mm raindrops, medium or 0.05 to 0.30 mm raindrops, and small or less than 0.05 mm raindrops.

Best's formulae for size distribution of the raindrops and terminal velocity of these raindrops have been used and adapted in the semi-empirical expressions for WDR intensity. One of them is the expression by Lacy (1965), who modified Equation 1 to include the raindrop terminal velocity and median raindrop size as a function of horizontal rainfall intensity:

$$R_{wdr} = 0.222 \times U \times R_h^{0.88} \approx 0.222 \times U \times R_h$$

<div align="right">**Equation 2**</div>

where 0.222 is the average WDR coefficient $[s/m]$

Equation 2 calculates WDR intensity not affected by any obstructions typically found closer to the ground level. Hence, this unobstructed WDR intensity is also referred to as the **free-field WDR intensity**, which can also be described as the flow of rain through a vertical area (1m² or 1ft²) in an imaginary airfield.

2.3.3 Obstruction Factors

As WDR reaches closer to the ground, the free-field WDR intensity becomes affected by any foliage, the terrains, urban landscapes, and the geometry on the building and façade of interest. These obstruction factors are accounted for in the two models presented next.

2.3.3.1 ASHRAE 160 Standard

ASHRAE 160 Standard provides a simplified method to predict the wind driven rain by combining Lacy's model. The coefficient 0.222 in Equation 2 was simplified as the empirical constant, FL, at 0.2 kg.s/(m³.mm). Obstruction factors that account for the levels of exposure due to topography, run-off and overhang factors are also accounted for. The wind driven rain prediction by ASHRAE 160 method is calculated as following.

$$R_{wdr} = F_E \times F_D \times F_L \times \cos(\theta) \times U(h) \times R_h$$

<div align="right">**Equation 3**</div>

R_{wdr} = WDR intensity on to a vertical surface [mm/hr.m²]

F_E = rain exposure factor depending on topography

F_D = run-off and overhang factor

F_L = empirical constant, 0.2 kg.s/(m³.mm)

θ = angle of the wind to the wall's normal

$U(h) =$ wind speed at the height of interest [m/s]

$R_h \ =$ horizontal rainfall intensity [mm/hr.m^2]

2.3.3.2 Straube and Burnett's method

Factors considered in this model include the raindrop diameter, wind speed at the height of interest, location on the façade, building aspect ratio and presence of overhang, and topography of the building.

$$R_{wdr} = RAF \ \times DRF(V_t) \ \times \cos(\theta) \times U(h) \times R_h$$

Equation 4

$R_{wdr} =$ WDR intensity on to a vertical surface [mm/hr.m^2]

$RAF \ =$ Rain Admittance Factor

$DRF(V_t) \ =$ Driving Rain Factor

$\theta =$ angle of the wind to the wall's normal

$U(h) =$ wind speed at the height of interest [m/s]

$R_h \ =$ horizontal rainfall intensity [mm/hr.m^2]

The Rain Admittance Factor, RAF, accounts for the obstruction factor due to the air flow around the wall geometry features, such as the wall's aspect ratio and the presence of roof overhangs. In addition, the WDR intensity also varies at the different locations on the wall surfaces, i.e. on the middle field area of the wall, compared to the top or bottom of the wall or the corners of the wall. RAF converts the free-field WDR intensity to WDR intensity on building façade. The values of RAF for three types of buildings are shown in Figure 6.

(a)

0.8 - 1.0
0.5 - 0.8

< 0.5

Low-rise Building H/W << 1

(b)

0.9 - 1.0+

0.5 - 0.9

< 0.5

Tall Building (>10m) H/W >> 1

(c)

< 0.20

0.20 to 0.35

0.35 to 0.50

< 0.35
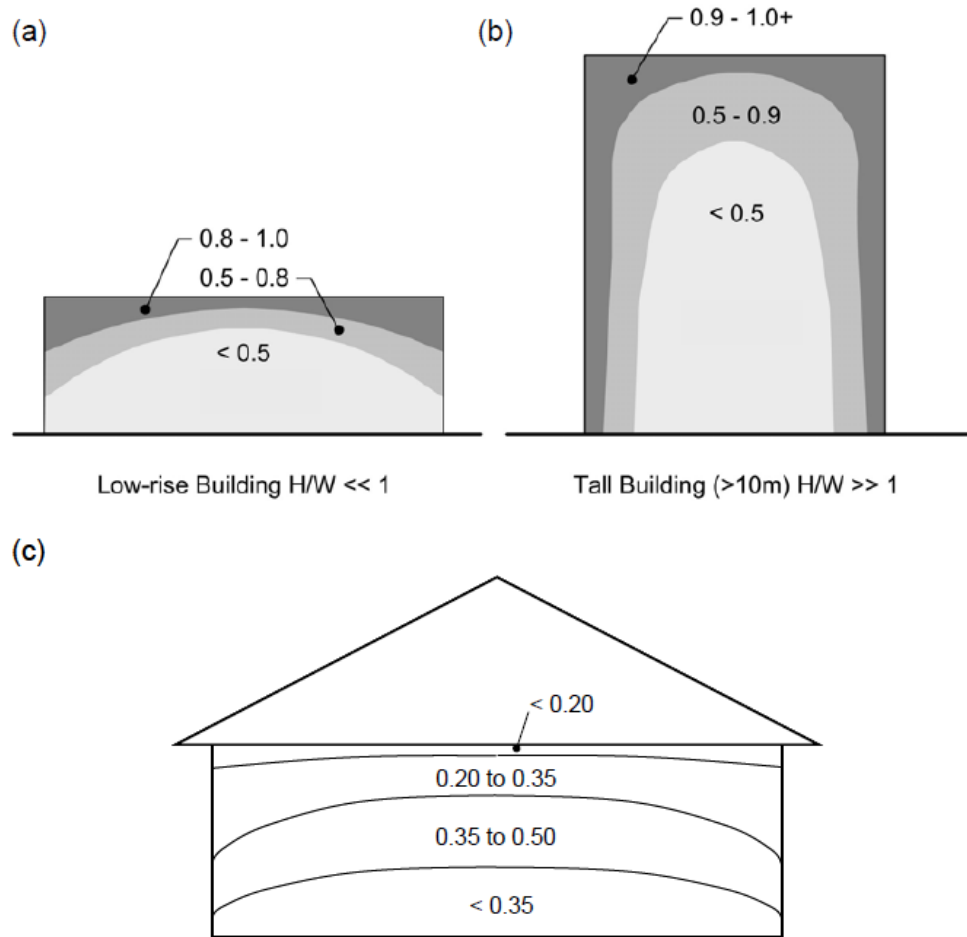
Figure 6. Rain admittance factors (RAF) for low-rise building with aspect ratio of less than 1 (a), for tall building of more than 10 m height and aspect ratio of more than 1 (b), and for a low-rise building with sloped roof and overhang (c). Extracted from Blocken and Carmeliet (Blocken & Carmeliet, 2010), based on Straube and Burnett (2000) and Straube (1998).

Straube and Burnett provide no RAF value estimates for low-rise building with aspect ratios closer to 1. However, similar to these RAF values, the values of Wall factor, W, tabulated in Figure 7 for multiple façade geometries with wall aspect ratios closer to 1, particularly for two to three storeys buildings are applicable for the WDR intensity calculation. Wall factor, W, is described by a European standard EN 13013-3:1997 (CEN., 1997) to account for the variation of the flow of air on the surface of the wall, to be used to calculate the driving rain index on vertical surfaces.

Description of wall	Average value	Distribution
Two storey gable	0.4	0.5 0.4 0.3 0.3 0.3 0.2
Three storey gable	0.3	0.5 0.4 0.3 0.3 0.3 0.2
Multi storey flat roof[1]	0.2 for e.g. ten storey, but higher intensity at top	0.5 for top 2.5 m 0.2 for remainder
two storey eaves wall	0.3	Pitched roof (20° or over) typical overhang 350 mm 0.3 0.3 0.3
three storey eaves wall	0.4	Pitched roof typical overhang 350 mm 0.4 0.4 0.4
two storey flat roof (pitch <20°)	0.4	0.5 0.4 0.2
1) These data apply to multi-storey blocks of normal aspect width; no data are available for exceptionally narrow buildings		

Figure 7. Wall factors, W, on multiple wall façade geometries, similar to the RAF values used in the European Standard EN 13013-3 for the calculation of driving rain index (CEN., 1997).

Driving Rain Factor, DRF, is the inverse of the terminal fall velocity of raindrops, V_t, which depends on raindrop size distribution, and horizontal rainfall intensity, R_h. The terminal velocity of raindrops, V_t (d), depends on the raindrop diameter, d. As recommended by Straube and Burnett (2000), a third-degree regression fit for raindrop diameters between 0.1 to 5.8 mm is by Dingle and Lee (1972) as follows:

$$V_t(d) = -0.166033 + 4.918441d - 0.888016d^2 + 0.054888d^3$$

Equation 5

V_t = raindrop terminal velocity [m/s]

d = raindrop diameter [mm]

The raindrop diameter in this model is the median diameter of raindrops, which is defined such that 50% of raindrops in the air are of a diameter less than this median diameter. The following semi-empirical equation is derived from the raindrop sizes distribution given by Best (1950a):

$$d_{50} = 1.30\, R_h^{0.232} \times 0.69^{1/n}$$

Equation 6

d_{50} = median diameter [mm]

R_h = horizontal rainfall intensity [mm/hr]

n = 2.25

Three most commonly used models for calculating WDR that are the two semi-empirical models by Straube and Burnett (2000) and by Lacy (1965), as well as a numerical model by Choi (1998). This thesis will focus on the semi-empirical models. More details on the numerical model by Choi can be found at the following articles: (Choi, 1994a; Choi, 1994b, 1994c, 1999, 2000). The different investigation methods used in WDR field are discussed next.

2.3.4 Investigation Methods in WDR field

Investigation methods into WDR are generally one of the following three types: experimental, semi-empirical, and numerical. Experiments to measure WDR in the field use wall-mounted WDR

gauges or free-standing WDR gauges. Historically, semi-empirical methods are used to investigate the relationship between WDR over horizontal area (R_h), wind speed and wind direction to the intensity of unobstructed, and free-flowing WDR (R_{wdr}). Hence, combination of horizontal rain gauges to measure R_h and anemometers to measure wind speeds and directions has been used to provide the typical meteorological data available from weather stations. On the other hand, numerical models for WDR studies are usually based on Computerized Fluid Dynamics (CFD) simulations, which may use wind tunnel studies to verify the models' prediction.

2.4 WOOD FRAME WALL'S HYGROTHERMAL ANALYSIS

The application of the WDR input data into the hygrothermal simulation could be grouped into two different approaches. The first approach is considered the traditional approach, where the total mass of all raindrops impacting an façade area of a building during a time interval of the rain event is averaged over time and space, and then input into a hygrothermal analysis boundary condition as an average of moisture flux (Abuku, et al., 2009a). The second approach is where the impinging raindrops are considered discretely and randomly.

When compared to field measurements, simulations using the traditional approach were found to overestimate the measured average moisture content of specimen cladding materials (Abuku, et al., 2009a). Possible causes of the overestimation include (1) the splashed and bounced raindrops that were in reality not absorbed by the cladding and (Timber Frame Housing 2002 Consortium) the difference between the evaporation / absorption flux assumed to be uniform over a given surface area and the more real discrete evaporation / absorption by the raindrops (Abuku, et al., 2009a).

Damage Mechanism in Wood-Frame Wall Assemblies

Wooden building materials fail by excessive moisture typically when infected by fungal / mold growth to the point where the wood is soft. In order to simulate the thresholds of building materials' failure, such as wood rot, hygrothermal analysis have included numerical models for predicting the extent of mold growth. Two commonly used mold growth prediction models are the empirical VTT

model and the theoretical biohygrothermal model (Krus, et al., 2010). Regardless of the differences between these two models, either of the two models can be used to yield a Mold Index, which is the percent coverage of wood surface by mold growth. Mold Index has been used as a rating of the extent of mold growth on the wood substrate (Krus, et al., 2010), providing a comparative measure among multiple mold growth prediction models. Although the focus of discussion here is on wood, both models are also used to analyze the mold growth in mineral-based building materials, such as bricks and stucco.

The parameters that determine mold germination and growth are the moisture conditions of the growth medium (surface humidity and moisture content of the substrate), temperature and time. As the moisture contents of the substrate reach equilibrium with the relative humidity closest to the substrate's surface, the surface's relative humidity is the common parameter used as an input for the mold growth models. The critical moisture conditions modeled in the laboratory based VTT mold growth model has been validated by a field study (Johansson, et al., 2013). More detailed discussions and comparisons among various mold growth prediction models are found in the review by Vereecken and Roels (2012).

2.5 BEST PRACTICES FOR WIND-DRIVEN RAIN MANAGEMENT IN WOOD FRAME CONSTRUCTION

As a response to the leaky condo crisis in 1990s, various reports and studies into the cause of those water leakage into wall assemblies were published (Alberta Municipal Affairs & City of Calgary, 2008; Bomberg, et al., 2002; City of Woodbury Building Inspection Division, 2011; Morrison Hershfield, 1996; Morse & Haas, 2010; RDH Building Engineering Ltd., 2001; Timber Frame Housing 2002 Consortium, 2002; Tom, 2001). In addition, the guidelines to moisture management within wall assemblies, standardized water tightness test procedures, and hygrothermal simulations of wall assemblies were developed. More recently updated guidelines on the best practices for

window installation in wall assemblies include the ASTM E2112-07: Standard Practice for Installation of Exterior Windows, Doors, and Skylights (ASTM, 2007) and CSA A440.4-07: Window, Door and Skylight Installation (CSA, 2007). Both standards documents provide 3D detail drawings to illustrate step-by-step guidelines of multiple approaches that users can follow to detail the window-to-wall interfaces. In both standards, windows are expected to leak at some point; hence, the wood framing around the windows are detailed such that incidental leakage water can be directed outside the assembly. The approaches vary according to the risk level of water ingress based on the wall assemblies' location, topography, and building geometry.

Three strategies for rain penetration management are described in the CSA A440.4 standard: face seal, concealed barrier, and rain screen. These are similar to the wall classifications by Straube and Burnett (1998) as shown in Figure 2 where face seal walls are non-realistic strategy of perfect barrier ("Fully Sealed") walls, concealed barrier walls are drained walls with no clear cavity, and rain screen walls are drained walls with dedicated drainage cavity. The main difference between concealed barrier assemblies to rain screen assemblies is the use of furring (e.g. strapping) to create the dedicated air cavity/drainage plane in rain screen assemblies. To determine which of these rainwater management strategies are suitable for a wall of a particular building geometry at a particular topography and climate, the exposure rating of the building is first assessed through the Moisture Index (MI) of the building location, the overhang ratio, and the terrain factor. The Moisture Index for several cities in Canada are listed in a table reproduced from the National Building Construction Code. The overhang ratio is calculated by as the ratio of the width of roof overhang to its height above the window sill. The types of terrains, such as urban, suburban, rural, or exposed terrain (e.g. on a hill, or facing a lake or sea) are listed as part of the building exposure nomograph, on which a line can be drawn connecting the three micro-exposure conditions (CSA, 2007). Three exposures rating from the nomograph are high, moderate, or low exposure. For example, a two-storey building with first level windows and with less than 1 foot overhang located in Burnaby, BC, Canada (MI of 1.93) with few large trees or surrounding buildings have a high

exposure rating. For high exposure rated walls, the suggested water management strategy is the rain screen wall design.

2.5.1   Test Procedures for Water Penetration through Wall Assemblies

The challenges in testing wall assemblies for water tightness revolve around how to simulate WDR as the potential water ingress source (boundary conditions) in a time frame that is suitable for the construction industry, as well as the parameters that time resolution of weather data for hygrothermal response of the wall was one of the parameters questioned for the development of standard water tightness test methods and for hygrothermal analysis of building components exposed to the WDR. While hourly average rainfall and wind data are typically provided at weather stations, higher time resolutions, for example at 1 minute, 5 minutes or 10 minutes, may capture more realistic weather. For the purpose of water penetration testing, short durations of occurrence of strong windward gusts during a rainfall may more likely cause water penetration through a wall defect. Shorter duration strong winds and heavy rainfall intensities would have been reduced and become undetected in the hourly average. An analysis of the influence of the time resolution of the weather input data on the hygrothermal simulations was done by Blocken and Carmeliet (2007) and it was found that on several rain events, hourly data led to large underestimations of wall materials moisture content.

A 5-minute averaging time have been selected to be the suitable higher time resolution for use in many water penetration testing and hygrothermal simulations (Krpan, 2013; Sahal & Lacasse, 2008). An equation to convert the more commonly available hourly average wind speed to 5-minute averages and the procedure to determine the 5-minute wind driven rain intensity were described by Choi (1998). In Choi's article (1998), the 5 minute time resolution was chosen as a case study. Wu (2011) compared the effect of the hourly time resolution vs. the 5-minute data when each were used for hygrothermal response at a wall in Toronto, Ontario climate, and found that there was no significant difference. However, Wu cautioned that this may not be true at climates with higher

annual rainfall, such as in Vancouver, and at more complex wall locations, such as where windows are involved (Wu, 2011).

2.5.2   ASHRAE Standard 160

The ASHRAE Standard 160 - Criteria for Moisture Control Design Analysis in Buildings (ASHRAE Standard, 2009) was developed for a systematic building envelope moisture performance evaluation. This standard is intended to be a guide that helps building designers decide on building envelope assembly designs suitable for the building's climate, based on the evaluation of the potential moisture load on that assembly. The standard also attempts to take moisture design into a performance-based procedure, rather than its usual prescriptive measures, while standardizing design assumptions and requiring more transparency in the design, boundary condition inputs in simulations, and materials assumptions (TenWolde, 2011). As one of the moisture load source, rain penetration is addressed in Section 4.6 of this ASHRAE standard by first calculating the design rain loads on the wall assembly, and then a portion of that rain load is assumed to penetrate the wall as follows.

> "In the absence of specific full-scale test methods and data for the as-built exterior wall system being considered, the default value for water penetration through the exterior surface shall be **1% of the water reaching the exterior surface**." (ASHRAE Standard, 2009)

The "exterior surface" is further clarified by the ASHRAE Standard 160 to be on the exterior side of the water resistive barrier; in other words, the intention of the design is to limit the exposure of the water resistive barrier to a maximum of 1% of the rain load. The 1% default value, however, is arbitrarily determined based on an unpublished research on brick walls due to a lack of supporting data (TenWolde, 2008). The correlation between the rain penetration and the wind-driven rain parameters is a knowledge gap that still needs to be filled from field investigations.

2.6   SUMMARY OF RESEARCH PROGRESS ON WDR STUDIES

In response to these findings of the past and ongoing moisture-related wall failures, the building science industry is gaining interest in predicting the wetting and drying performance of a wall assembly in the wall's respective particular climate conditions (Tariku, et al., 2007). As the role of hygrothermal performance simulations is increasing in building envelope assembly designs, benchmarking rain leakage as a moisture source against field observations is becoming more important. The results of hygrothermal performance simulations are sensitive to the boundary conditions and the internal moisture sources used as input. However, current hygrothermal analysis still uses assumptions regarding the location and the magnitude of the rain leakage moisture source inside a wall (Dalgliesh, et al., 2005).

Similar to the Limit State Design approach used in structural engineering, the Limit State Design concept and procedure have been suggested for the evaluation of the drying performance of wall systems to the moisture load that it is likely to experience (Mao, et al., 2011). Using the Limit Stated Design concept, the drying capacities of well-performing wall systems must be higher than the moisture load the wall systems are predicted to experience in the climate zones the walls are built in. In other words: Drying capability > Moisture load.

The drying capabilities of several wall systems have been characterized through laboratory testing. A field study on the wetting and drying of wood framing due to vapour pressure gradients from vapour diffusion and wind driven rain load on the wall cladding has been done as well by Tariku, et al. (2015). However, rain penetration as a primary source of moisture loading has not been studied enough using real climate's moisture loading. Examples of moisture loading methods used in previous studies by others include placing a water tray on the bottom plate in the stud cavity (Mao, et al., 2011), wetting a piece of cloth held against the wood sheathing board (Weston, et al., 2010), and using a water spray rack with or without air pressure (Nelson & Norris, 2009). The amount of moisture load in these moisture loading methods is typically determined assuming the worst case scenario, i.e. 100% saturation of an area of wood framing or presence of liquid water on

the bottom plate, or as prescribed by a water testing standard, or decided based on the experimenter's professional experience.

2.7   PROBLEM STATEMENT

Based on the literature review above, two research problems were identified:

1. Although there is a need to determine the magnitude of rain penetration leakage relative to the wind driven rain and the wall system, no real-time, field tested data are available.

2. Although simpler, due to the different rain penetration management at different wall systems, the one-size-fit-all leakage amount estimate proposed by the ASHRAE 160 Standard will not be suitable for all wall cladding systems. If the industry and the research progress are moving towards hygrothermal performance simulations and limit state design concept, leakage amount estimates for different wall cladding systems and for different rain intensities are needed.

2.8   HYPOTHESES

Based on the literature review and problem statement discussed above, the following hypotheses for the defined scope of the study are made:

- The sheathing membrane behind vinyl siding walls is expected to experience less moisture load than the sheathing membrane at the stucco walls. However, as the sheathing membrane is concealed behind the stucco cladding, the hypothesis is that this moisture load will be small compared to the amount of rain that the exterior surface of the stucco experiences.

- The moisture load and the potential leakage amount are different at stucco walls compared to vinyl siding walls; higher potential leakage amount is expected at stucco walls.

- Sill corner location is expected to have higher potential leakage amount than at any other locations around the window perimeter.

- Higher wind driven rain intensity is expected to result in higher amount of leakage.

CHAPTER 3: RESEARCH APPROACH

3.1   OVERVIEW

The experiment will include the construction of vinyl sidings and non-rain screen stucco clad wood frame walls in one façade of a test building. The walls will be two storeys high with a window on the first level to allow the most rain load from the upper level.

In essence, two types of walls based on the measurement/ monitoring method will be built. The first type, water-collecting wall, quantifies the potential rain load that contributes to a leakage into the wood framing cavity. The second type, long-term performance wall, replicates the simulated defect of the first one and monitor the moisture content of the wood framing components, and the relative humidity inside the wood framing cavity. The pattern of the drainage of water on the sheathing membrane and the quantity of the drainage water are also monitored on the long-term performance walls. The magnitudes of the leakage and the drainage water are then compared to the wind driven rain (WDR) gauges and other weather parameter measured by the weather station on the building.

In total, three water-collecting walls were built: W1, W2, and W6. W1 and W2 were vinyl sidings clad walls, while W6 was a stucco clad wall. A total of five long-term performance walls were built: W3, W4, W5 were vinyl sidings clad walls, while W7 and W8 were stucco clad walls. W3 and W8 also served as control walls where typical construction details were built and no simulated defect was introduced as a variable.

3.2   EXPERIMENTAL VARIABLES

To meet the objective set in this study, the focus of the study is broken down into 3 elements of experimental variables as shown in Table 1 below.

Table 1. Three elements of investigations and the related measuring devices or sensors and the specimen wall types.

Element	Devices/Sensors	Wall type
1. Relative amount of rain going through defects	Leakage gauges (Modified tipping-bucket rain gauges)	Water-collecting walls
2. Amount of rain that is retained by wall cladding or is draining on the WRB behind cladding	Aluminum trough, tubing, collecting bottles, graduated cylinder and graduated syringe.	Long-term performance walls
3. How different wall systems perform given specific defects or details	Thermocouples, Moisture pins, RHT sensors and moisture detection tapes	

These three elements translate to three different measurement activities. The first one – amount of rain going through defects – is measured in mL using a modified tipping bucket rain gauge. The second one – how much water is retained by wall cladding – is measured in mL using a 50 mL capacity graduated cylinder and a 5 mL capacity graduated syringe. Water that flows on the building paper is collected at the bottom of walls and then measured. The third element – how different wall systems perform given specific details – is monitored for longer time period, i.e. more than one year, using thermocouples, moisture pins, relative humidity and temperature or RHT sensors inside wall cavity, and moisture detection tapes on the outside of WRB. The third element is studied as a response of the wall to the given deficiency.

3.3   ANALYSIS METHODS AND RESULT PRESENTATION

First, the weather data is analyzed, starting from the horizontal rain, the wind driven rain (WDR) on the wall rain gauges, and the wind speed. Trends and summary of the horizontal rain and WDR intensity are presented, Rain Admittance Factors (RAF) are also calculated to be compared to Straube and Burnett's estimated values. The relative quantities of water draining on the sheathing membrane as the moisture load that managed to past the cladding are summarized and analyzed for any patterns.

The rain leakage quantities at the wall and window interfaces of the water-collecting walls are analyzed on event-basis. The trends of the leakage events are compared to the horizontal rain and WDR intensity along the timeline of the study. Then, any possible correlations are analyzed, first by scatterplots of the moisture load (WDR) and the leakage amounts as the response to the moisture load. A second further analysis is done to find additional contributing parameters to the leakage amount using multiple linear regression models. The models are evaluated using statistics criteria. At the long term performance walls, hourly moisture content and relative humidity averages are plotted to analyze for any trends along the research timeline and to be compared to the timing of the leakage detections. The trends at the variable walls are compared to the trends at the control walls.

The main goal of the study is to present a proportion or percentage of the leakage amount at the different wall types compared to the moisture load, in this case, the wind driven rain.

CHAPTER 4: EXPERIMENTAL SET UP

4.1   OVERVIEW OF TEST FACILITY

The experimental tests were conducted using the South East façade of the Building Envelope Test Facility (BETF) at British Columbia Institute of Technology (BCIT), Burnaby campus. As shown in Figure 8, the test facility is located in an open field area, surrounded by a grassy area on the North side, a parking lot towards the West, another parking lot to the South past a small downhill area of about 4 feet (1.2 meters) high, and the closest wind driven rain obstacle is approximately 80 feet (24.4 meters) from the South East corner. Up to 16 feet (4.9 meters) high wall panels can be accommodated by the test facility. The interior condition of the test facility is maintained at approximately 21°C and 50% RH on the interior throughout the year. The exterior of the test panels are exposed to naturally occurring weather conditions, which are monitored by a weather station located on campus, mounted on the roof of the test facility, BETF, for the rainfall intensity, wind speed and wind direction.

Figure 8. Overview of the test facility from Google Map. South East façade shown (Google Maps, 2015).

Measuring devices that are relevant for this study at the weather station include the horizontal rain gauge at the rooftop of the BETF, and the anemometer that records the wind speed and direction. The horizontal rain gauge is a tipping-bucket rain gauge type. The count of bucket tipping is read by the data acquisition system every minute and averaged for hourly calculation. The horizontal rain gauge tips once 2 grams of rain is collected. Similarly, the wind speed and direction is recorded every minute. Based on the catchment area, the 2 grams or mL of rainwater is equal to 0.1 mm of rainwater.

The environmental conditions of outdoor and indoor of the BETF were monitored by the weather station, pyranometer, relative humidity sensors, temperature, and moisture sensors on the building.

4.2   DESCRIPTION OF THE TEST PANELS

The test facility is built with separate structural support for the second storey wall panels. In this study, while the exterior finishes of the wall panels were continuously cladded to the full 16 feet height, only the ground level 8 feet high panels were newly constructed and incorporated with sensors and measuring devices. Figure 9 shows the eight test panels and their relative position on the BETF. The previously framed upper level wall panels were built up to the same depth or preserved to allow the continuous cladding. Each wall panels are isolated on all four sides from the surrounding panels with extruded polystyrene, XPS, rigid insulation. The components of the wall assemblies from inside to outside consist of the following:

- Gypsum board
- 6 mil polyethylene sheet as vapour barrier
- 2x6 SPF wood framing filled with batt insulation
- 1/2" plywood sheathing
- 2 layers of 30-minute building paper
- Vinyl sidings or stucco cladding.
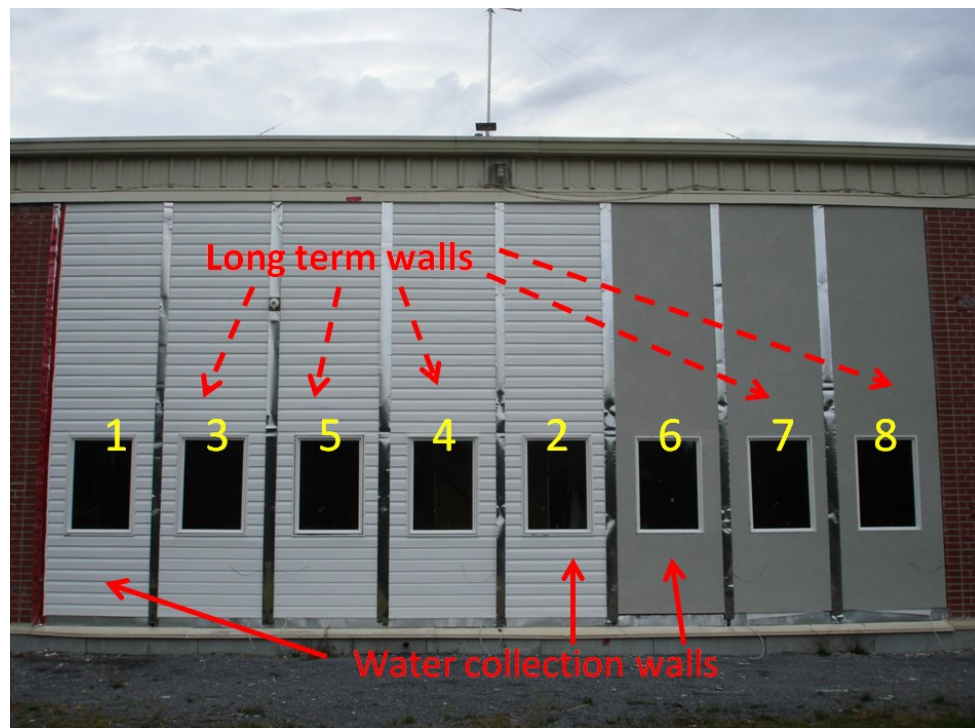
Figure 9. Configurations of water collection and long-term performance, vinyl sidings, and stucco cladded walls on SE facade of test facility. The numbers represent the specimen panel

number, e.g. specimen panel W1 is labelled as "1" in the photo. This photo was taken prior to the installation of wall rain gauges.

The vinyl sidings are the horizontal double 5" Dutch-lap panels with woodgrain finish from ABTCO. Accessories used include 5/8" J-channels, undersill trim, starter strips, and drip caps. The vinyl sidings were installed following ASTM D4756-06 (2006).

The stucco cladding consists of 1 inch x1 inch chicken wire type metal lath, ¼ inch thick scratch coat, ½ inch thick brown coat to build up to the thickness of the ¾ inch casing beads, and completed with grey, smooth-texture acrylic finish coat, most commonly used in BC. In addition to the standard lime, sand, cement and water as the ingredients for the stucco cladding, fibers and plasticizer additives were added to the stucco mixtures as commonly applied. Galvanized roofing nails of 1.5 inch length were used to fasten the metal lath onto the wall framing. Figure 10 shows the stucco scratch coat layer and the metal lath.

Figure 10. The application of stucco scratch coat over the metal lath on W7 panel.

The windows used in this study are 30 inch x 43 inch vinyl windows with nailing flanged, manufactured by Jeld-wen and ordered from Home Depot. The windows were installed following ASTM E2112-07 standard (ASTM, 2007).

The exterior sealant used around the perimeter of the window between the window frame and the stucco and vinyl siding trims is the Quad Advanced formula exterior sealant by LePage, which was selected because it passed the adhesion pull test on a vinyl siding J-trim among multiple sealants tested, as shown in Figure 11. The interior window perimeter sealant used between the window frame and the self-adhered membrane on the wood framing is the Sonolastic NP1 polyurethane sealant, which is a commonly used sealant to seal air leakage.

Figure 11. LePage Quad Advanced Formula exterior sealant passed the adhesion pull test on a vinyl siding J-trim as the sealant showed cohesive failure, instead of adhesive failure when pulled away from the substrate.

All wall framing construction, windows and vinyl sidings installation were completed by the author and the staffs at BCIT Building Science Centre of Excellence department. The stucco cladding was installed by an experienced contractor from "Hemlock Stucco and EIFS" company under the supervision of the author to minimize damages to the sensors.

The wall types undergoing these tests are subdivided into 2 categories: Water collection walls and long term performance walls. Figure 12 below shows the location of each wall types on the façade. Instead of creating specific defects on the five vinyl siding walls, variations in wall construction details were made. Wall specimen W1, W2, W3 and W5 simulate typical vinyl sidings installation with no head window flashings. W1 is a water collection wall with collection area below the left sill corner. Similar to W1, W2 collects the rainwater that is present along 6 inch length at the quarter point of the window sill. W3 is a long-term performance control wall specimen as a replicate for W1. Panel W5 is also a variation of the control long-term performance specimen, with a bead of sealant between the window frames and the vinyl siding J-trims all around. W4 is the only specimen with vinyl drip cap accessory along the head of the window.

Three stucco cladded panels labelled as W6, W7, and W8 were installed on the North end of the SE façade. W6 is a water collection wall with two missing sealant defects/collection areas: the first one at the left sill corner, with a controlled length of 4 inch up the jamb – to be referred to as the "W6 corner" defect, and the second one at the right quarter point of the sill for approximately 6 inch long of missing sealant – to be referred to as the "W6 middle" defect. W7 is a long-term performance wall that repeats the W6 corner defect. W8 is a long-term performance wall with no designed defect, to function as a control specimen.
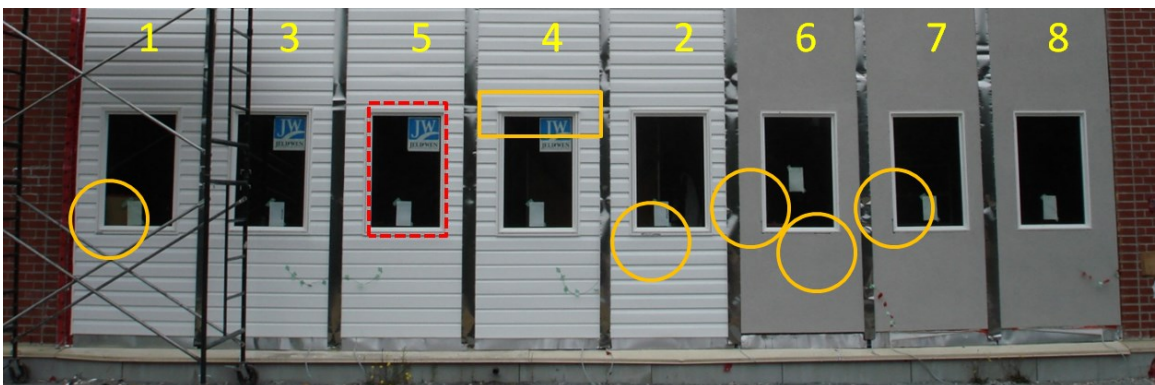
Figure 12. Locations of defects or features of the different wall panel specimens.
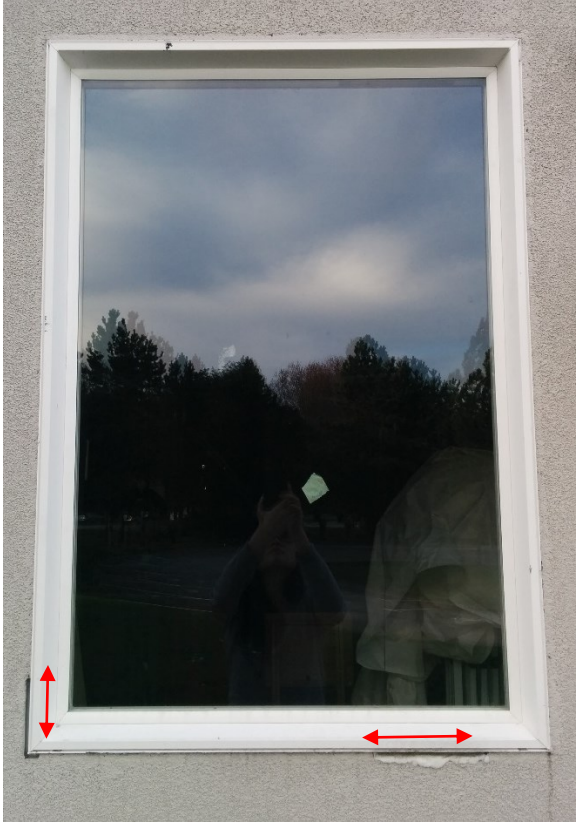
The following Table 2 summarizes the features in each wall panel specimen and the intent of each panels.

Table 2. Summary of the feature, intent, sensor and/or equipment at each wall panels.

Panel No.	Photo of Wall Panel	Features, Intent & Sensor / Equipment
W1		• Vinyl siding • Typical construction with no head flashing • **Water collection wall at the sill corner** • Leakage gauge • MDT as control sensors.

Panel No.	Photo of Wall Panel	Features, Intent & Sensor / Equipment
W2		• Vinyl siding • Typical construction with no head flashing • As a comparison to W1, **W2 collects water at the quarter point of the window along the sill J-trim** • Leakage gauge • MDT as control sensors.
W3		• Vinyl siding • **Typical construction with no head flashing** • A control wall for long-term performance monitoring • Thermocouples, moisture pins, RHT sensors, and moisture detection tapes • Bottom-of-wall trough and collection bottles.

Panel No.	Photo of Wall Panel	Features, Intent & Sensor / Equipment
W4		• Vinyl siding • **Vinyl drip cap was installed above the head of the window** • For investigation of the effect of a head flashing • Thermocouples, moisture pins, RHT sensors, and moisture detection tapes • Bottom-of-wall trough and collection bottles.
W5		• Vinyl siding • No head flashing • **Sealant applied between the vinyl head, jambs and sill J-trims and the window frames** • For investigation of the effect of sealing the gap between the J-trims and the window frames, such that no direct WDR enters the gap, and no run-off water exits from the gap. • Thermocouples, moisture pins, RHT sensors, and moisture detection tapes • Bottom-of-wall trough and collection bottles.

Panel No.	Photo of Wall Panel	Features, Intent & Sensor / Equipment
W6		• Stucco • Typical construction with no head flashing, sealant at gap between window frame and head, jamb, and sill casing beads • **Two missing sealant locations: 4" upwards from left sill corner & 6" long at the right quarter-width point along the sill** • As a comparison to W1 & W2, to collect water as potential leakage source • Leakage gauges: "W6 corner" and "W6 middle" • MDT as control sensors.

Panel No.	Photo of Wall Panel	Features, Intent & Sensor / Equipment
W7		• Stucco • Typical construction with no head flashing, sealant at gap between window frame and head, jamb, and sill casing beads • **Replicates W6 corner missing sealant defect and monitors the condition of the sheathing board and the framing under the window sill** • Thermocouples, moisture pins, RHT sensors, and moisture detection tapes • Bottom-of-wall trough and collection bottles.
W8		• Stucco • Typical construction with no head flashing, sealant at gap between window frame and head, jamb, and sill casing beads • **No designed defect** • Monitors the condition of the sheathing board and the framing under the window sill for comparison to W7 • Thermocouples, moisture pins, RHT sensors, and moisture detection tapes • Bottom-of-wall trough and collection bottles.

4.3   WALL RAIN GAUGES

The wall rain gauges consist of tipping bucket rain gauge apparatus connected to receive rain from square / diamond shaped catchment metal plates. Initially, in September 2013, four existing wall gauges were placed on the brick wall panels at the North and South ends of the SE façade. In October 2013, eleven more wall gauges were added after the preliminary test in the middle area of the façade. Figure 13 shows the layout of these 15 wall gauges.
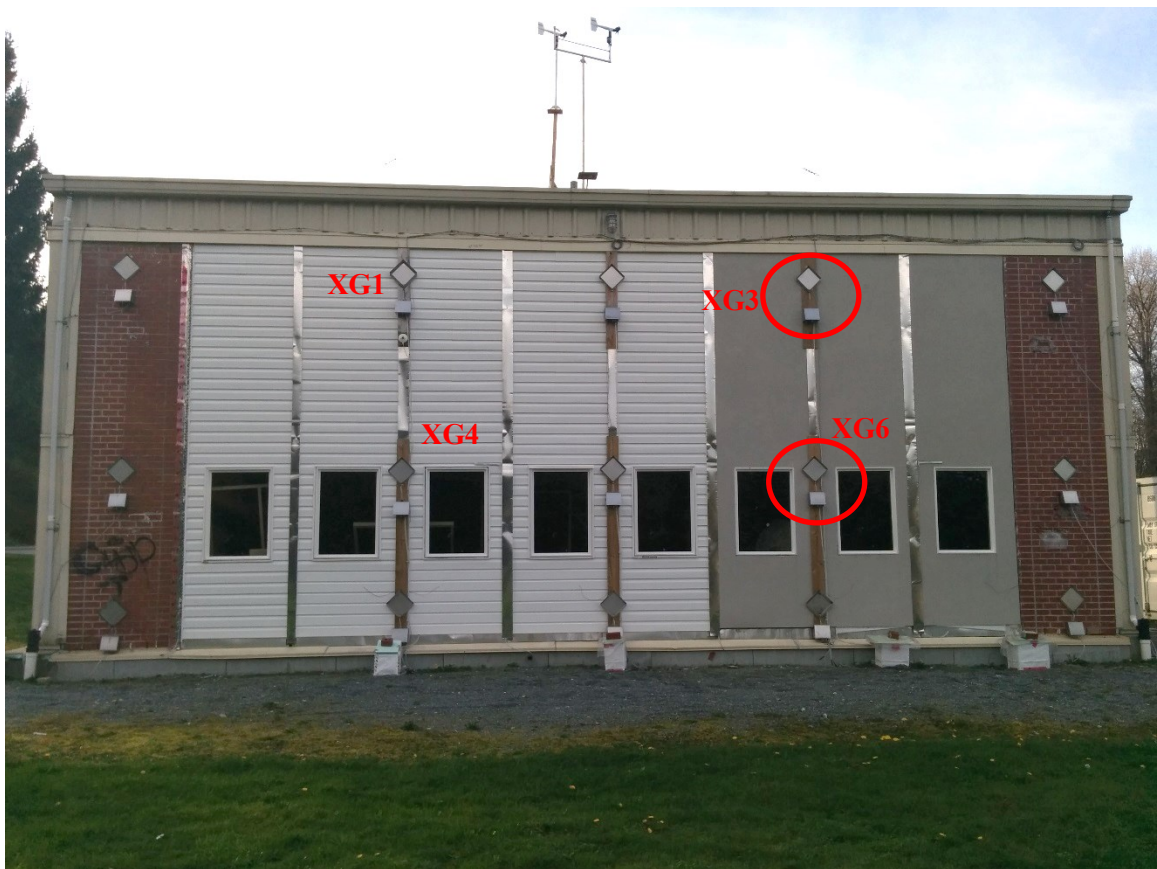
Figure 13. Locations of 15 wall rain gauges on the South East facade. In the analysis of the leakage into water collecting walls, the closest top and the middle gauges were used. For example, the circled gauges XG3 and XG6 were used for the analysis of the leakage at W6.

The wall rain gauges apparatus also measures 2 grams or mL of collected rain/tip. With the 9 inch x 9 inch catchment area, this is equal to 0.038 mm/tip. The rain gauges are also read by the data acquisition system once every minute.

4.4   LEAKAGE GAUGES

The leakage gauge is a modified version of the similar tipping bucket rain gauge used in a wall rain gauge. The modification increases the sensitivity of the gauges so that they tip after smaller amount of leakage water is collected. On average, the gauges were calibrated to 1.5 ± 0.1 mL of water/tip. The calibration of the leakage gauges is described in Appendix A. The table from Appendix A, is reproduced here as Table 3, which summarizes the sensitivity of each leakage gauges used.

Table 3. Calibrated amount of leakage gauges at water collection walls.

Location of Leakage Collection	Calibrated amount mL/tip
W1	1.482
W2	1.336
W6 Corner	1.613
W6 Middle	1.511

The framing of the water-collection walls are slightly different than that of long-term walls due to the shelves that hold the tipping bucket rain gauges as shown in Figure 14 and Figure 15. For corner water collection walls, the shelf is offset further to the panel's side. An approximately 4 or 6 inches wide by 1 inch high slots are cut through the plywood sheathing to allow aluminum troughs that direct any rainwater that can potentially infiltrate the wall assembly past the building paper water resistive barrier into the leakage gauge collection bucket. The troughs were made from paint coated, corrosion-resistant aluminum flashing sheet. Around the slot opening, self-adhesive membrane or peel-and-stick are applied as if the slot is a rough opening of a window, except that the overlapping of the membrane is to direct the water onto the triangular trough.
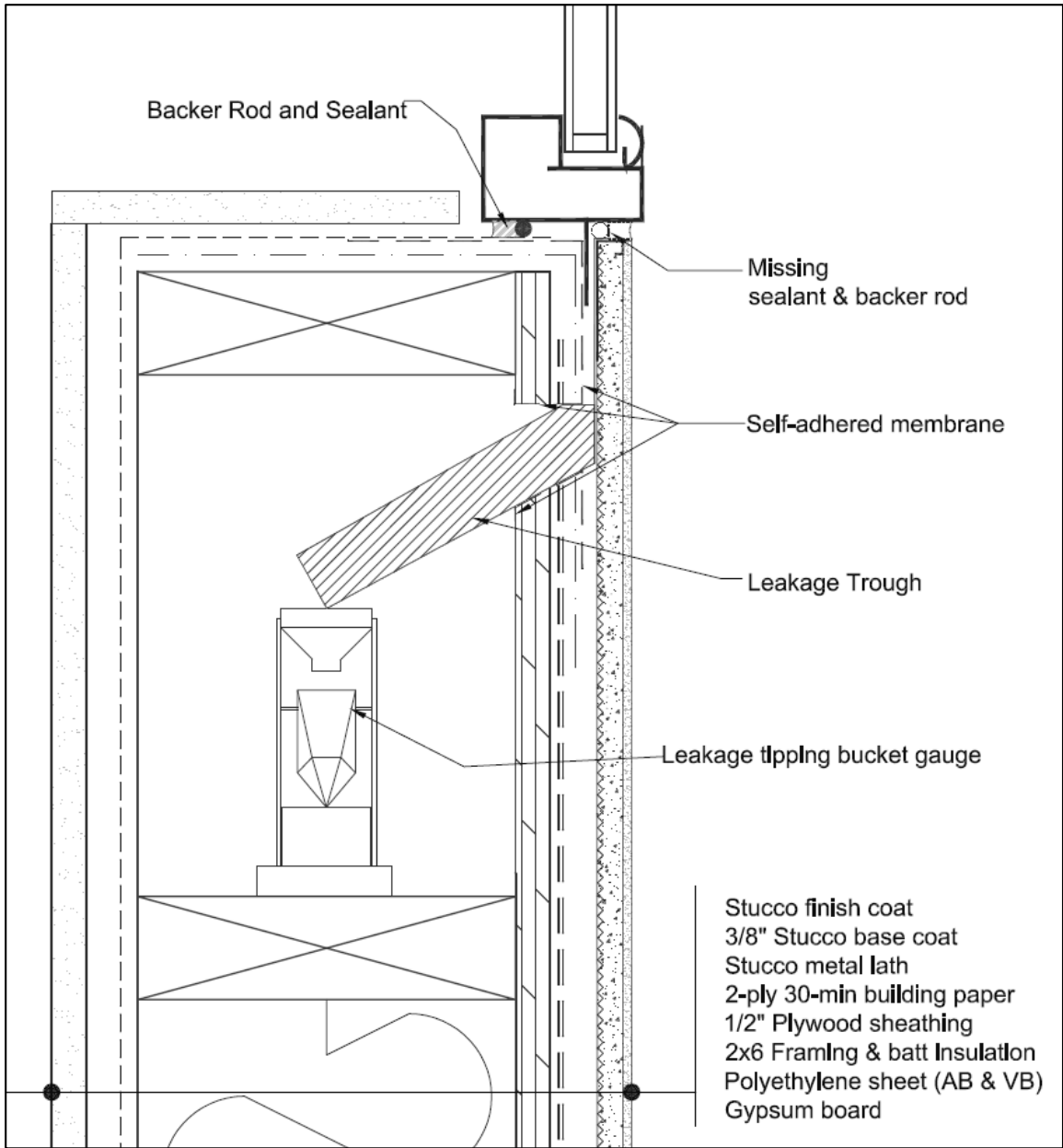
Figure 14. Detail drawing of water collection stucco wall W6 with missing sealant defect. The wall assembly cross section is typical for all stucco walls.

Figure 15. Left: Framing for the leakage gauge shelf of middle collection area for W2 panel. Right: Leakage gauges placed in assembled W2 and W1 panels; note the offset shelf in W1.

Figure 16 shows a close up view of a typical leakage gauge and the aluminum trough inside the shelf.
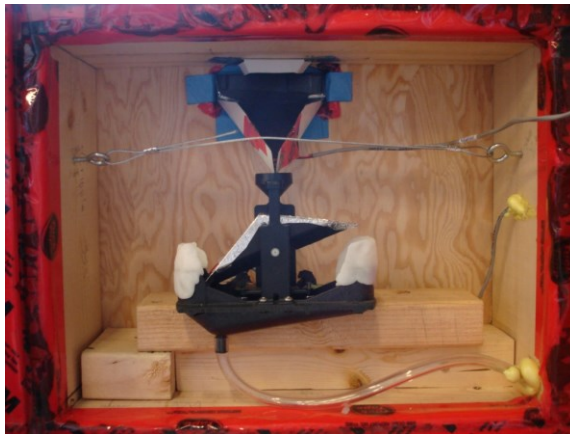
Figure 16. Close up view of a typical installed leakage gauge.

The installed leakage gauges are the results of many trials of modifications, which include:

- Adding a plate of cut-out aluminum flashing material to the tipping buckets and then wrapping the buckets with aluminum tape. This aluminum plate fills up the volume of the

bucket and directs water to the edges of the buckets; therefore, reducing the amount of water required to tip the buckets.

- Fine-tuning the height of the screws under the tipping bucket support for balance and reduction of water requirement. One error associated with the increased height of the screws is the bouncing of the buckets. To solve this issue, the original plastic nuts at the end of the screws were replaced with neoprene foams that were trimmed to a round shape. The neoprene foam material dampen the momentum of the bucket as it lands.

- Adding a moldable thermoplastics to each sides of the catch basin to catch the water spillage when the buckets tip since the buckets are now resting higher on their supports.

As shown in Figure 17, the triangular aluminum trough extends vertically up and its top edge folded to form a ledge. This folded ledge is later set to sit on top of the window sill stucco stop / casing bead or vinyl J-trim.
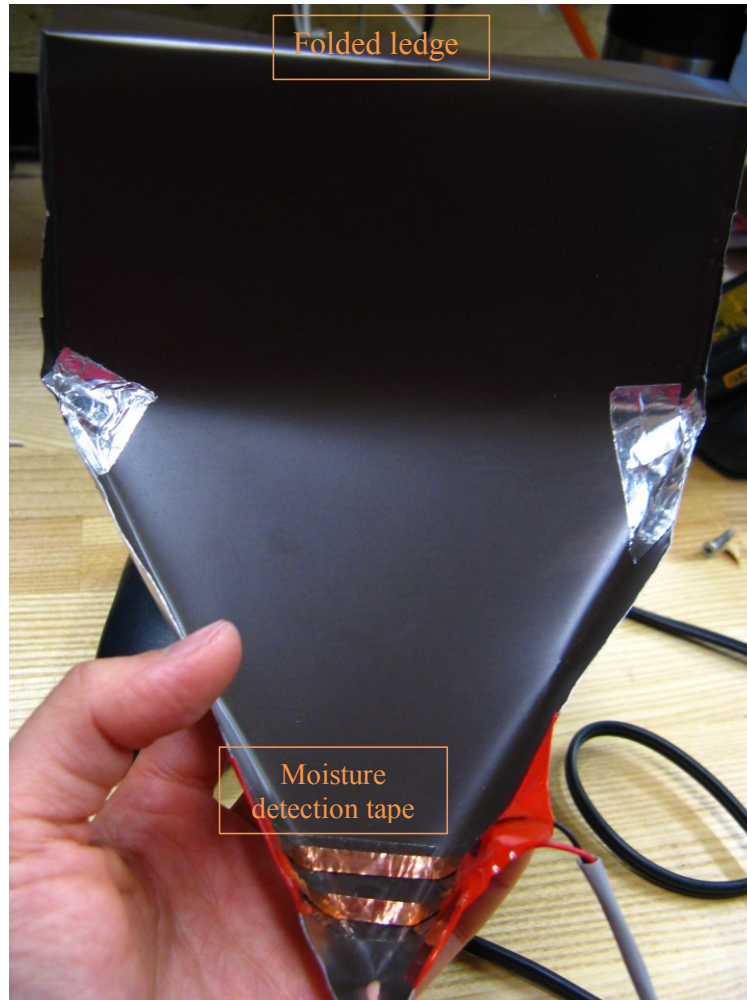
Figure 17. A typical triangular aluminum trough with a moisture detection tape labelled as W1GtMdR, W2GtMdC, W6GtMdR, and W6GtMdC for the water collection troughs at W1, W2, W6 sill corner and W6 middle locations respectively.

The collection area and the triangular trough are offset such that the sill corner lines up to approximately the middle of the triangular trough. Therefore, at a sill corner collection area such as at W1, the horizontal flat area of the aluminum trough is partially cut and then folded up behind the depth of the jamb J-trim of that corner – as shown in Figure 18 by the dotted lines. The ends of the folded ledge are taped to the vinyl J-trim using an aluminum tape at vinyl siding walls, while at stucco wall W6, the ends of the folded ledge is held down with the moldable thermoplastics.

Figure 18. Sill corner collection area details for the aluminum triangular trough at W1.

An additional flashing piece is installed over the open aluminum trough at the sill corner area – as shown in Figure 19– so that the water that runs behind the wall vinyl siding and the jamb J-trim is not directed into the leakage gauge. A short piece of moisture detection tape is then attached near the bottom tip of the aluminum trough as a control monitoring sensor to confirm whether or not water passes through the aluminum trough during a leakage event. The moisture detection tape is further discussed in section 6 of this chapter.

Figure 19. Additional flashing piece over the open aluminum trough at the sill corner area.

4.5   LONG-TERM IN-CAVITY MONITORING SENSORS

Wall panels W3, W4, W5, W7 and W8 are the long-term performance walls. The wall cavities of these long-term performance walls were instrumented with moisture pins, thermocouples, and the RHT sensors. As shown in Figure 20, the sets of moisture pins and thermocouples are installed on the plywood sheathing board, the underside of the window sill, the studs, and the plates. Thermocouples are installed to provide temperature references for the moisture pins, but also on the exterior surface of the stucco and vinyl sidings and on the interior surface of the gypsum board. In total, each long-term performance walls have 15 thermocouples and 15 moisture pins installed. Except for the tip and the pin heads, the moisture pins were insulated. After the installation, the pins heads and the wood/pin interfaces were sealed with epoxy.

Figure 20. Typical overview of moisture pins, thermocouples, and RHT sensor installation in a wall cavity under the window sill.

One RHT sensor is installed in one wall cavity at each long-term performance walls. The RHT sensor is held suspended in the middle of cavity using a string as shown in Figure 21. Also, each pair of moisture pins are approximately 1 inch from each other and from its reference thermocouple. The sensor wires are held in place permanently by the expanding foam sealant where they pass through any studs in order to isolate each wall cavities. The isolation of each wall cavities reduces moisture migration from one cavity to the next by air leakage through the wiring holes. The fiberglass batt insulation helps support the wires in the middle of the cavity depth.
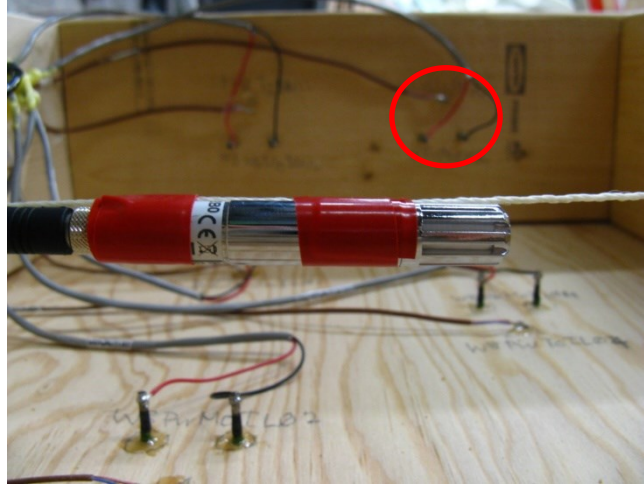
Figure 21. Close up view of RHT sensor installed and suspended mid-depth of the wall cavity. Note the typical configuration of each set of the moisture pins and a thermocouple – as circled in the background.

Labelling of Sensors

Prior to introducing the long term performance sensors, this section explains the logic of the sensor naming. For this project, a total of 75 thermocouples, 75 moisture pins, 5 RHT sensors, and 48 moisture detection tapes are used. The labelling of the sensors follow the general format of **W#AaBb*LOC***, where:

- **W#** refers to the wall number, e.g. W3 for Wall 3.

- **Aa** refers to the material or wood framing component on or within the wall assembly that the sensor is attached to or placed in, as following:

    Bp for bottom plate, **Cd** for cladding, **Gs** for gypsum board, **Gt** for leakage gauge's trough, **La** for stucco metal lath, **Pw** for plywood, **Sm** for sheathing membrane, **Tr** for trimmer wood, and **Ws** for window sill.

- **Bb** refers to the sensor type: **Tc** for thermocouple, **Mo** for moisture pin, **Md** for moisture detection tape, **Rh** for RHT sensors, and **Rg** for tipping bucket rain gauge used in the 4 leakage gauges.

- **LOC** refers to the approximate location of the sensor within the wall or on the wood framing component. The **LOC** code range from 1 to 4 characters, and consist of alphabet and /or digits. Generally, it includes vertical code (**U** –Upper, **M**-middle, **L**-lower, **T**-Top, and **B**-Bottom), depth code (**O**-Outside, and **I**-Inside), and horizontal code (**L**-Left, **C**-Centre, and **R**-Right). The labels for thermocouples, moisture pins, and moisture detection tapes also include a unique number.

Among the five long-term performance monitoring walls, most sensors are replicated at similar locations on the respective walls. To simplify the discussion of the long term monitoring sensors, the **LOC** code is used as a reference.

Figure 22 is a schematic drawing showing the typical labeling and locations of the moisture pins, thermocouples, and RHT sensors.
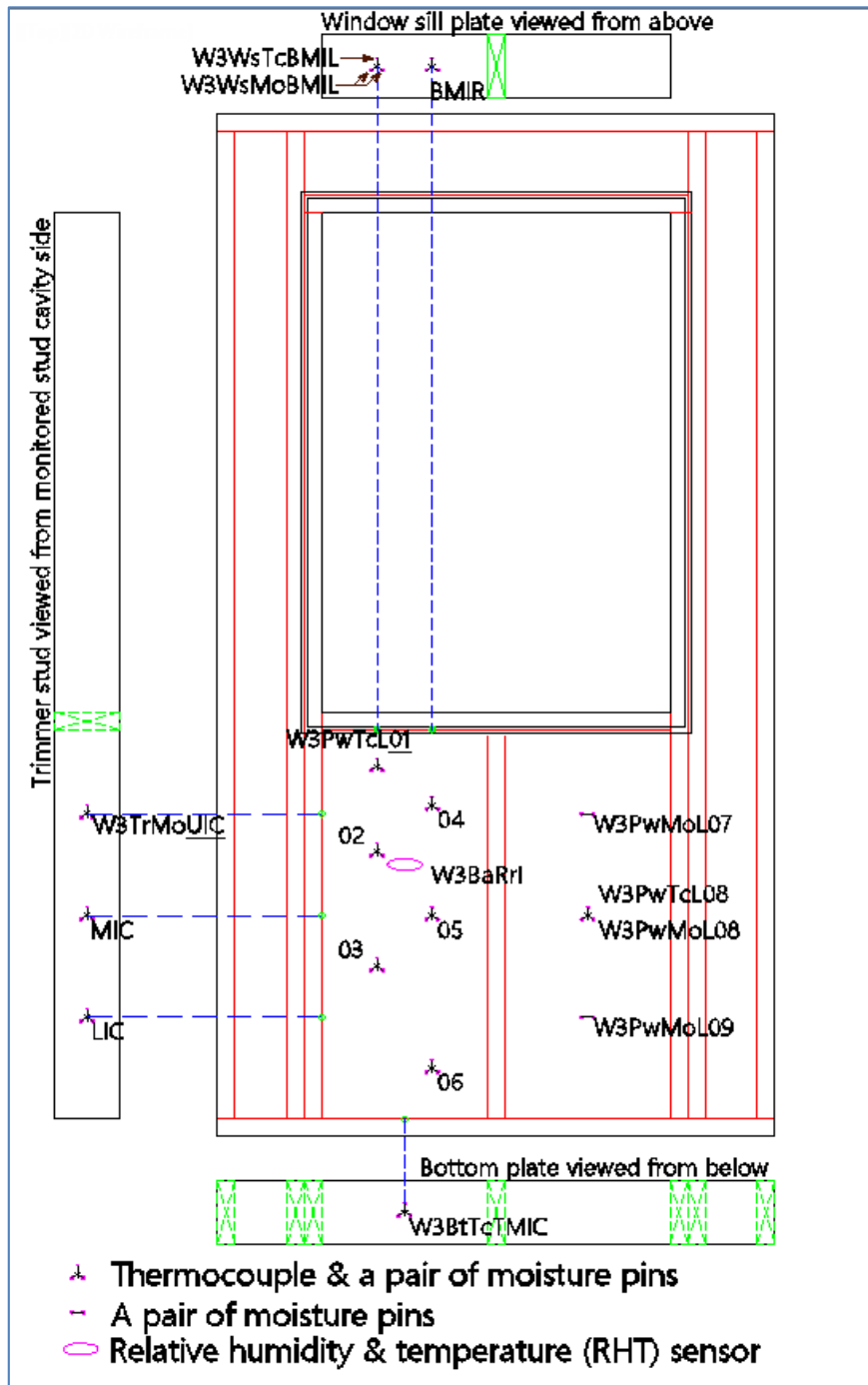
Figure 22. Locations and labelling of typical interior sensors in the wall cavity of long-term performance walls, with W3 as an example.

4.6   MOISTURE DETECTION TAPES

Moisture detection tape (MDT) consists of 2 strips of metal conductors that adhere to a plastic tape. It detects presence of water that flows over and connects the two conductor strips. The tapes are used on the long-term performance walls to trace the path of water draining behind the cladding on the building paper as WRB. Figure 23 shows the typical layout of MDT for vinyl siding long term performance walls. The multiple moisture detection tapes were arranged to capture the presence of water draining on the building paper and their wiring is arranged to minimize the obstruction of the water path to the lower tapes.
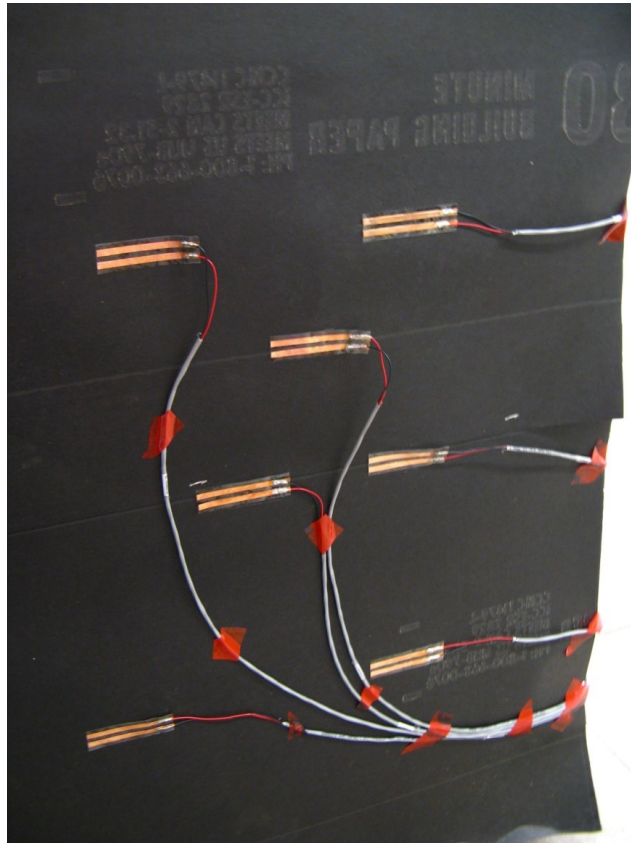
Figure 23. Typical layout of strips of moisture detection tapes (MDT) on the outside of building paper.

A schematic drawing showing the labelling and the locations of the moisture detection tapes on the long-term performance monitoring walls is presented in Figure 24.

Figure 24. Locations and labelling of moisture detection tapes (MDT) viewed from the exterior on the sheathing membrane of long-term performance walls, with reference locations of interior sensors on sheathing board. W3 is used as an example.

The locations of the moisture detection tapes on the stucco clad long-term performance monitoring walls are shown in Figure 25 for wall W7. While the seven MDT locations 10-16 are similar at all

long-term monitoring walls, location Ref was added only to W7 to compare between the side with sealant defect and the side with no sealant defect.

Corner
Missing
Sealant
Defect

W7LaMdOL10

11

Ref

12

14   13

16   15

Bottom Trough
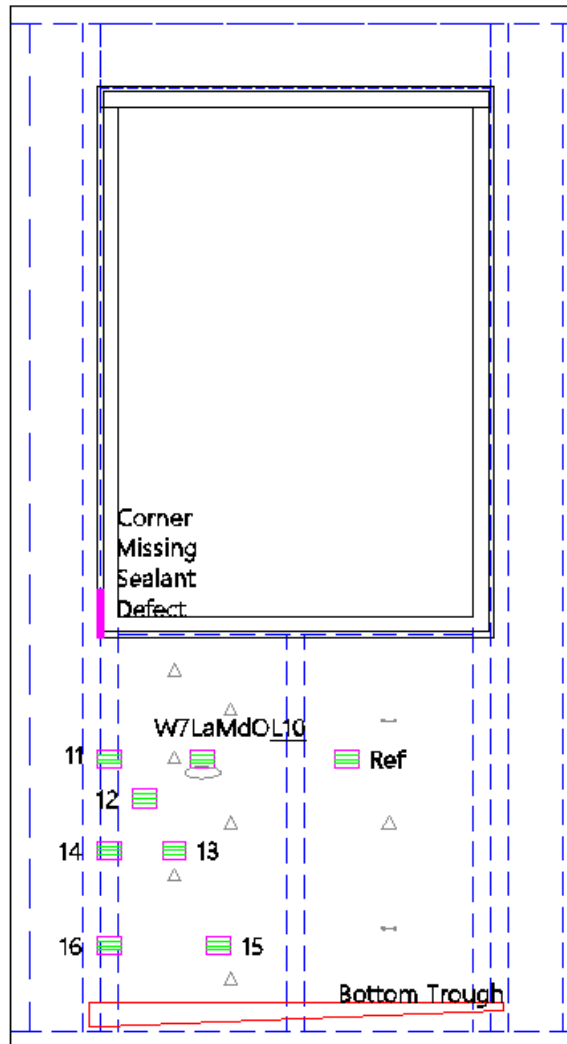
SENSORS ON EXTERIOR OF SHEATHING MEMBRANE:
▤ Moisture detection tape (MDT)

SENSORS ON THE INTERIOR SIDE OF SHEATHING BOARD:
△ Thermocouple & a pair of moisture pins
⊷ A pair of moisture pins

Figure 25. Locations of moisture detection tapes on wall W7 viewed from the exterior on the sheathing membrane of long-term performance walls, with reference locations of interior sensors on sheathing board.

A piece of polyethylene was added over all of the MDTs on the stucco walls W7 and W8 to prevent the conductor strips from touching stucco cladding as shown in Figure 26.

Figure 26. A small piece of a polyethylene sheet installed over the MDT for stucco.

The moisture detection tapes are also used on the water collection walls for control purposes, e.g. to see if potential leakage water was missed from being directed by the troughs onto the leakage gauges as shown in Figure 27.

Figure 27. A long piece of moisture detection tape under the triangular trough collection area viewed on W2.

A schematic drawing showing the locations of these control MDTs is presented in Figure 28.

Figure 28. Locations and labelling of moisture detection tapes (MDT) viewed from the exterior on the sheathing membrane of water collecting walls, with reference locations of interior sensors on sheathing board. W1 is used as an example.

The locations of control MDTs in the above figure are similar for W2. However, wall W6 has one extra MDT as there are two water collecting locations as shown in Figure 29.

Figure 29. Locations and labelling of moisture detection tapes (MDT) at W6 as viewed from the exterior on the sheathing membrane of water collecting walls, with locations of interior sensors on sheathing board shown as a reference.

4.7 BOTTOM-OF-WALL TROUGH AND WATER COLLECTION BOTTLE

At the bottom of the long term performance walls W3, W4, W5,W7 and W8, the amount of rain that was retained by stucco cladding, and/or was drained on the WRB behind vinyl siding or stucco cladding, was captured by a trough along the bottom of the wall claddings. The water in this trough was then directed via plastic tubes into bottles that are housed in boxes made out of extruded polystyrene insulation (XPS) as shown in Figure 30. The XPS boxes were made to minimize evaporation of the collected water from the bottles. The water collected in these bottles were periodically measured manually using 50 mL capacity graduated cylinder and 5 mL capacity graduated syringe – the type that is sold as an oral medicine dropper. Efforts were made so that the measurements of the collected water are done within 3 hours after the end of rain events during daytime, or in the early morning if the rain events ended at night. This was also to reduce the loss of collected water due to evaporation. Occasionally, intermediate measurements were also taken several times during a long period of rain, as the bottle waters were limited in sizes. At stucco walls W7 and W8, 1 L jar and bottle were used, while at vinyl siding walls, 500 mL bottles were used.

Figure 30. XPS housing for the bottles collecting drainage water from W3 and W5 vinyl siding walls.

The building paper is lapped over the back leg of the aluminum trough, as shown in Figure 31. For the vinyl siding walls, the bottom-of-wall aluminum trough at a vinyl siding wall is also hidden behind the bottom-most vinyl siding panel, to prevent the trough from collecting rainwater run-off on the outer surface of the vinyl siding panels.
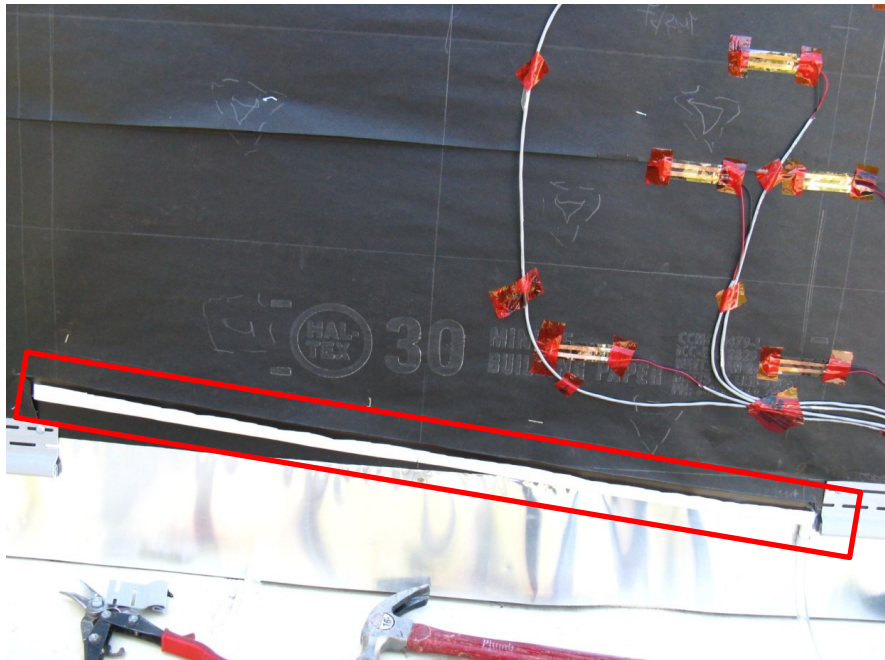
Figure 31. Bottom-of-wall aluminum trough at a typical vinyl siding long term performance walls.

On the other hand, for the stucco walls, the bottom-of-wall troughs are installed below the stucco stop/ casing beads of the stucco claddings, while still maintaining the overlap of the building paper onto the back leg of the aluminum trough, as shown in Figure 32.
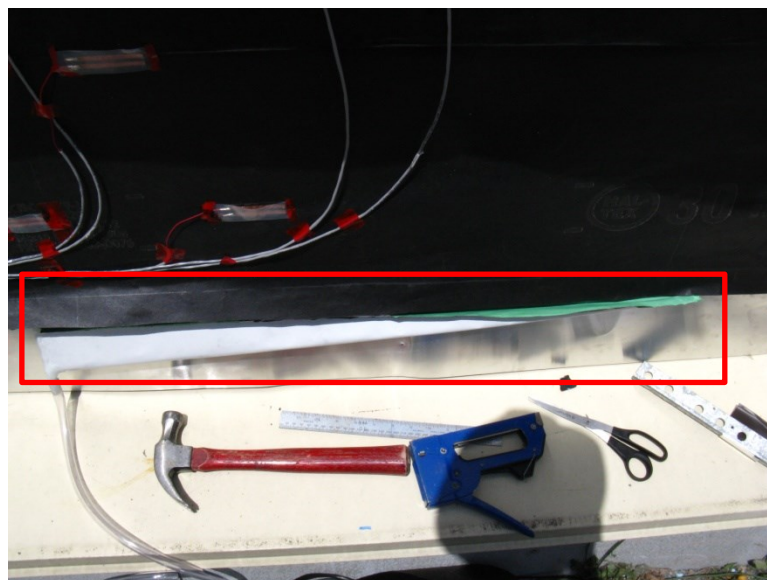
Figure 32. Bottom-of-wall aluminum trough at a typical stucco clad long term performance walls.

CHAPTER 5: RESULTS AND ANALYSIS

The data from November 1, 2013 to June 19, 2014 are presented in this section, starting from the weather conditions, i.e. rain intensities, wind speed and direction; the leakage data from W1 and W6 corner defect; as well as the data on the drainage water from behind the cladding that were collected by the troughs at the bottom of the five long-term performance walls. Finally, the hygrothermal data from the long-term performance walls are presented.

5.1   WEATHER CONDITIONS

5.1.1   Rain Intensities

The rain loads that the test facility were exposed to in November 1, 2013 to June 19, 2014 are presented in Figure 33 as hourly horizontal rain intensities, measured by the horizontal rain gauge on the weather station. The majority of the hourly rain intensities is less than 5 mm/hr. Rain intensities between 5 – 10 mm/hr are observed in 7 cases.
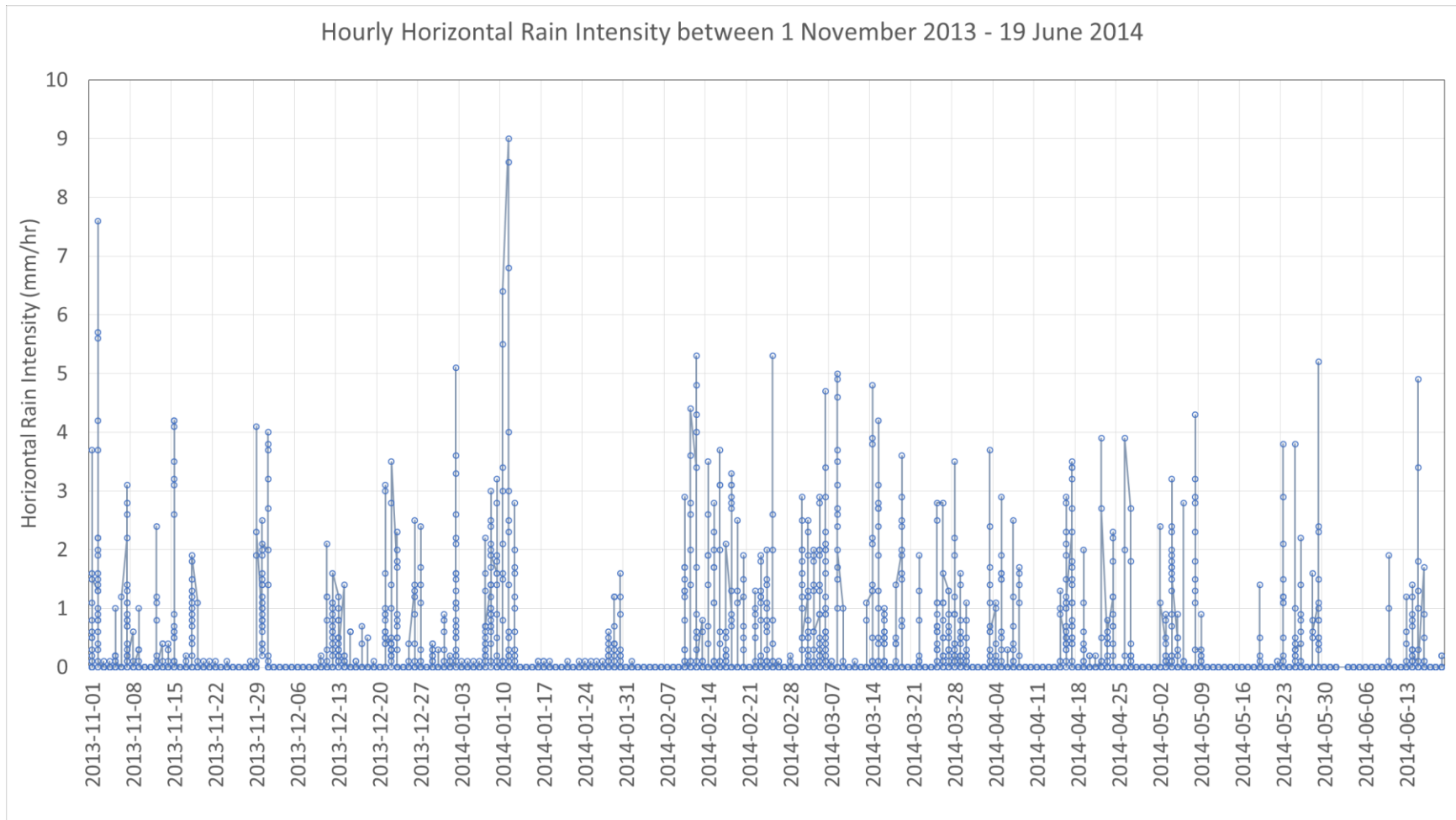
Figure 33. Horizontal rain intensity during the period of 1 November 2013 – 19 June 2014.

Monthly total horizontal rain during this monitored period of time is presented in Figure 34. Overall, 1179.6 mm of horizontal rain was recorded during November 1, 2013 to June 19, 2014.
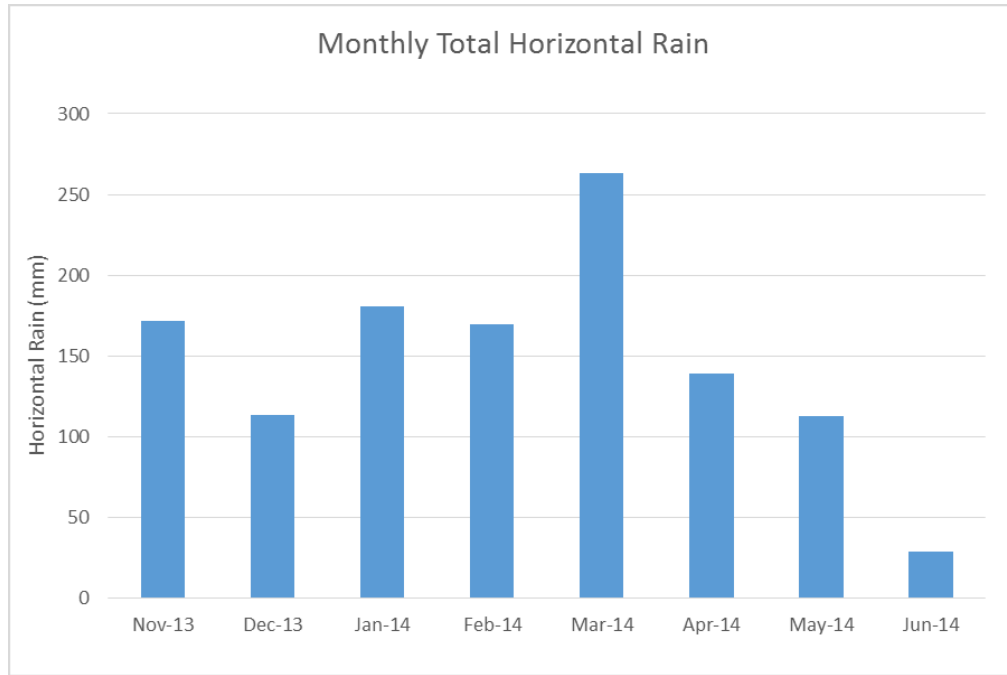
Figure 34. Horizontal rain summarized by the months.

Based on the horizontal rain intensities and the recorded wind speed, the free-field wind driven rain (WDR) intensities were calculated following the Straube and Burnett's method. Figure 35 compares the monthly total of these free-field WDR to the monthly total of maximum WDR measured by the wall rain gauges. To calculate the monthly total of maximum WDR, the maximum WDR intensities were determined among the multiple rain gauges on South East façade every hour and then summed for the monthly totals. As expected, the measured WDR totals are less than the free-field WDR. Although horizontal rain is the highest in March 2014, WDR is the highest in February 2014, followed closely by March 2014.
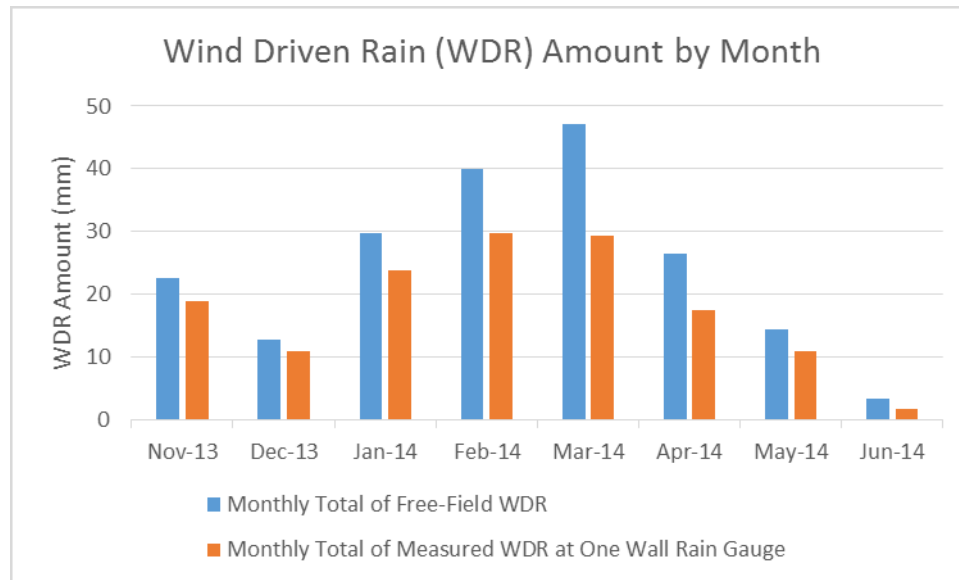
Figure 35. Monthly total of measured wind driven rain (WDR) by a wall rain gauge and free field WDR calculated following Straube and Burnett's method.

Several wall rain gauges were found to record excessive amount of WDR as they were affected by leaking eavestrough on South East façade and were therefore excluded from analysis; these were the three wall gauges on the left brick wall cladding and the middle wall rain gauge on the right brick wall cladding. The rest of the eleven wall rain gauges were used in the calculation for the bar chart in Figure 35. Wall rain gauges XG1, XG4, XG3, and XG6 (see Figure 13) were analyzed in more details as these were analyzed for the leakage gauges analysis in Section 3 of this chapter.

The measured wind driven rain amount at XG1 and XG4 is presented in Figure 36. Each points in this graph represent the hourly wind driven rain amount. There were missing WDR data from around 6 pm to 1 pm on June 1, 2014 to around 1 pm on June 11, 2014, due to power issues with the wall rain gauges data acquisition equipment. Overall, higher amount of WDR is measured by the top wall gauge XG1 than the middle wall gauge XG4. The maximum hourly WDR amount measured by XG1 is 1.6 mm, while the maximum measured at XG4 is approximately 0.7 mm.
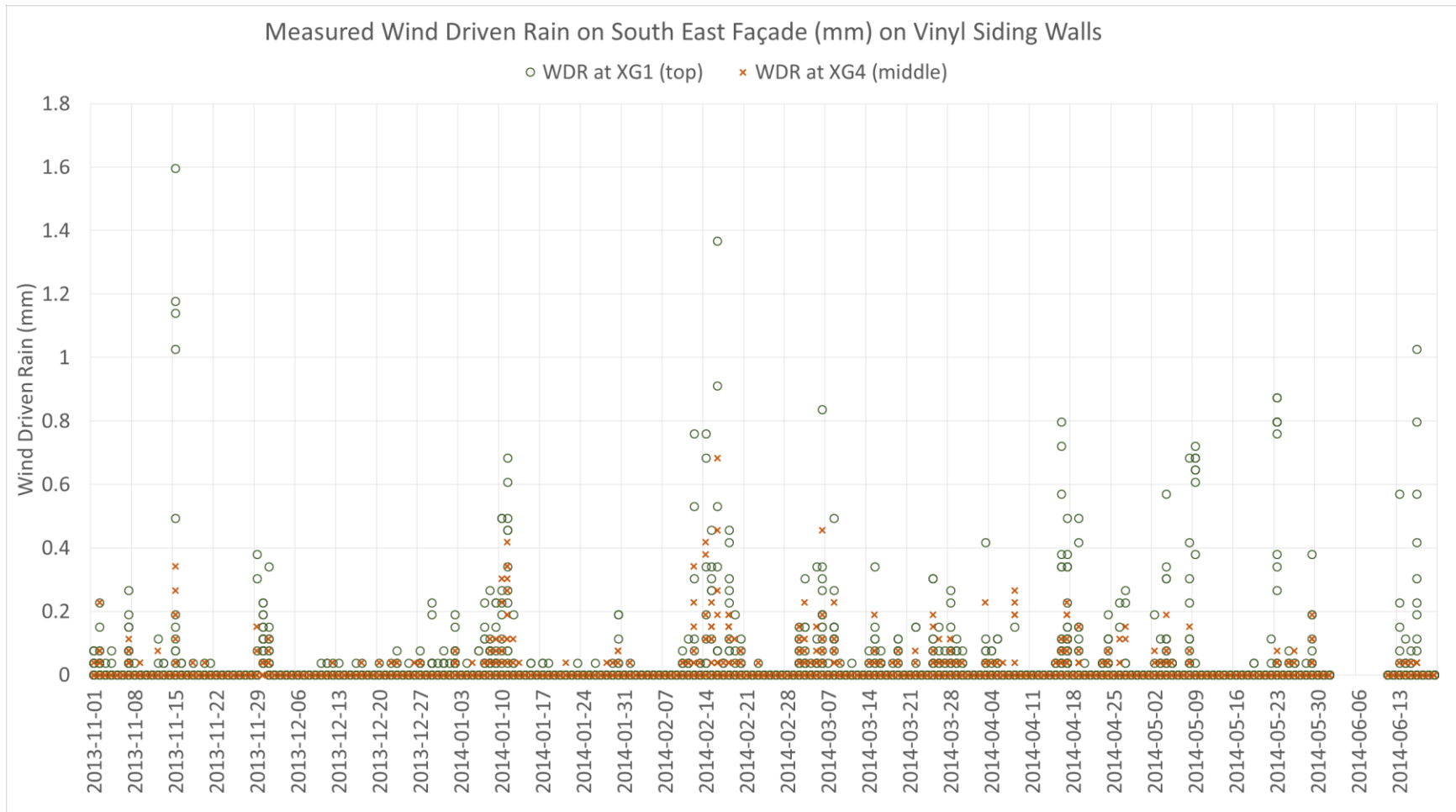
Figure 36. Measured wind driven rain amount by wall rain gauges XG1 and XG4 near vinyl siding walls during November 1, 2013 to June 19, 2014.

Figure 37 presents the hourly measured wind driven rain at XG3 and XG6. There were missing WDR data for XG3 wall gauge from around 6 pm on June 1, 2014 to around 1 pm on June 11, 2014, due to power issues. Similar to the observation in Figure 36 for vinyl siding walls, higher amount of WDR is also measured by the top wall gauge XG3 than the middle wall gauge XG6. The maximum hourly WDR amount measured by XG3 is 1 mm, while the maximum measured at XG6 is approximately 0.75 mm.
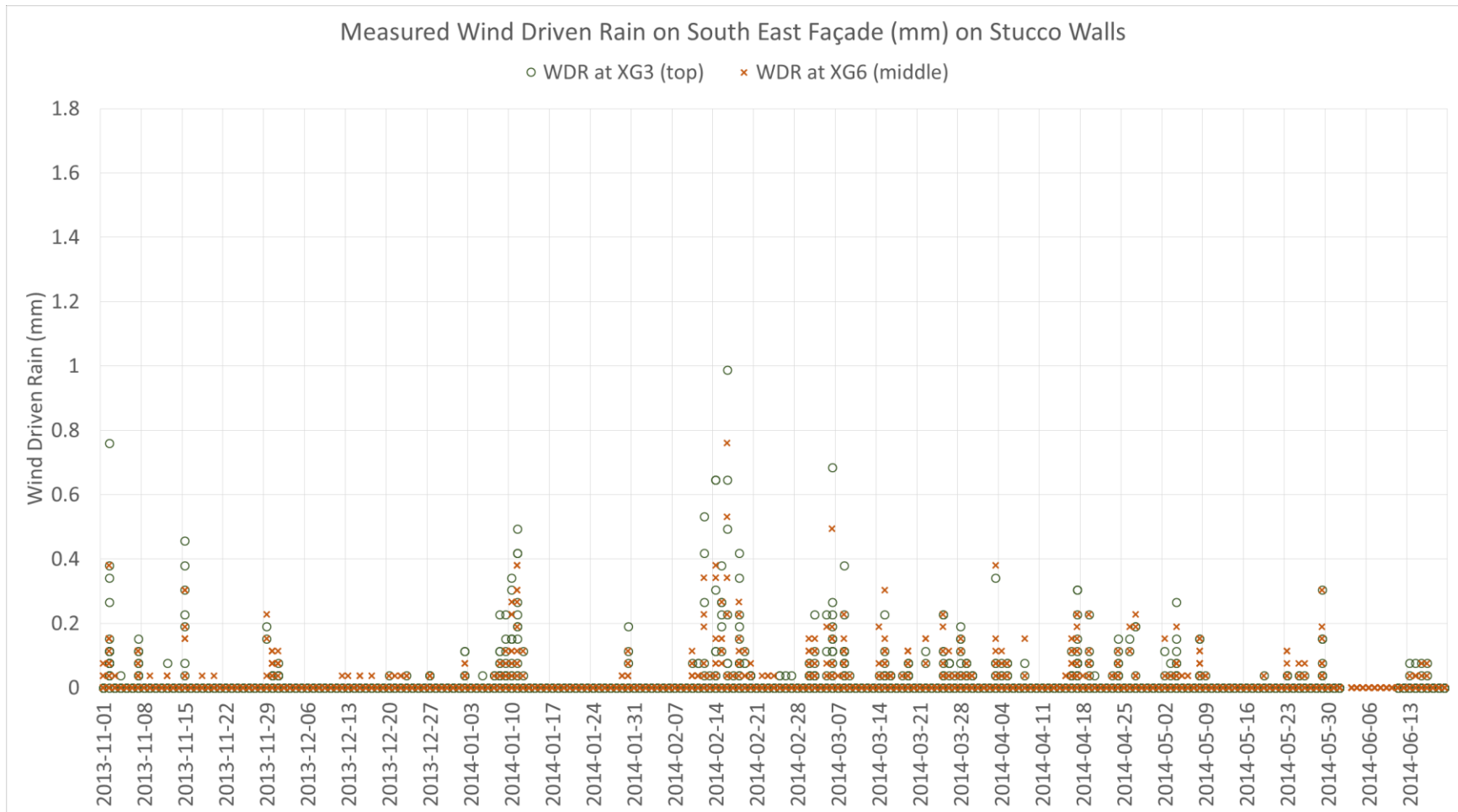
Figure 37. Measured wind driven rain amount by wall rain gauges XG3 and XG6 near stucco walls during November 1, 2013 to June 19, 2014.

The free-field WDR was calculated using the measured hourly horizontal rain and the measured hourly wind-speed normal to the South East (SE) façade applying Equation 4 without the RAF or Rain Admittance Factor. Figure 38 shows the plot of the hourly measured wind driven rain at XG1 and XG4 near W1 against hourly free-field wind driven rain. Essentially, the slopes of this plot account for the geometry of the building at the SE facade and for the location of the gauges on the wall, which is represented in Straube and Burnett's method as an RAF.
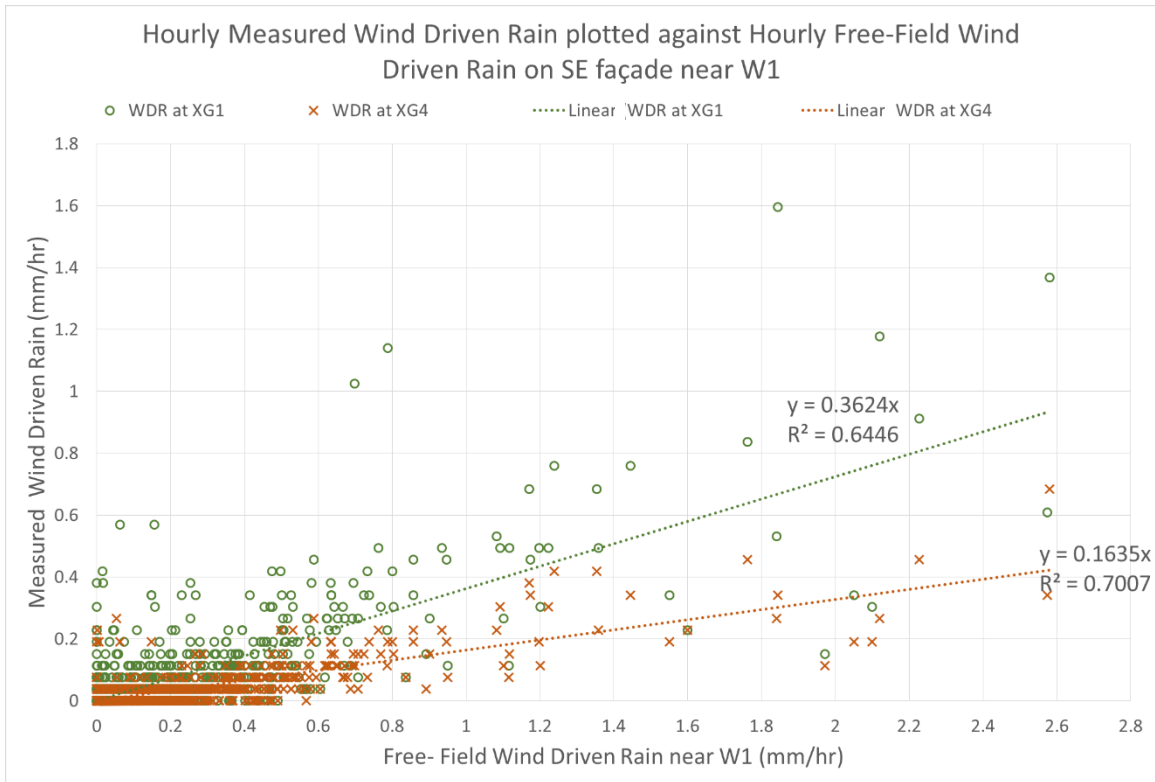
Figure 38. Hourly measured wind driven rain plotted against the free-field wind driven rain near W1. The slope of the regression lines reflects the Rain Admittance Factors (RAF).

As a comparison to the WDR gauge near W1 vinyl siding wall, Figure 39 shows the plot of the hourly measured wind driven rain at XG3 and XG6 near W6 against hourly free-field wind driven rain. Compared to XG1 and XG4, the hourly measured wind driven rain amounts at XG3 and XG6 are less. The R-squared values at all four slopes are similar, ranging from 0.64-0.72, indicating that there were no unusual errors among these four WDR gauges.
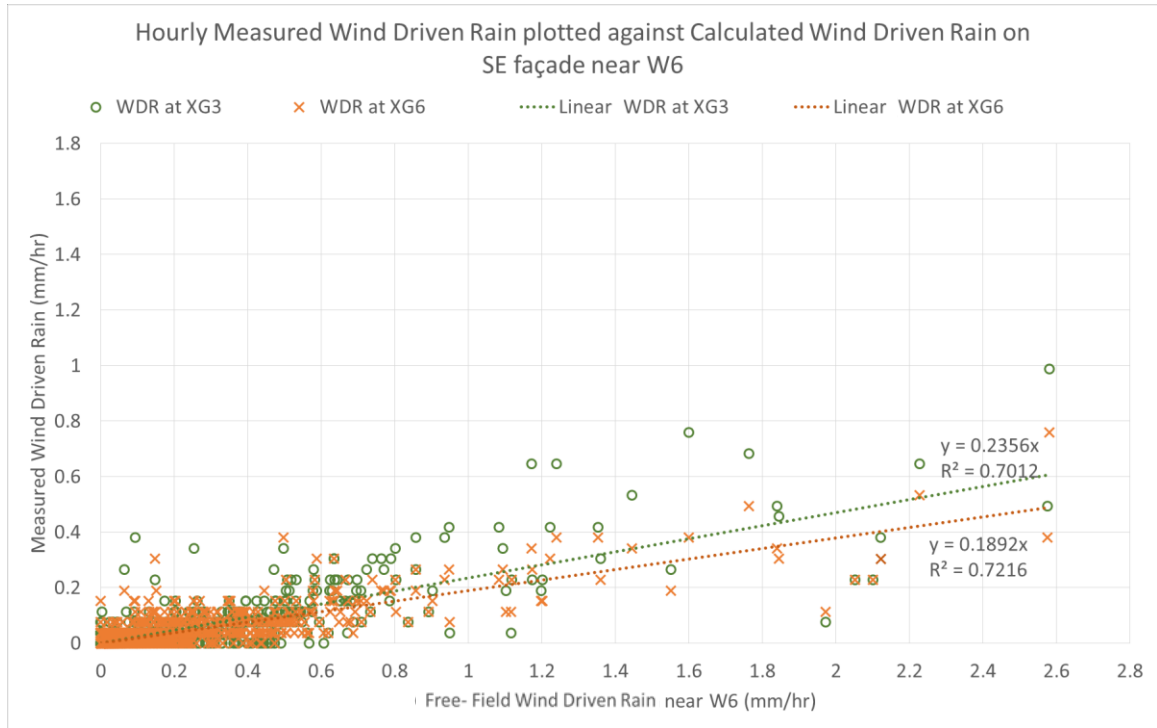
Figure 39. Hourly measured wind driven rain plotted against the free-field wind driven rain near W6. The slope of the regression lines reflects the Rain Admittance Factors (RAF).

The plots in Figure 38 and Figure 39 were repeated for the rest of the functioning wall gauges and the slopes of the regression lines from these plots are shown in Figure 40 as the RAF values at the respective wall gauges. The RAF at the upper row of the rain gauges ranges from 0.21 to 0.36, while the RAF at the middle and lower rain gauges ranges from 0.10 to 0.49. As mentioned above, rain gauges on the left brick cladding data were not analyzed due to the leaky gutter. In addition, the middle rain gauge on the right brick cladding recorded unusually higher amount of WDR compared to the free-field measurements due to the backsplash of rain dripping from the top wall gauge's tubing onto the middle wall gauge's box. Therefore, the middle wall gauge was also excluded from the analysis.

Figure 40. Rain Admittance Factors (numbers in yellow) calculated based on the measured WDR at the respective wall rain gauges and the free-field WDR as calculated following the Straube and Burnett's method.

As the aspect ratio of the BETF building is approximately 0.4, the RAF values were expected to match the range of RAF values, or wall factors, W, in Figure 7 for the two storey building with flat roof, i.e. RAF of 0.2 to 0.5. The RAF values found for the upper row of rain gauges are much lower than the expected range of RAF of 0.5. It is possible that the eavestrough along the top edge of the SE façade may have a role in these results – the lower-than-expected RAF values.

The two RAF values at the bottom WDR gauges near the vinyl sidings walls, 0.32 and 0.49 are higher than those near the bottom of stucco walls, which are at 0.10 and 0.15. A possible cause for this is that the two XPS housings for the bottom trough water collecting bottles in front of the vinyl sidings walls distorted the wind flow as obstacles and therefore may have increased the wind driven rain captured by these two WDR gauges.

5.1.2   Wind Speed and Direction (Wind Characteristics)

Hourly averages from minute records of wind speed and direction data in November 1, 2013 to June 19, 2014 were used to generate the wind rose charts in Figure 41 (a) and (b). The two wind roses show that wind blew most frequently from between South East and East directions, both during all weather conditions (top rose) and during rain periods only (bottom rose). Wind of less than 1 m/s occurred most frequently during all weather conditions. Wind speed of less than 1 m/s and wind speed between 1 to 2 m/s were most frequent during rain periods.

Frequency Distribution of Wind Speed and Direction At Any Weather Conditions - Nov 2013 - June 2014
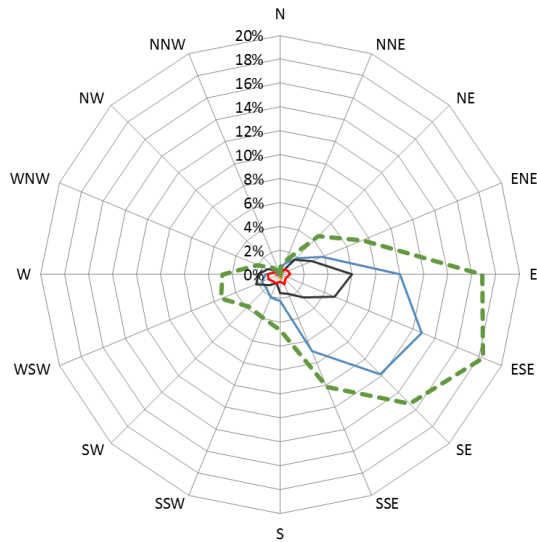
Frequency Distribution of Wind Speed and Direction During Rain - Nov 2013 - June 2014
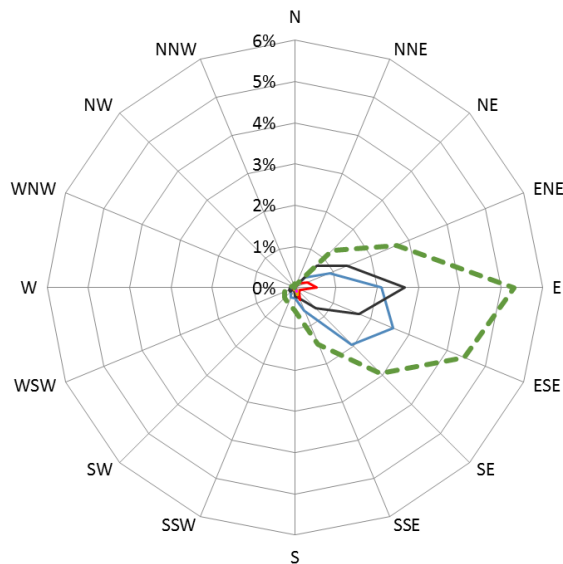
Figure 41. Frequency distribution for hourly averages of minute records of wind speed and direction in November 1, 2013 to June 19, 2014 period at: (a) any weather condition, i.e. rain or dry conditions (top rose), and (b) during rain periods only (bottom rose).

Figure 42 compares the hourly average wind speeds between wind occurring only during rain and wind occurring any time from November 1, 2013 – June 19, 2014 at each compass direction for the test facility. Figure 42 shows the maximum wind speeds from the hourly averages for each wind directions.

Average and Maximum Wind Speed from 16 Compass Directions in Nov 2013 - June 2014
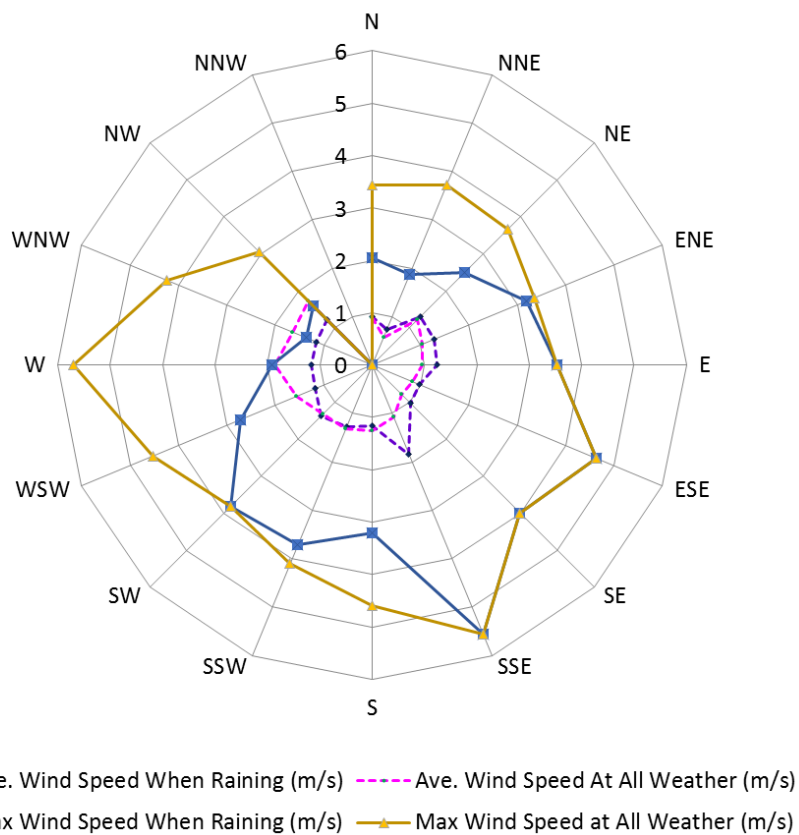
Figure 42. Hourly averages and maximums of minute records of wind speed at each wind directions during rain and at all weather conditions for BCIT Burnaby in November 2013 – June 2014.

The three wind roses above confirm that SE façade was the windward-facing wall and that the mean of wind speed during rain was greater than that at any time.

5.2 MOISTURE LOAD CONTRIBUTING TO LEAKAGE AMOUNT AT W1 AND W6 CORNER DEFECT

To analyze the moisture load contributing to leakage amount at the locations of leakage water collections, first, the measured WDR that most likely had contributed to the collected leakage amount was identified. This approach was based on the premise that the contributing WDR occurred during the rain event that started for a period of time before the first detection of a leakage by the leakage gauge.

Defining the start and end of the relevant rain event was a challenge. For example, are two periods of back-to-back rain separated by a 1 hour of dry period considered as 1 rain event or two separate rain events? Often low intensity rain may give rain gauge readings of only 0.1 mm or 1 tip in 1 hour. Determining which rain events contributed to a leakage event was further complicated by the delay of leakage detection by the leakage gauges as certain amount of time was required for the tipping bucket to fill up and tip to be counted. This delay became a part of the error in the analysis of the leakage. The sources of error in the analysis were further discussed at the end of this section, following the discussion of the results and leakage model analysis.

In this rain leakage analysis, only rain events where WDR was detected were considered. The start of each relevant rain event was defined as the first horizontal rain gauge reading prior to a WDR wall gauge reading, where no rain was detected 1 hour before. The readings were further filtered out to focus on the events that contributed to leakages. One leakage event started after at least 1 WDR gauge detection, but could last after WDR had stopped. This was observed in several events, which reflected the delay in leakage gauge detection compared to the WDR gauge readings.

Table 4 summarizes the total number of rain events that results in a leakage; it gives the highest amount of leakage in any one rain event, and the total leakage amount measured at each of the four leakage gauges during the study period of November 1, 2013 to June 19, 2014. As no leakage was detected at W6 middle leakage gauge and only one event led to leakage detection at W2, the analysis on the leakages was focused more on W1 and W6 corner locations.

Table 4. Overall comparison between W1, W2, W6 corner and W6 middle.

Leakage Gauge Location	W1	W2	W6 corner	W6 middle
Number of rain events resulting in leakage	39	1	40	0
Highest amount of leakage in a rain event	146.7 mL	1.3 mL	151.6 mL	0
Total leakage amount measured for the period of November 1, 2013 to June 19, 2014.	856.6 mL	1.3 mL	985.5 mL	0

Figure 43 shows the measured WDR at XG1 and XG4 near W1 together with the leakage gauge measurements at W1 corner collector. In general, when most of the higher wind driven rain was recorded, leakage at W1 occurred, indicating that most rain events with WDR on this façade provided enough moisture load for a sill corner leakage at typical vinyl siding wall.
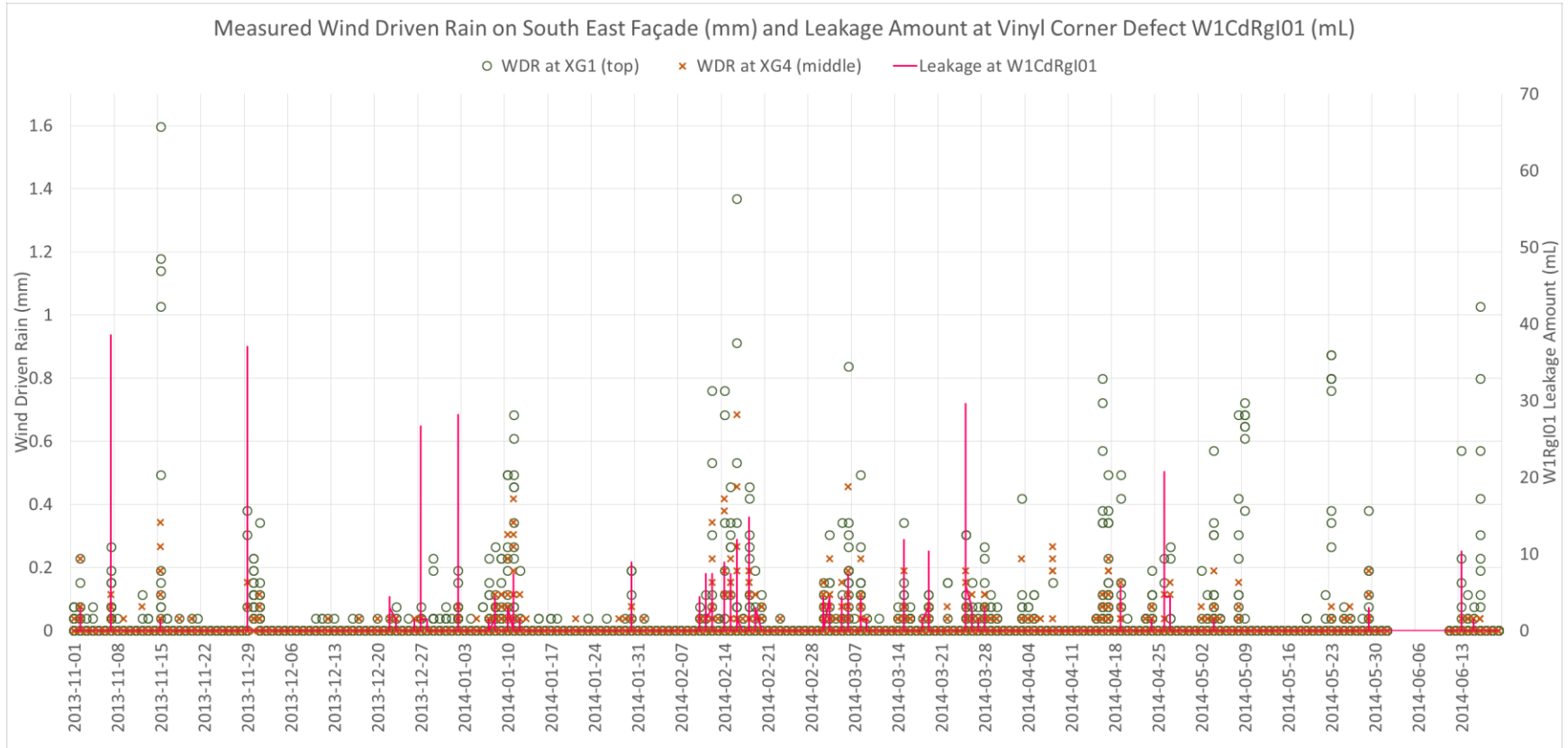
Figure 43. Measured hourly wind driven rain intensity on South East Façade in November 1, 2013 – June 19, 2014, overlapped with the leakage amount at W1 (window sill corner collection of the vinyl siding wall).

Similarly, measured WDR at XG3 and XG6 near W6 have been plotted together with the leakage gauge measurements at W6 corner collector in Figure 43. Most rain events with higher WDR on this façade also provided enough moisture loads for a potential sill corner leakage at typical stucco walls.
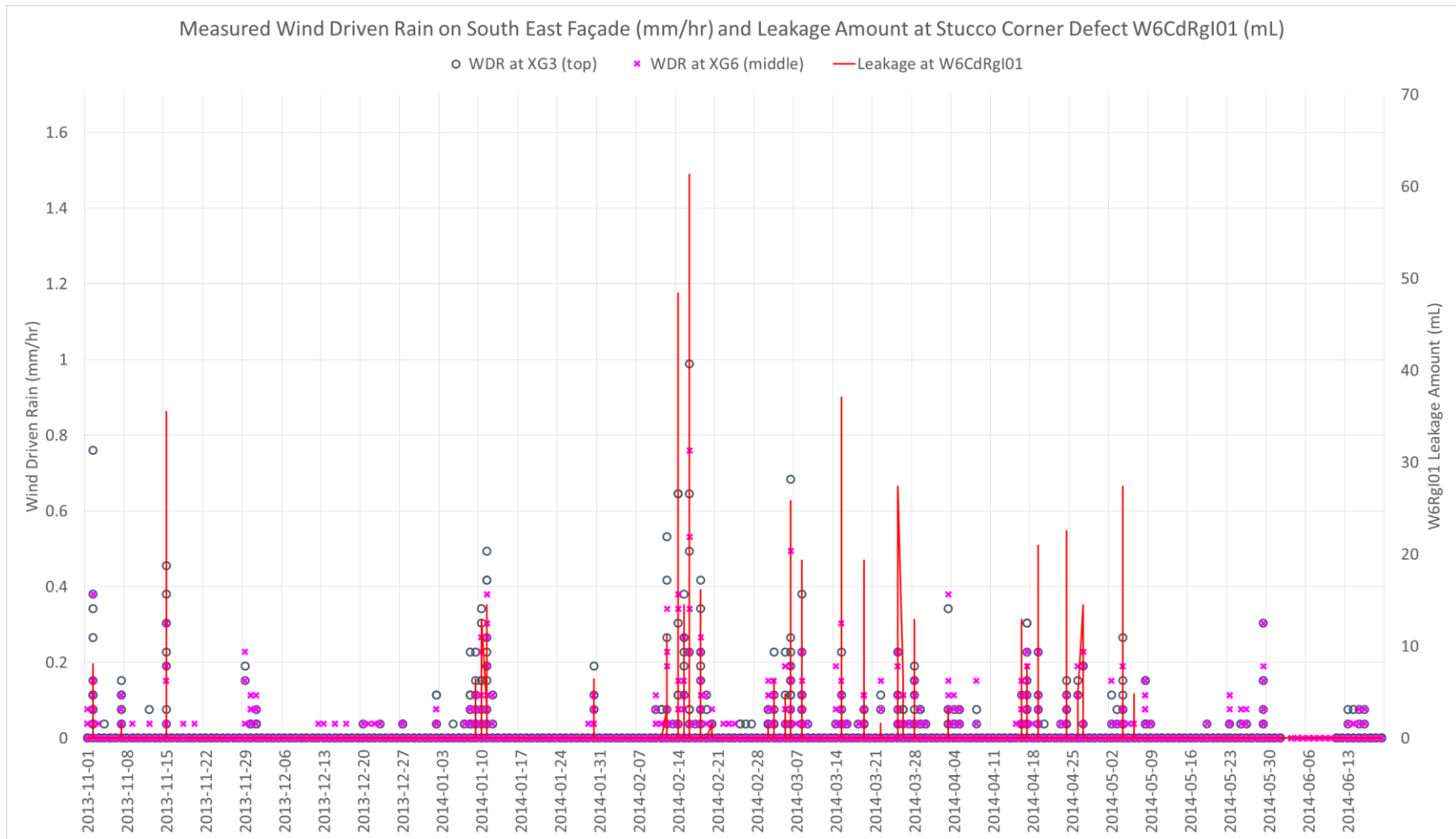
Figure 44. Measured hourly wind driven rain intensity on South East Façade in November 1, 2013 – June 19, 2014, overlapped with the leakage amount at W6 (window sill corner defect at the stucco wall).

As a control measure, the short strips of moisture detection tapes (MDT) were installed near the tip of the leakage trough above the leakage gauges at W1, W2, and W6 in order to detect the passing of water leakage prior to the water being measured by the gauges. However, Figure 45 shows that this method was not always successful. Despite the multiple leakage events recorded at the W1 corner defect, only a few significant voltage readings were detected. It appears that the leakage water bypassed the conductors of the MDT at W1.
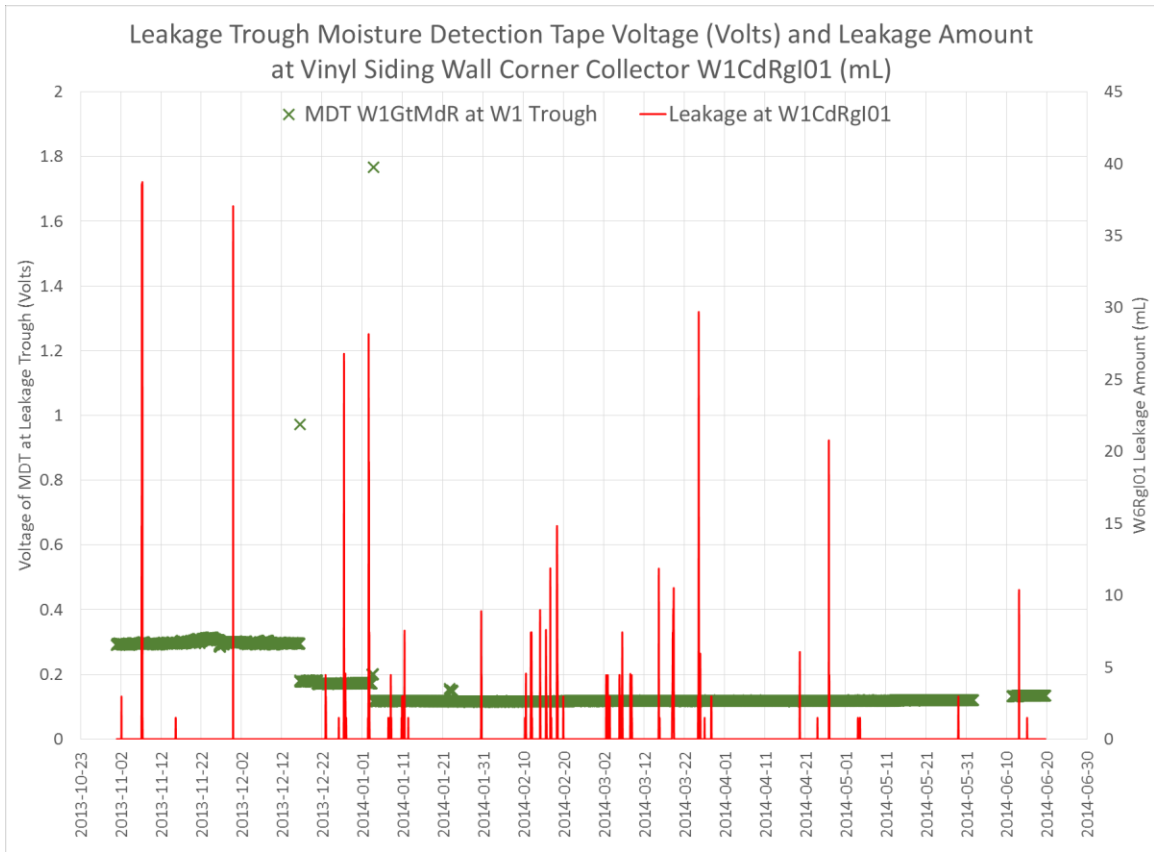
Figure 45. Leakage trough moisture detection tape voltage compared to the leakage amount at vinyl siding corner defect.

On the other hand, the MDT at the W2 middle leakage collector trough recorded significant voltage readings primarily around one leakage event. On February 17, 2014, multiple water leakage passes through the MDT as shown in Figure 46, followed immediately by the measurement of this leakage event by the leakage gauge. Two other significant voltage readings

were also observed prior to the leakage event on February 17, 2014. However, it appears that these amounts of leakages were insufficient to tip the bucket of the leakage gauge.
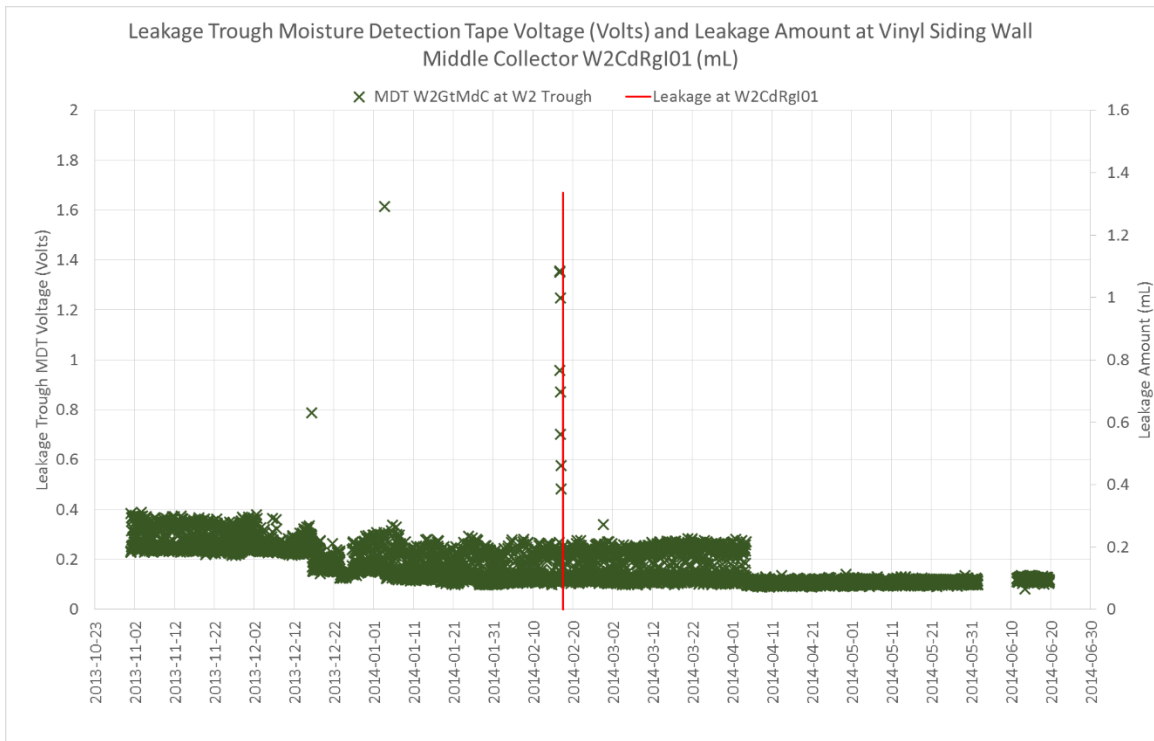
Figure 46. Leakage trough moisture detection tape voltage compared to the leakage amount at vinyl siding middle collection gauge.

Similarly, multiple flow of water though the MDTs were detected, followed by the measured leakages soon after, as shown in Figure 47. Several MDT readings in between the leakage events were also observed, indicating that some leakage amount collected was not enough to tip the leakage gauge's bucket.
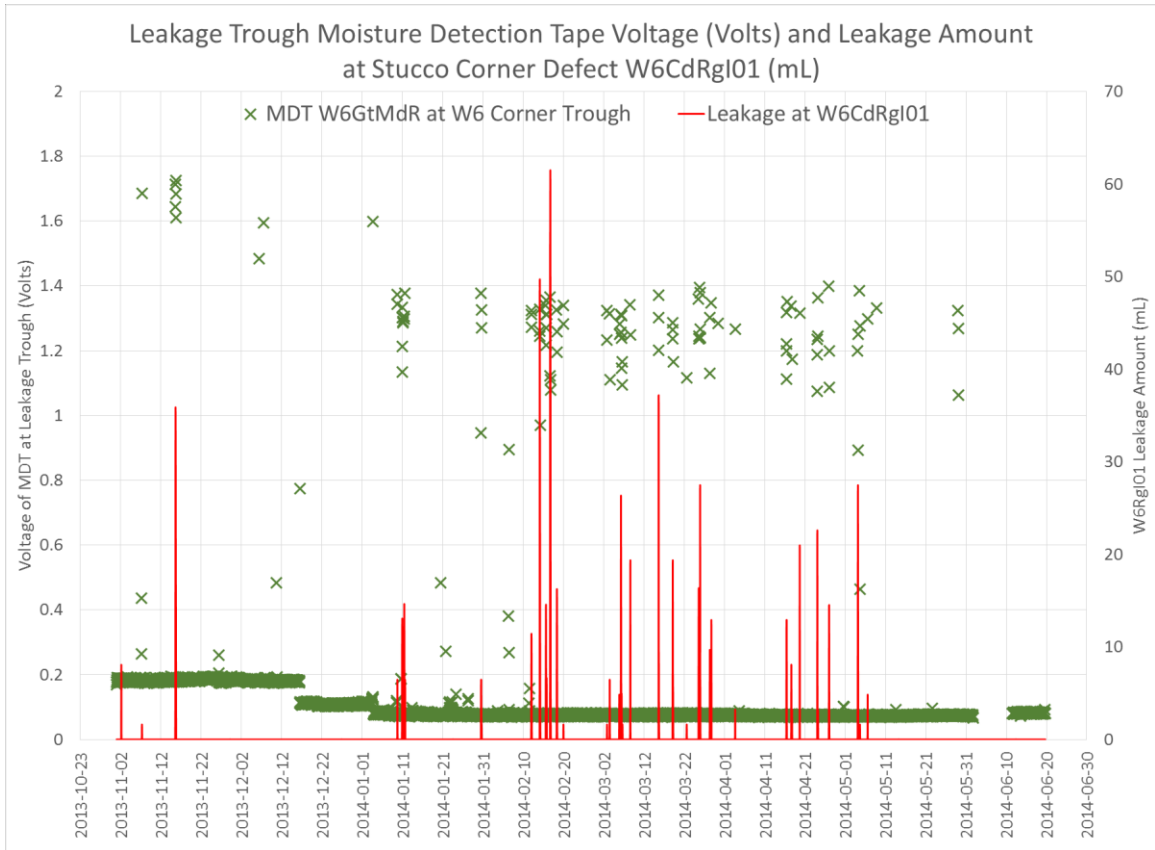
Figure 47. Leakage trough moisture detection tape voltage compared to the leakage amount at stucco wall W6 corner defect collection gauge.

Only three single flows of leakage water were detected at W6 middle water collector as shown in Figure 48. The amount of leakages from these three flows was too low to tip the leakage gauge's bucket. No leakage amount was measured at this W6 middle water collector.
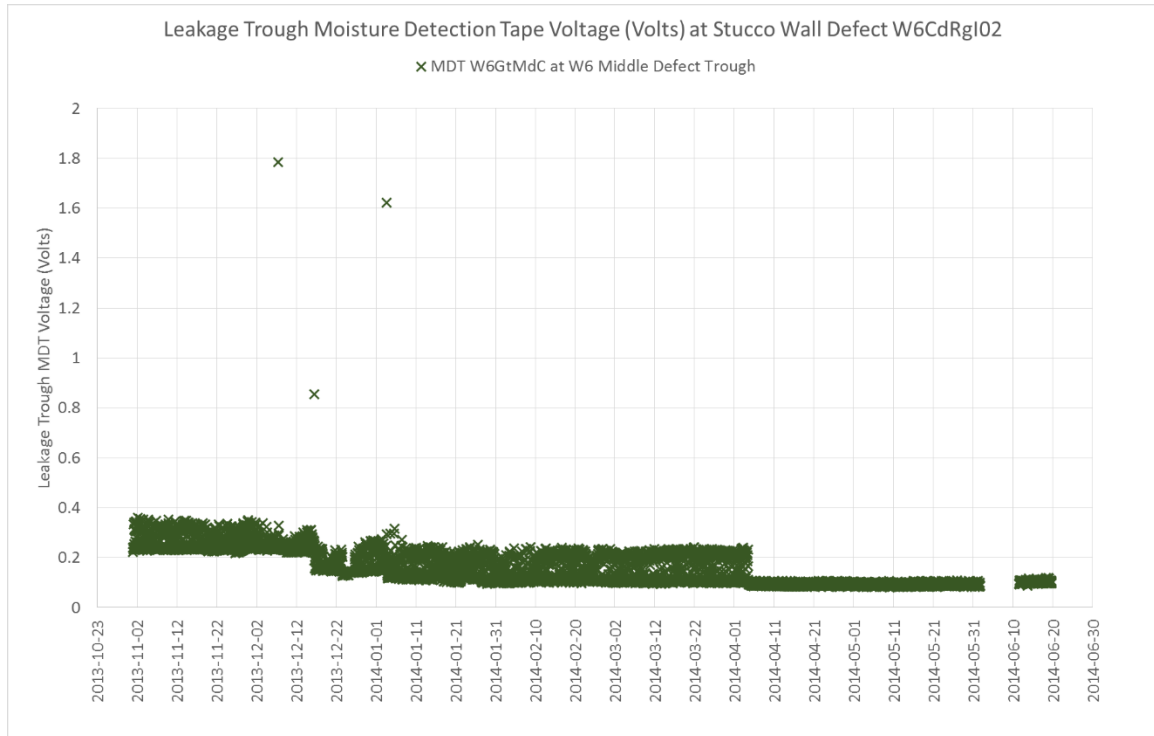
Figure 48. Leakage trough moisture detection tape voltage compared to the leakage amount at stucco wall W6 middle defect collection gauge.

5.3   RAIN LEAKAGE AT WALL / WINDOW INTERFACES – EVENT-BASED DATA ANALYSIS

Similar to the preliminary results analysis from Stucco Wall W6 (Ngudjiharto, et al., 2014), the initial assessment of W1 and W6 corner defect leakage data from November 1, 2013 to June 19, 2014 includes the simple plotting of the leakage amount at W1 and W6 defects against measured wind driven rain amount at the nearby top wall gauge.

Although run-off analysis is not in the scope of study for this thesis, part or all of the amount of WDR intensity captured by the upper wall rain gauges is expected to run down the wall cladding by gravity and contribute to the leakage, in addition to any direct WDR amount around the leakage location. Therefore, the WDR amounts on these uppermost gauges are expected to correlate better to the leakage amount. The uppermost wall rain gauges are thus chosen for the leakage amount analysis. It is also expected that the upper wall rain gauges experiences higher intensity WDR due

to the flow pattern of the wind as it approaches the building façade, as reflected by the Rain Admittance Factor (RAF) values, shown in Figure 40.

For W1, as the closest wall gauges on the left brick cladding were affected by the leaky eaves-trough, wall rain gauge XG1 is used in this analysis instead. Figure 49 shows the simple plot of leakage amount at W1 to the measured WDR intensity on the wall rain gauge XG1. The WDR in eight leakage events, highlighted by the red rectangle, were suspected to be underestimated due to the use of XG1 instead of the closest top wall rain gauge on the left corner of the façade, which hypothetically should experience higher WDR intensities than XG1. These unusual leakage events had leakage amount above 30 mL, despite the low amount of wind driven rain of less than 2 L/m^2 measured at XG1. These 8 unusual leakage events are considered outliers and are excluded from the data analysis.
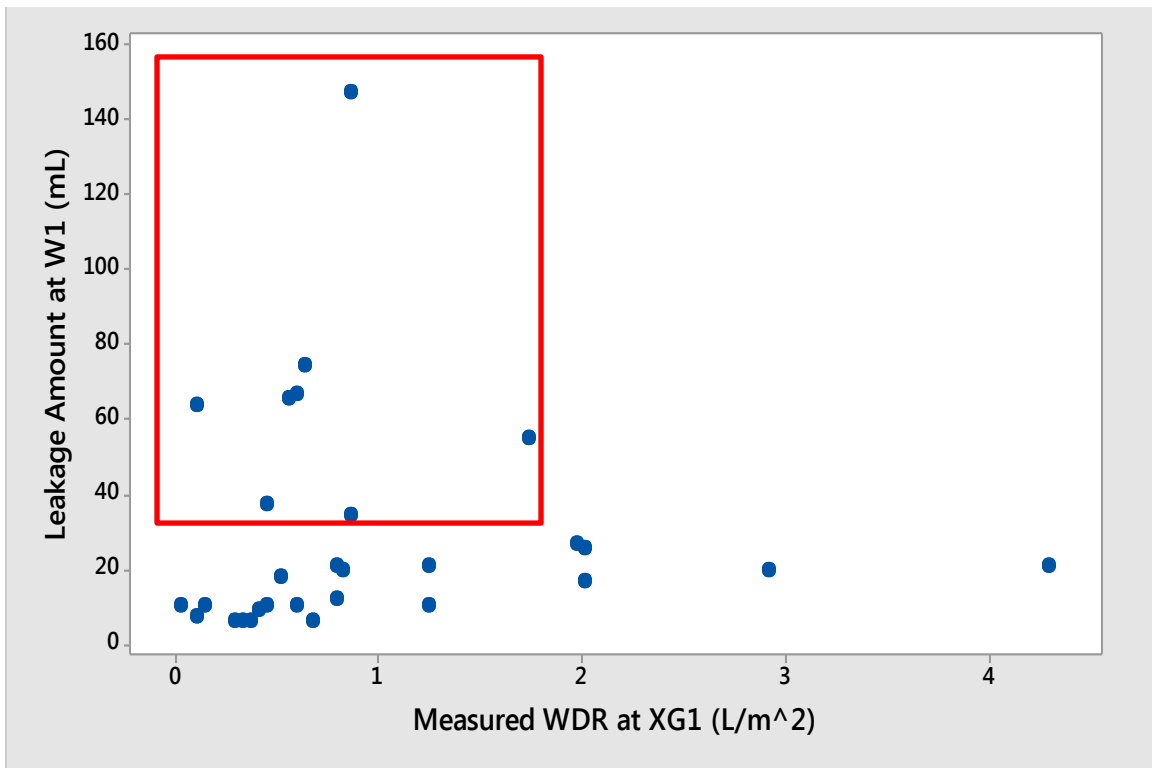
Figure 49. Plot of leakage amount at W1 leakage gauge collector to measured WDR amount at wall rain gauge XG1. A red box highlights unusual leakage events, where the leakage amount is more than 30 mL but the measured WDR is less than 2 L/m^2.

In addition, all leakage events of 2 tips or less, i.e. 2.96 mL or less are considered potential errors, as it was often observed that small leakage amount that is less than 1.48 mL remains on the leakage gauge tipping bucket after a rain event ends. Hence, for any leakage amount of 2 tips, there is a possibility that up to 50% of these recorded leakage amount is from the previous leakage event. Therefore, leakage events with 2 tips or less leakage amounts are also excluded from the data analysis. Figure 50 repeats the scatterplot of the leakage amount at W1 vinyl siding wall to wind driven rain amount at XG1 with exclusion of these two groups of leakage events. To conform to the proportion of leakage amount to WDR amount as suggested in ASHRAE Standard 160, a linear regression line analysis through the origin is fitted using the Minitab 17 software. For W1, however, two lines appeared to fit better across the data as shown in Figure 50. The red regression line across the two data points of Group 3 indicates that at higher WDR amount of around 2.5 mm or more, the leakage amount may no longer dependent on the WDR amount. More data points at higher WDR amount are needed to further study this observation. A linear regression line is fitted from the origin across the data points in the lower WDR amount range (Group 1) with an R-squared value of 82.8%. The equation of this Group 1 fitted regression line, as drawn in blue, is:

$$Leakage\ amount_{W1} = \ 13.38 \times R_{wdr-gauge}, when\ Rwdr - gauge < 2.5\ mm$$

Equation 7
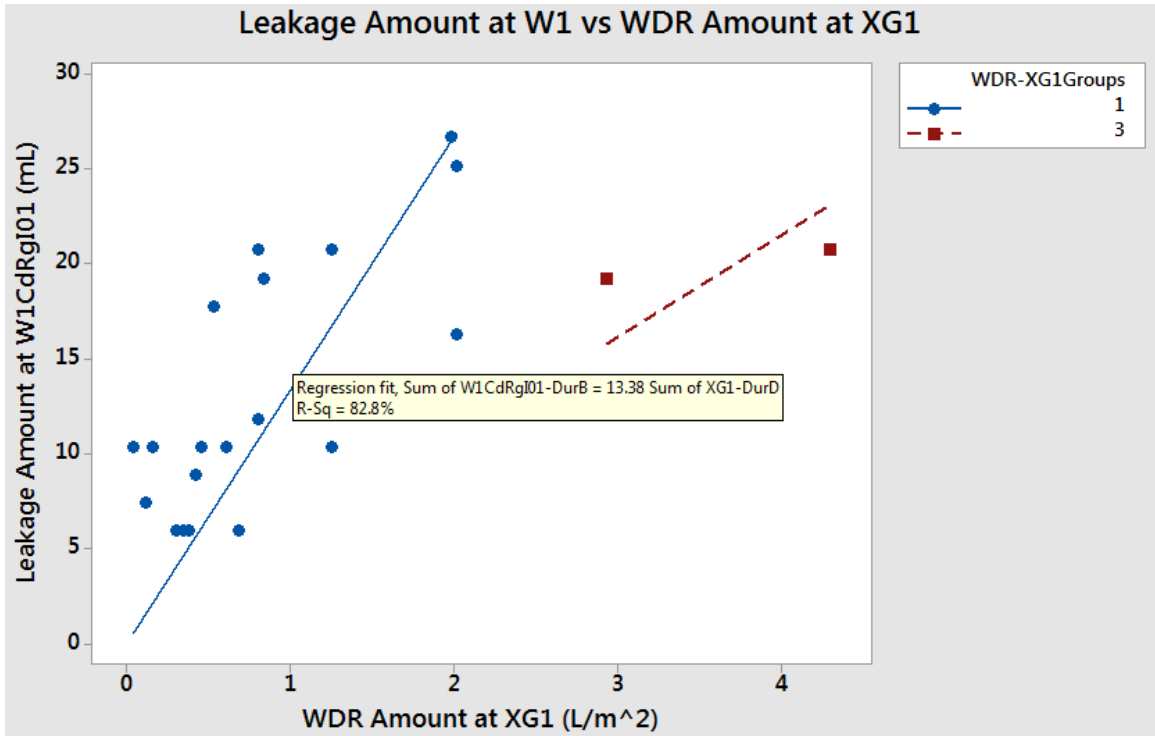
Figure 50. Scatterplot of leakage amount at W1 vinyl siding wall against wind driven rain amount at XG1, after the exclusion of unusually high leakage events as outliers and leakage events with 2 tips or less.

Assuming that the leakage events occur due to the WDR impinging on ½ area above the window and then run-off by gravity towards the window, i.e. approximately 2.42 m² area – see Figure 51, the percentage of the rain moisture load at the sill corner collection area that leaked into the leakage gauge at W1 is 0.55%. This percentage is calculated by dividing the slope by the approximated area and by the conversion factor of 1000 mL/L.
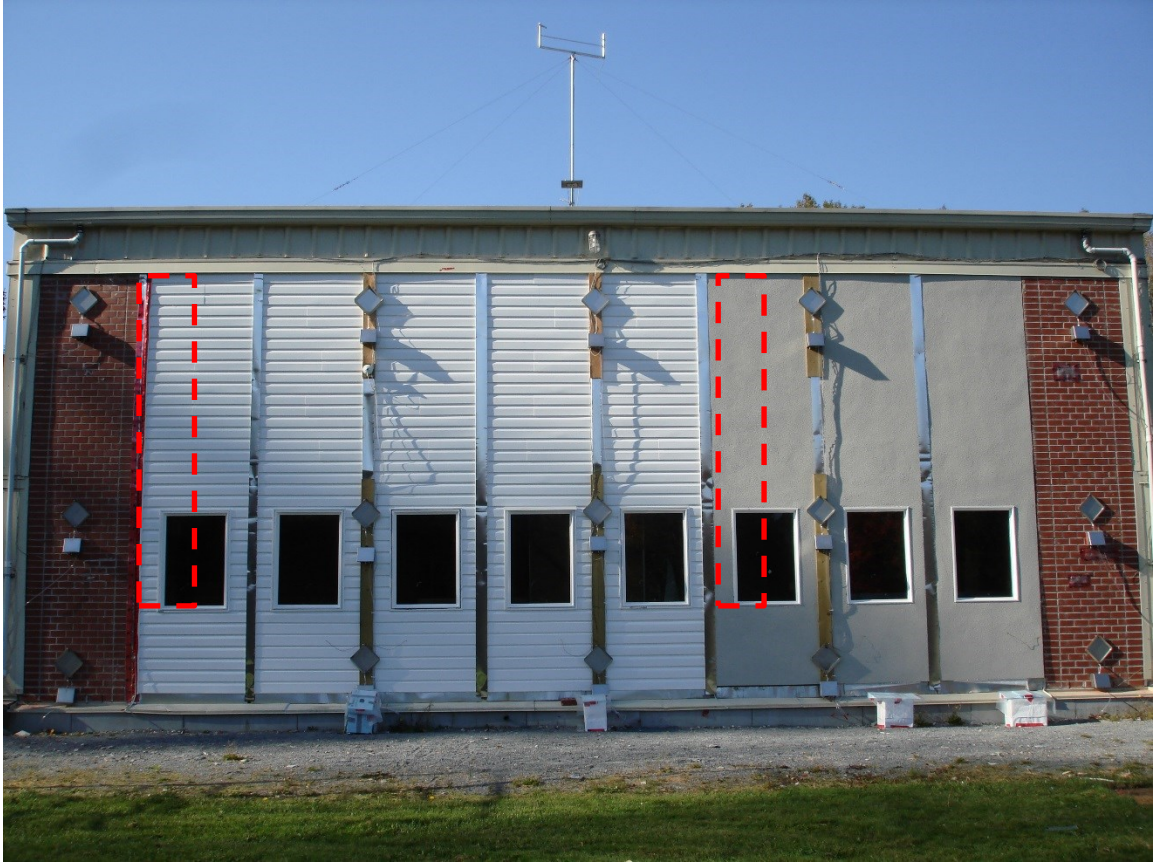
Figure 51. Areas of 2.42 m² each above the windows of W1 and W6, assumed to be catchment area of the WDR contributing to the leakage amount at the sill corners leakage collection points.

Similar scatterplot analysis was done for the leakage rain events at W6 stucco wall corner collector. Figure 52 shows the plot of leakage amount at W6 corner collector to the measured WDR intensity on the wall rain gauge XG3. Again, leakage events with 2 tips or less leakage amounts are excluded from the data analysis. The linear regression line fitted across the data has an R-squared value of 70.8%. The equation of the fitted regression line, as drawn in red, is:

$$Leakage\ amount_{W6corner} = 36.42 \times R_{wdr-gauge}$$

Equation 8
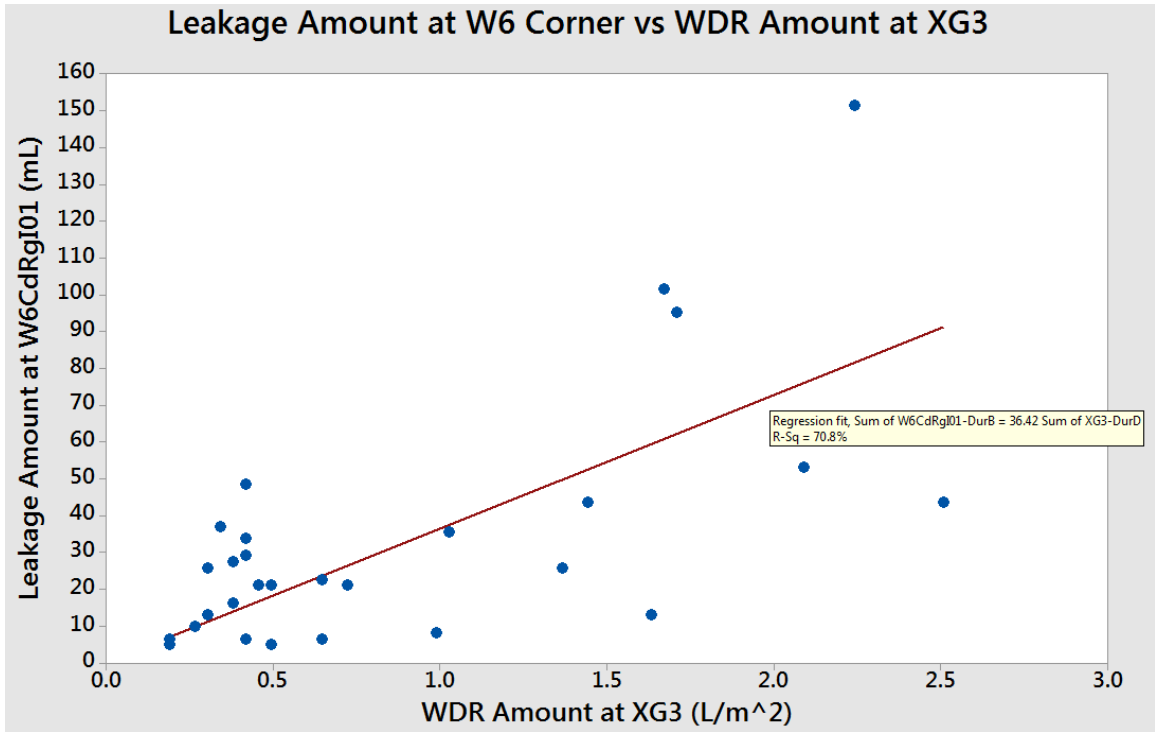
Figure 52. Plot of leakage amount at W6 corner leakage gauge collector to measured WDR amount at rain gauge XG3. Leakage events with 2 tips or less at the leakage gauge measurement are excluded.

Using the same assumption as at W1, that the rain load was collected over the 2.42 m² area which is the left half of area above the W6 window – see Figure 51, the percentage of the rain moisture load at the sill corner collection area that leaked into the leakage gauge at W6 corner is 1.5%. In comparison to W1, W6 corner leakage gauge collected approximately 3 times higher leakage amount, even though the upper WDR gauge showed that W1 experienced approximately 1.5 times more WDR load at the top of the wall than at the upper area of W6.

5.4   STATISTICAL MODEL

To determine the factors that may have contributed to the variations in the leakage amount at W1 and W6 corner, semi-empirical statistical models for the leakage amounts at W1 and W6 were generated using the multiple regression analysis in Minitab 17 Statistical Software. The Assistant

function in the software was used to generate a model from the leakage events input into the database.

In a multiple regression analysis, the relationship between the dependent values, Y, and all the predictors, or X variables is tested for statistical significance, i.e. $p<0.10$. Furthermore, the percentage of variation explained by the model, i.e. the R-squared value, must be closer to 1. The regression analysis run by the Assistant function includes the following selected options:

- Continuous predictor standardization by subtraction of the mean and then division by the standard deviation.

- Stepwise method selection of terms, with $\alpha=0.1$ to enter and to remove a term.

The output provided by the Assistant function is further evaluated by comparing R-squared, R-sq, and adjusted R-squared values, R-sq(adj), of the different models generated. In addition, the normal probability plots for each models are evaluated to ensure that the regression model gives unbiased coefficient estimates with the least variance. Regression models also assume that the residuals are normally distributed. In a normal probability plot of residuals, if the residual points generally lie in a straight line, this normality assumption can be deemed valid.

The hourly data from the three gauges, i.e. horizontal rain gauges, wall rain gauges, and leakage gauges, are processed on event basis, and are extracted according to the start and end of the rain events and/or leakage events. The raw data output from the data acquisition are arranged following the time stamp of the data acquisition system. Ranges of time stamps for each gauges are marked with the related leakage event identification number for the start and end of the related event duration. To prepare for the data extraction, several duration types are identified:

- Duration A is defined based on the horizontal rain event that contributes to a leakage event that occur after the start of this horizontal rain event. Duration A starts on the first tip of the horizontal rain gauge bucket until the last tip of leakage gauge, or until the last tip of the horizontal rain gauge if the leakage event continues on after the horizontal rain has stopped.

- Duration B is the leakage event duration which starts on the first tip of leakage gauge bucket to the last tip of leakage gauge and is typically included in Duration A.

- Duration D is similar to Duration A, except it is based on the wind-driven rain event of a particular wall rain gauge. Duration D starts on the first tip of the wall rain gauge bucket until the last tip of leakage gauge, or until the last tip of the last tip of the wall rain gauge bucket if the WDR on that wall gauge stops earlier than the end of leakage event.

As the main focus of this analysis is on what contributes to the leakage event, any horizontal rain and wind driven rain after the end of the leakage event are typically excluded. Although each duration type is defined based on the tipping of the related gauges, these duration types can be also applied to the data from the non-related gauges. For example, consider a hypothetical typical leakage event where the leakage event ends prior to the end of the horizontal and wind-driven rain events. Not all of the horizontal rain recorded within Duration A, R_{h-DurA}, contributes to the leakage event, as wind direction typically changes and may not always drive the wind driven rain towards the façade of interest; in which case, the sum of horizontal rain during Duration D, R_{h-DurD}, may be a better fit for the model. However, in the case where runoff from a roof with no overhang or eavestrough may be a factor, R_{h-DurA} may potentially be a better predictor for the model.

Several parameters that are considered as potential predictors to the model are listed as following:

- R_{h-DurA} is the sum of horizontal rain during horizontal rain event Duration A leading up to and during the leakage event [mm/m^2]. The sum of horizontal rain during Duration A is considered as a contributor to the leakage amount for the cases where rain run-off may play a larger role in the leakage, rather than the wind-driven rain.

- R_{h-DurD} is the sum of horizontal rain during wind driven rain event Duration D leading up to and during the leakage event [mm/m^2]. As discussed above, this parameter will narrow down the horizontal rain that occurs during the time that Wind Driven Rain is detected and

may be a predictor in the cases where both rain run-off and the wind-driven rain are important factors for the leakage.

- $R_{wdr-gauge}$ is the sum of measured amount of wind driven rain at the closest upper wall rain gauge, during wind driven rain event leading up to and during the leakage event [mm/m^2], i.e. during Duration D. This is the primary contributor to the leakage that is always considered in all initial model generation in the leakage analysis.

- t_{DurA} = length of time period starting from the start of horizontal rain measurement, leading up to and during the leakage event, i.e. Duration A [hr].

- t_{DurD} = length of time period starting from the start of wind-driven rain measurement, leading up to and during the leakage event, i.e. Duration D [hr].

- U_{Max} is the maximum of 5-min averages of wind speed normal to wall during each leakage events [m/s]. The wind speed, $U_{Max-5min}$ was determined by first calculating 5-minute averages of the wind speeds normal to the wall, and then selecting the maximum among the average values for each leakage event to capture the gust wind speeds assumed to have contributed to the leakage.

- The Prior Rain Index, PRI_{48}, accounts for how recent the last WDR intensity was detected by the wall rain gauges, if that last WDR occurred within 48 hours. This parameter is typically for absorptive cladding types such as stucco, a parameter that attempts to account for the effect of the retained moisture in the cladding has on the leakage amount. Therefore, it is included in the model generation for stucco wall, but not for vinyl siding wall.

To calculate PRI_{48}, first, the number of hours between the time stamp of the first WDR detection of the leakage event and the last time stamp of the previous WDR detection by the wall rain gauges was calculated as t_{prev}. If t_{prev} is less than 48 hours, then PRI_{48}= 48 − t_{prev}. Otherwise, PRI_{48}=0.

Leakage events with prior WDR at less than 48 hours are given scores in PRI$_{48}$ as the prior WDR is assumed to contribute to the current leakage event. The more recent the prior WDR event, the higher the PRI$_{48}$ scores. The 48-hour threshold was initially arbitrarily determined. To test the relevance of this 48-hour threshold, the model building for stucco wall W6 corner collector was also repeated for 12-hour, 24-hour, and 36-hour thresholds; however, at these three thresholds, the PRI was not found to be significant.

The process of statistical-based leakage models generation at W1 and W6 corner collector is presented next.

5.4.1 Statistical Leakage Model for W1

Using the same sample set of 21 data points used to generate the scatterplot in Figure 50, the seven parameters discussed above were used in an iterative approach of generating a regression models. The simplest model generated by the Assistant function of the Minitab 17 with the highest R-squared value of 80.76% for W1 leakage amount is as following:

$$L_{W1-stats} = 3.46 + 8.14 \times R_{wdr-gauge} + 1.12 \times t_{DurD} - 1.61 \times R^2_{wdr-gauge}$$

Equation 9

where, L$_{W1-stats}$= Leakage amount measured at W1 [mL] – **Statistical multi-regression model**.

R$_{wdr-gauge}$ = Sum of measured wind driven rain captured by wall gauges XG1 during rain event leading up to leakage and during the leakage event [mm/m^2]

t$_{DurD}$ = Length of time period starting from the start of wind-driven rain measurement, leading up to and during the leakage event [hr].

Below are the statistics for this model, followed by the model's normal probability plot in Figure 53 which shows a generally straight line of residual points.

- Sample size, i.e. number of leakage events, n = 21

- p<0.001

- R-sq=80.76%

- R-sq(adj)=77.36%
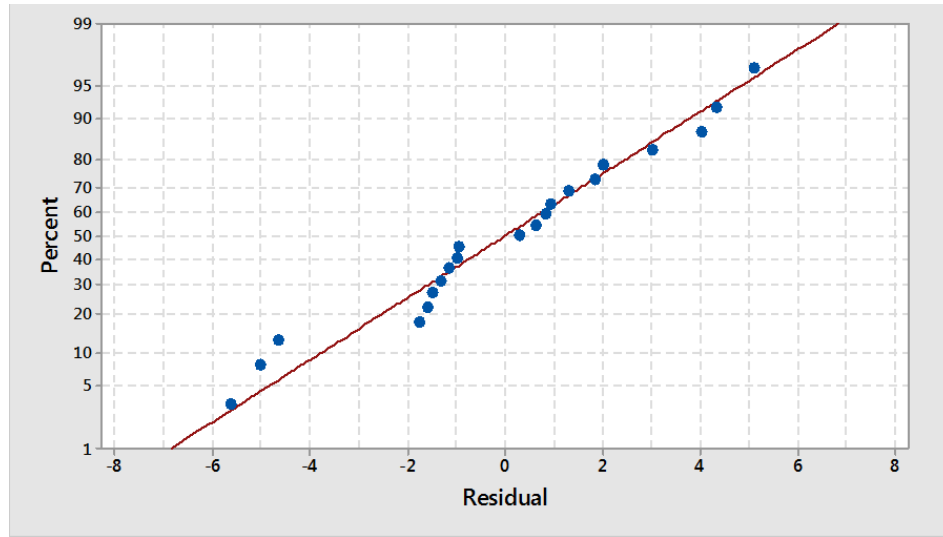
Figure 53. Normal probability plot from Minitab 17 for W1 statistical leakage regression model.

The statistical multi-regression model for W1, Equation 9, indicates that the primary predictors for the leakage amount at vinyl siding wall sill corner location are the wind driven rain intensity and how long the wind driven rain occurs. As expected, the PRI_{48} or the Prior Rain Index, although was initially included in the model generation for W1, was found to be irrelevant to predicting the variance to the leakage amount at the non-absorptive vinyl siding cladded wall. Neither is the U_{Max}, which is the maximum normal wind speed on the wall; most likely due to the presence of the horizontal air cavity gaps behind the vinyl sidings.

5.4.2 Statistical Leakage Model for W6 Corner Defect

A sample set of 29 data points, the same ones used plotted in Figure 52, were used to generate a multiple linear regression model in Minitab 17. Four regression models were initially found with R-Sq value above 80% and were discussed in Appendix B. The best-fitting model with R-squared value of 86.01% includes the variables: sum of horizontal rain starting from the first WDR detection up to and during the leakage event, sum of WDR collected by XG3 top wall gauge, and the maximum of 5-minute averages of wind seed normal to wall, as following:

$$L_{W6-stats} = -8.4 + 20.2 \times R_{wdr-gauge} + 2.37 \times R_{h-DurD} - 1.06 \times U_{Max} - 3.253 \times$$

$$R_{wdr-gauge} \times R_{h-DurD} + 7.79 \times R_{wdr-gauge} \times U_{Max} + 0.704 \times R_{h-DurD} \times U_{Max}$$

Equation 10

where, $L_{W6-stats}$=Leakage amount measured at W6 corner leakage gauge [mL] – **Statistical model**

R_{h-DurD}= Sum of horizontal rain during rain event starting from the start of WDR detection and during the leakage event [mm/m^2]

$R_{wdr-gauge}$=Sum of measured wind driven rain captured by top wall gauge XG3 during rain event leading up to and during the leakage event [mm/m^2]

U_{Max} = Maximum of 5-min averages of wind speed normal to wall during each leakage events [m/s]

The following are the statistics for this model, as well as the model's normal probability plot in Figure 54, which showed that the assumption of residual normality is met, with several outliers.

- Sample size, i.e. number of leakage events, n = 29

- p<0.001

- R-sq=86.01%

- R-sq(adj)=82.19%.
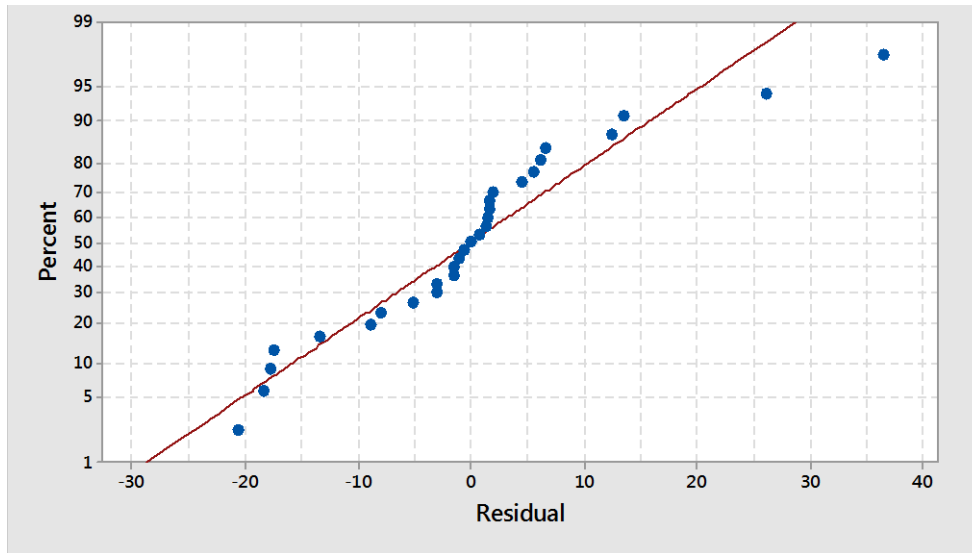
Figure 54. Normal probability plot for the statistical regression model of W6 corner leakage amount.

One of the initial 4 models considered for W6 Corner included the PRI_{48}, but was later eliminated after the statistics evaluation shown in Appendix B. The best-fitting model for W6 corner, Equation 10, indicates that there are several variables that contribute to the variations in the leakage amount at W6 corner. As the amount of horizontal rain is one of the contributing variables, it appears that rain run-off either finds its way to the rainwater sill corner entry location or is absorbed by the mass and enters that sill corner location with the help of another contributing variable, U_{Max}.

5.5   MOISTURE DETECTION TAPE READINGS AT WATER COLLECTING WALLS

The charts in Figure 55 to Figure 57 show the detection of water presence or passing though the moisture detection tapes, in comparison to the occurrence of the leakages. The MDT labelled with "01" ending are the tapes located directly under the location of water collection area. Refer to Figure 28 for the schematic drawing of the approximate locations of these moisture tapes. Figure 55 shows that more water passes through the middle sensors W1SmMdO01 and W1SmMdO02, compared to the bottom corner sensors along the jamb. More water presence is detected at the

sensor directly below the aluminum trough directing water into the leakage gauge, indicating there may be additional moisture load that could potentially add to the leakage amount.
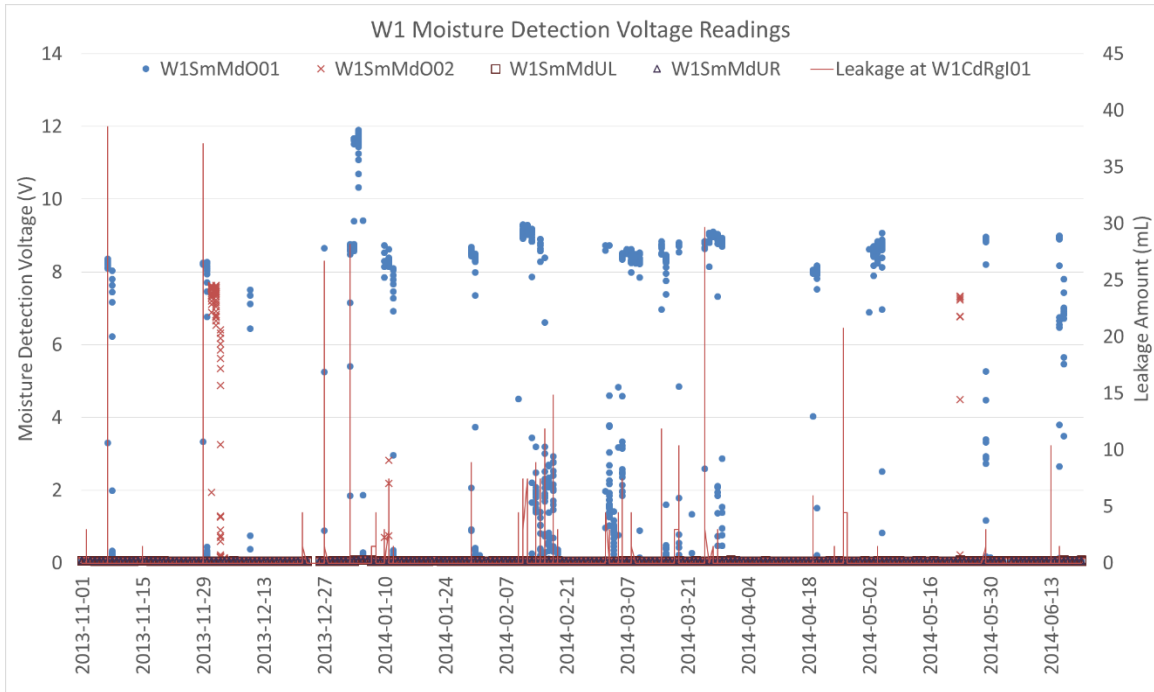
Figure 55. W1 moisture detection tape voltage readings from November 2013 – mid June 2014 compared to the measurements at leakage gauge W1.

More water presence is detected by the control MDTs at vinyl siding wall W2 with middle water collector as shown in Figure 56. Similar to what is observed at W1, the middle sensors W2SmMdO01 and W2SmMdO02 also detected more water presence, compared to the bottom corner sensors along the jamb. However, the W2SmMdO02 has higher frequency of water detection than at W2SmMdO01.
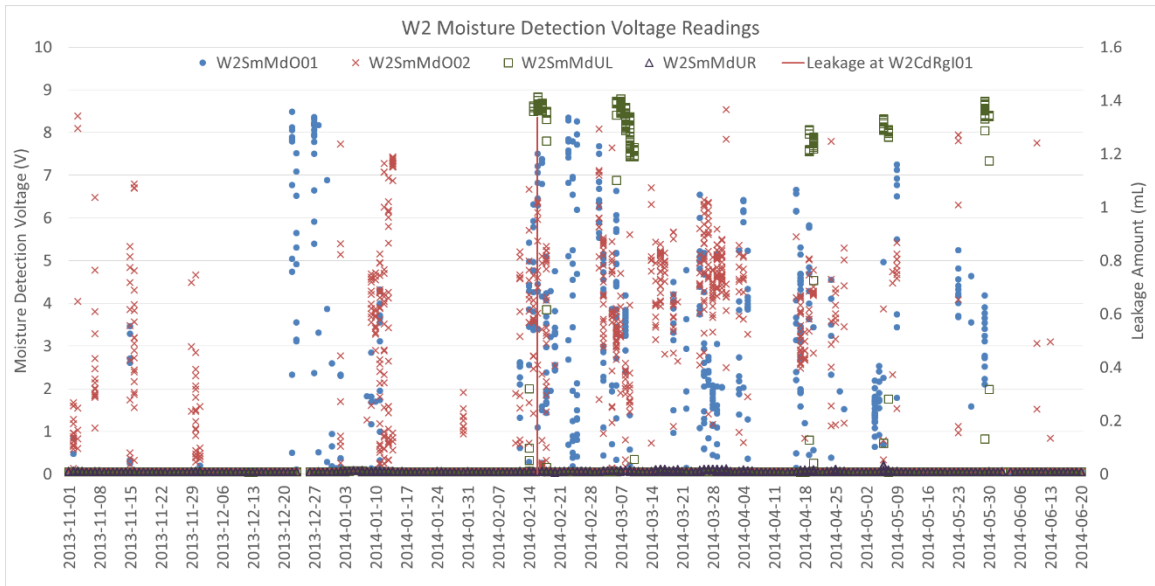
Figure 56. W2 moisture detection tape voltage readings from November 2013 – mid June 2014 compared to the measurements at leakage gauge W2.

As for the MDT sensors on stucco walls, the readings are less well defined and it appears that the moisture remains in contact with the conductors for longer period of time. Figure 57 shows these readings. This may be caused by the additional plastic cover added over the MDTs. Therefore, the control MDTs data for W6 cannot be used for the data analysis.
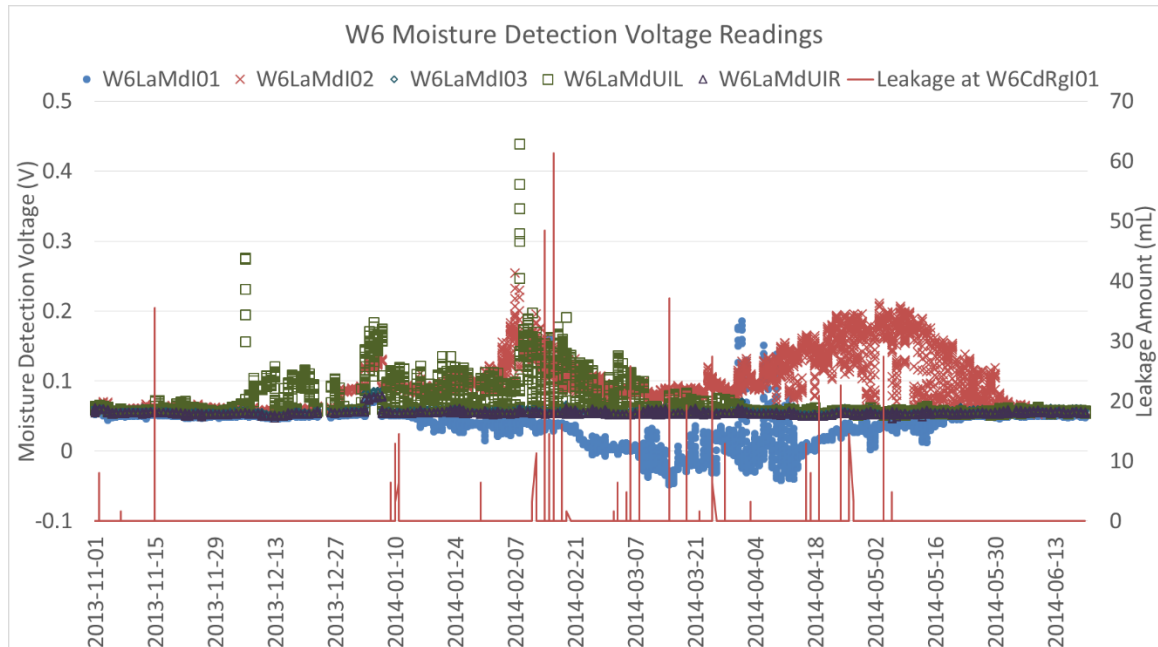
Figure 57. W6 moisture detection tape voltage readings from November 2013 – mid June 2014 compared to the measurements at leakage gauge W6 corner.

5.6 LONG TERM PERFORMANCE WALLS

This section presents the bottom trough water collection measurements and sensor readings of the long-term performance vinyl siding walls W3, W4, W5 and stucco walls W7 and W8, starting from the month of November 2013 to mid-June 2014, except for W8 moisture pin sensors readings that are only available starting from March 7, 2014. The sensors selected to be presented in the graphs of this section are the sensors that represent the typical trends, the sensors located closer to the window sill, and the sensors displaying atypical trends. The last sub-section of this chapter, numbered 5.6.5, presents and discusses the relative humidity levels in the monitored stud cavities of the five long-term performance monitoring walls.

As a brief reminder, the sensors monitor the long-term performance walls to correlate wetting and drying process of the walls with the water leakage collected at W1, W2, and W6 through the replicated construction details and/or simulated defects. W7 replicates the missing 4" vertical length of sealant at the window sill corner to be correlated to W6 corner water collection. W8 has no simulated defect and was monitored as a reference wall to W7. Vinyl siding wall W3 was built

to be correlated to W1 and W2, with no head flashing detail above the W3 window. W4 was built with head flashing drip edge over its window as a comparison to the W3 that has no head flashing; while at W5, the sealed gap between the frame and J-trim of W5 eliminates WDR through this gap as a moisture source for the wetting of the wall area below the window.

5.6.1 Bottom Trough Water Collection

The measured amount of water draining off the surface of the building paper behind the cladding during multiple rain events collected from the bottom trough of each of the five long-term performance walls are presented in Figure 58. The last measurement taken for the water drainage collection was on May 26th, 2014. This graph compares relatively the magnitude of rainwater draining from behind the vinyl siding cladding and for stucco walls; the rainwater that was absorbed across the thickness of the stucco wall and water that drained on the building paper within the small gaps behind the stucco cladding. The amounts measured for stucco walls at more than 500 mL are conservative measurements as typically the water bottle collectors were found full and more water were likely to have remained in the aluminum troughs.
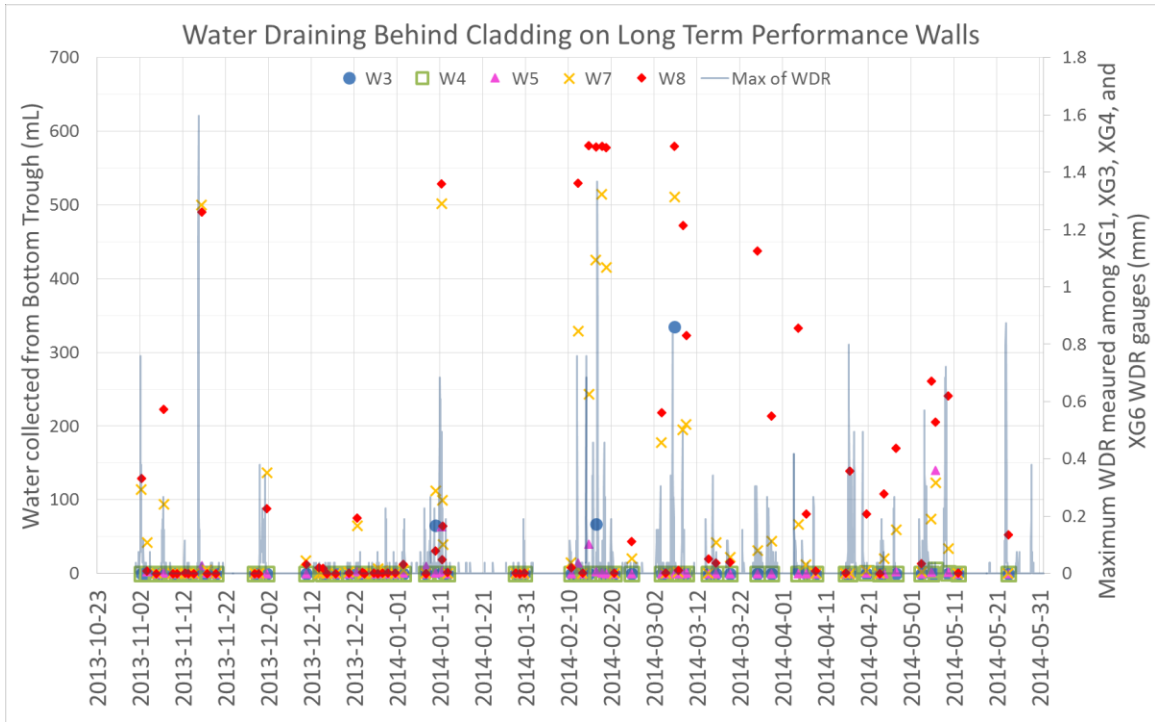
Figure 58. Amount of water draining behind cladding of long term performance walls from November 2013 to May 2014, compared to the maximum measured wind driven rain among XG1, XG3, XG4, and XG6 wall gauges.

Monthly total amounts of water draining behind the claddings of the long term performance walls are plotted in Figure 59. The highest amount of water was drained from the surface of building paper of W8 stucco wall, totaling close to 3 L in February 2014. W7 stucco wall also experienced the highest amount of water draining on its building paper in February 2014 at a total close to 2 L. The second highest total amount of water collected by both stucco walls occurred in March 2014. Typically, the amounts of water collected by stucco walls on other months range between 100 mL to 800 mL. On the contrary, for vinyl siding walls, less than 200 mL were typically collected monthly.
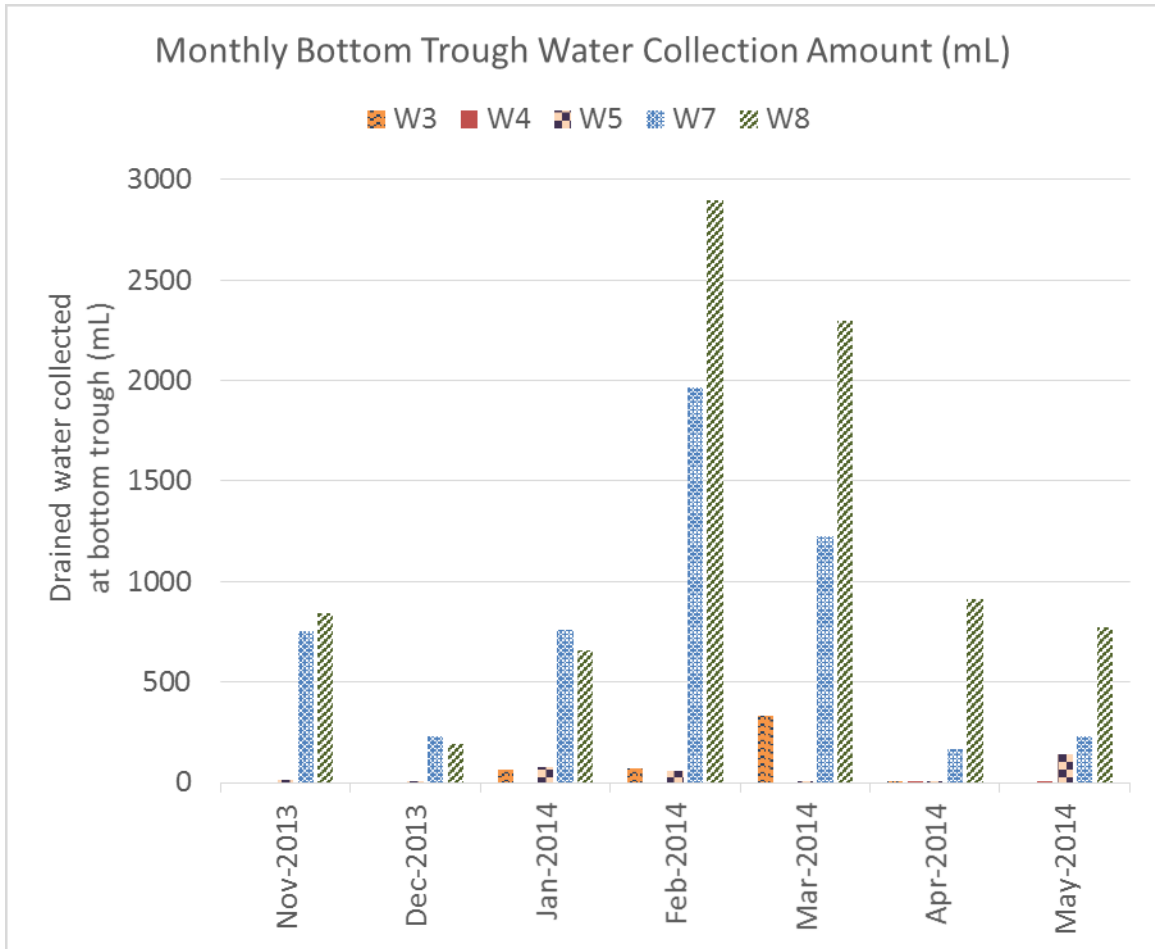
Figure 59. Monthly drainage water collection amount collected by bottom trough at the five long term performance walls.

Among the long-term performance vinyl sidings walls, the most frequent drainage water collection was observed from wall W5. In comparison, the drainage water from wall W3 was less frequently observed in the W3 collection bottle; however, when present, the amount of water collected was typically significantly higher than the water collected from W5. For example, at two measurements in January and February 2014, more than 65 mL were collected from W3, while less than 1 mL were typically collected from W5 during each measurement. The highest amount of drainage water collected among the vinyl siding walls was also collected from W3 at 334.5 mL in March of 2014. Overall, minimal amounts of drainage water were measured at vinyl siding wall W4. The highest amount collected for W4 was 5.0 mL on May 6, 2014. Only two other measurements of drainage

water from W4 were recorded; each was less than 0.5 mL. Since the difference between W4 and the other two vinyl siding walls was due to the head flashing trim installed above W4 window, these observations indicated that most of the water draining at the bottom of the walls of W3 and W5 appeared to be primarily contributed by the runoff rainwater on the surface of the vinyl sidings of the wall area above the windows that was captured by the head J-trims, channeled down along the jamb J-trims and was directed onto the surface of the building paper at the sill J-trim corners.

For stucco walls, in general, W8 were draining off the most amount of water, with W7 following closely. The observation that higher amounts of water were collected from W8 than from W7 may be attributed to the location of W8 which was closer to the end of the façade. The observation that both stucco walls drained more water than vinyl siding walls is consistent with the fact that stucco cladding has the characteristics of an absorptive cladding, where rainwater is retained and then drained once the water retaining capacity of the stucco is exceeded.

Assuming that only the WDR that impacted the stucco wall areas directly above and below the window has contributed to these collected amounts of drainage water, i.e. approximately 4.2 m^2, the proportion of monthly total amount of rainwater draining on the exterior surface of the building paper to the wind driven rain amount can be estimated. Using the maximum amounts for W8, in February 2014, 2.9 L of rainwater was collected by the bottom trough out of the approximately 30 mm total measured by the WDR gauge, as summarized in Figure 35, over the assumed 4.2 m^2 area, or roughly 126 L of WDR. In other words, up to 2.3% of the WDR load was draining on the exterior surface of the building paper of W8 in February 2014. This is more than double the limit of maximum exposure of water resistive barrier to the rain set by ASHRAE 160 Standard (ASHRAE Standard, 2009). Future testing for verification of the findings at the two stucco walls is therefore needed and the catchment area of WDR contributing to these collected drainage amounts should be defined to eliminate the assumption of area used in this calculation.

5.6.2 **Moisture Detection Tapes and Moisture Pins Readings at Long-Term Performance Walls**

For each walls, the moisture detection voltage readings on the building paper and moisture content readings of plywood sheathing and wood framing are graphed across the period of November 1, 2013 to June 19, 2014, except for the moisture content graphs for W8, which start from March 7th. For each graphs, the leakage amounts at W1 and W6 corner location, respective to the cladding type of the walls, are also included (at secondary vertical axes) to mark the occurrence of leakage events. At the end of each cladding types, close-up view charts of the same months of data are zoomed-in over the 1-month period of March 2014 – the month where the rain events were frequent, but no extreme weather conditions were measured.

The readings from nine thermocouples and ten moisture pin sensors were found illogical, for example, several negative moisture content readings were in the order of millions percent. These sensors were excluded from the charts as these sensors may have been damaged during their installation or their wiring became disconnected. Temporary power outages or voltage disruptions and fluctuations may also cause the sensors reading to be temporarily incorrect; one of these instances to note is during the period of January 3 to January 7, 2014.

Table 5 summarizes the thermocouple and moisture pin sensors that gave error readings and were therefore excluded from the charts presented in the next few pages. In addition, problems with nine thermocouples result in incorrect related moisture content readings as the moisture pins used the temperature readings from the thermocouples. Note that W7PwMoIR07, W7PwMoIR08, and W7PwMoIR09 depended on the temperature readings by W7PwTcIR08, which had issues and were therefore excluded. The error readings by W8PwTcIL04 were discovered early before November 2014; the sensor was then excluded, while the respective W8PwMoIL04 moisture pin was reset to depend on the nearby W8PwTcIL01 thermocouple readings.

Table 5. Summary table of sensors with errors and are therefore excluded from analysis.

Wall No.	Thermocouple	Moisture Pins
W3	None	None
W4	W4PwTcIL02 W4PwTcIL05	W4PwMoIL02 W4PwMoIL05
W5	None	None
W7	W7PwTcIL05 W7PwTcIL08 W7TrTcUIC W7WsTcBMIL	W7PwMoIL05 W7PwMoIR07 W7PwMoIR08 W7PwMoIR09 W7TrMoUIC W7WsMoBMIL
W8	W8PwTcIL04 W8TrTcLIC W8WsTcBMIR	W8TrMoLIC W8WsMoBMIR

The next two sub-sections: 5.6.3 and 5.6.4 discuss the moisture detection tape and moisture pin readings at the vinyl siding walls W3, W4, W5, and stucco walls W7 and W8.

5.6.3   Long Term Monitoring Sensors at Vinyl Siding Walls

5.6.3.1 Moisture Detection Tape Readings

Among the three vinyl siding long-term performance walls, W3 had the most frequent moisture detection tape readings. The voltage readings occurred at three tape locations: 11, 14, and 16 as shown in Figure 60. Referring back to the schematic drawing in Figure 24, locations of moisture detection tapes 11, 14, 16 were directly below the window sill corner. The moisture detection coincided with seven leakage events recorded at W1.
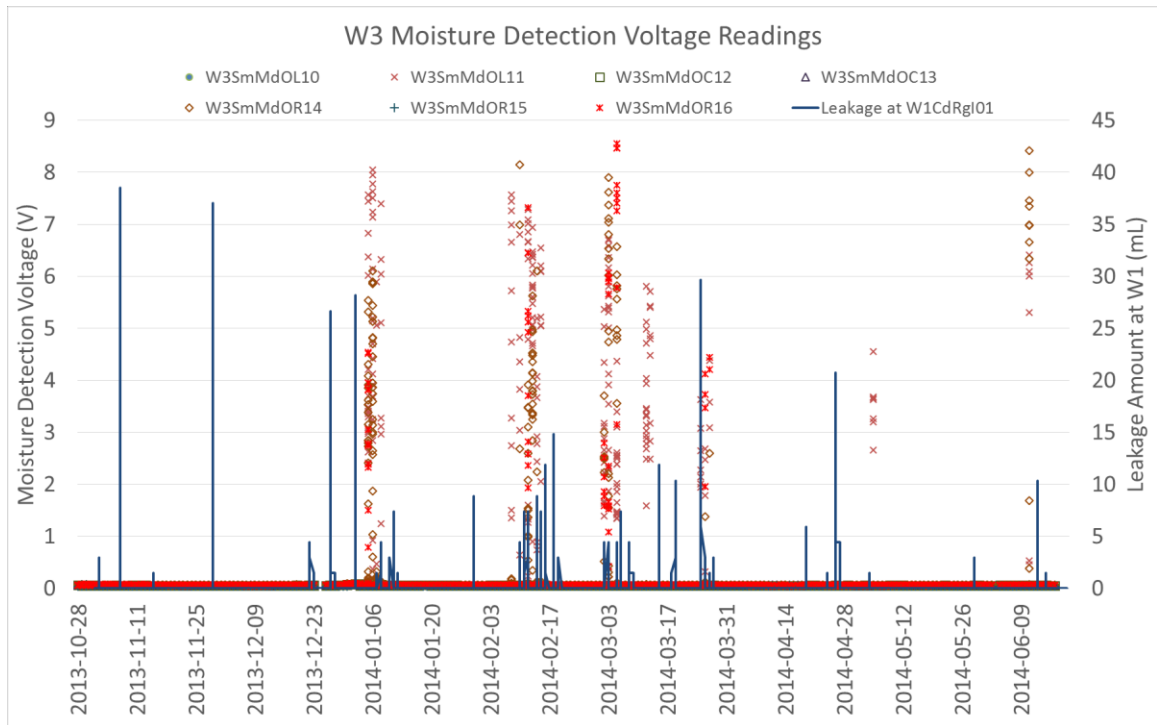
Figure 60. W3 moisture detection tape voltage readings from November 2013 – mid June 2014.

For W4, no significant moisture detection tape voltage readings above 0 V were detected as shown in Figure 61. This is consistent with the minimal amount of drainage water collected and measured at the bottom trough water collector. As the construction difference between W4 and W3 is the head flashing with drip edge over the window of W4, the lack of water draining over the building paper indicates the significance of the window head flashing in deflecting the water from above the window head of W3. In addition, this also suggests that most of the water draining on the building paper below the window appears to enter the space behind the vinyl siding cladding at or above the window head level.
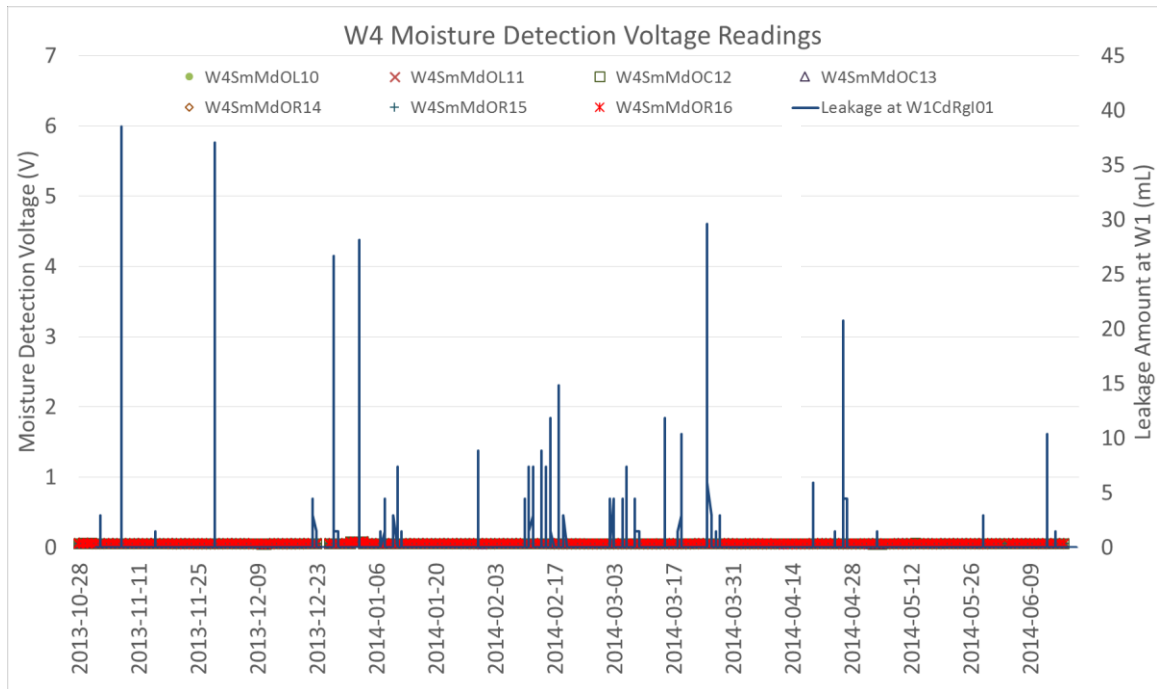
Figure 61. No significant moisture detection voltage readings were observed at W4.

Detections of water flow over the moisture detection tapes at vinyl sidings wall W5 occurred during one rain event that also caused a leakage event at W1. Water was detected passing through locations 11, 14 and 16 on May 3rd, 2014 at 1 am – 8 am.

The sealant at the gap between the window frame and the J-trims was applied as an attempt to eliminate any WDR from entering this gap. Therefore, the water flow detected by these readings at tape locations 11, 14, and 16 (all under sill corner area) appears to have originated from the surface rain run-offs on the wall area directly above the window head J-trim as the only other sources and paths of rain loads. However, it is unclear why only the May 3rd, 2014 WDR event resulted in these moisture detections at W5, but no other WDR events did.
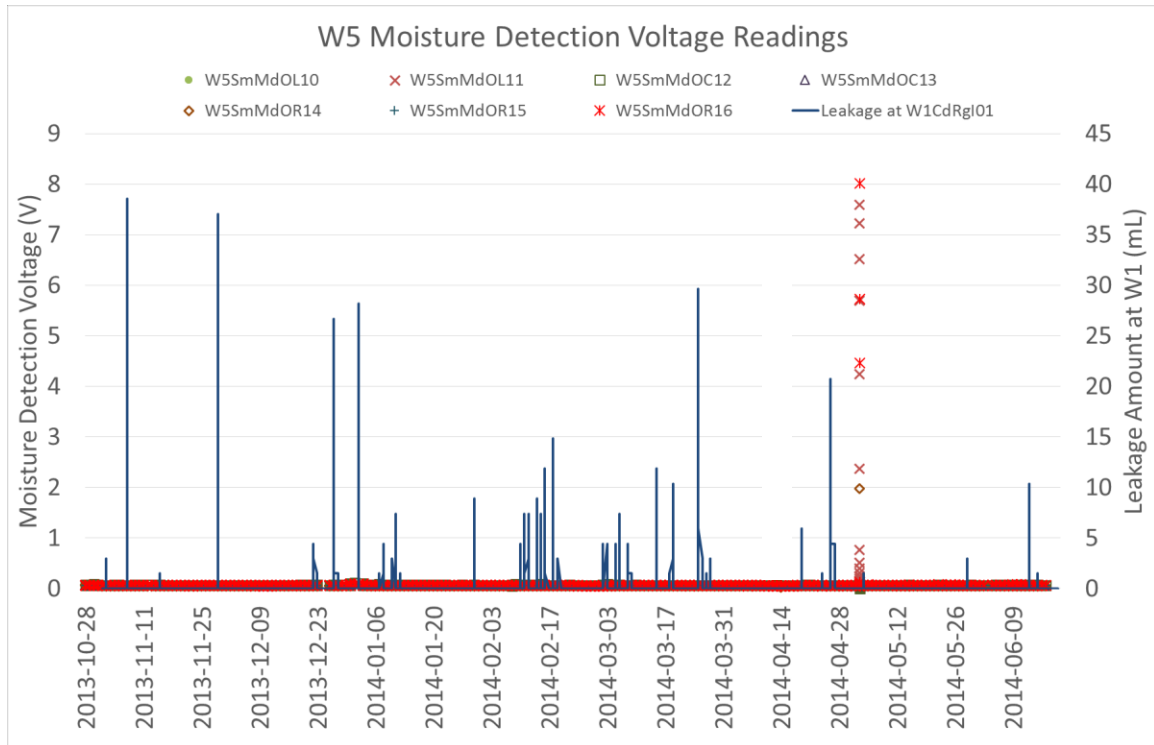
Figure 62. W5 moisture detection tape voltage readings from November 2013 – mid June 2014.

The frequency of the moisture detection tape at W3 was higher than the frequency of its drainage water collection at the bottom of the wall. However, the amount of drainage water collected from W3 was the highest among the three vinyl sidings as previously discussed and shown in Figure 58. On the other hand, at W5, rainwater appeared to drain more frequently behind the sidings in smaller amounts. Further studies need to be done to determine the cause of these findings regarding the frequency and drainage amounts at W3 and W5.

In both W3 and W5, moisture detection tapes at locations 11, 14, and 16 detected the presence of water most frequently. These three tape locations are all aligned as one column directly below the window sill corner. This observation further highlights the notion that the area directly below the window sill corner is the most exposed to the presence of water during a rain event and is therefore, the most susceptible area for damage from rainwater ingress.

5.6.3.2 Moisture Content Readings at Plywood Sheathing Boards

Figure 63 shows the moisture contents (MC) of plywood at W3 for moisture pins at locations L01, L04, and R07. The leakage amount at W1 is plotted at the secondary vertical axis. The moisture contents at L01, L04, and R07 vary between 7% and 13% and appear to show the seasonal trends. The higher level moisture contents were recorded in late January to mid-April. The drying phase appears to start in the spring.
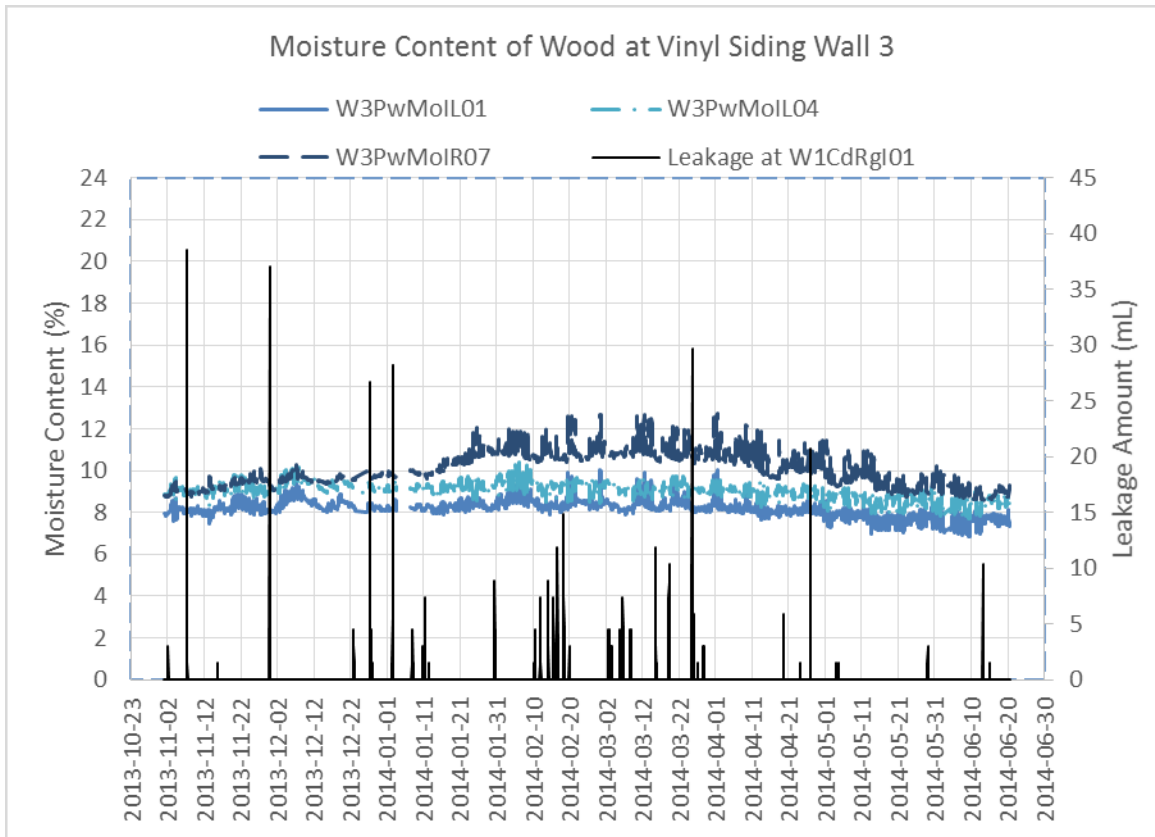
Figure 63. W3 Moisture content of plywood at upper moisture pin locations L01, L04, and R07, compared to the leakage amount at W1 as a reference to leakage events.

At W4, similar fluctuations and trends to the W3 are observed as shown in Figure 64. The MC of the plywood of W4 at location L01 is more stable than the typical MC of the plywood in W3. Overall, the moisture contents at the plywood of W4 also vary between 8% and 12%, with the seasonal trends of gradual increase in the winter towards the spring and decrease towards the summer.
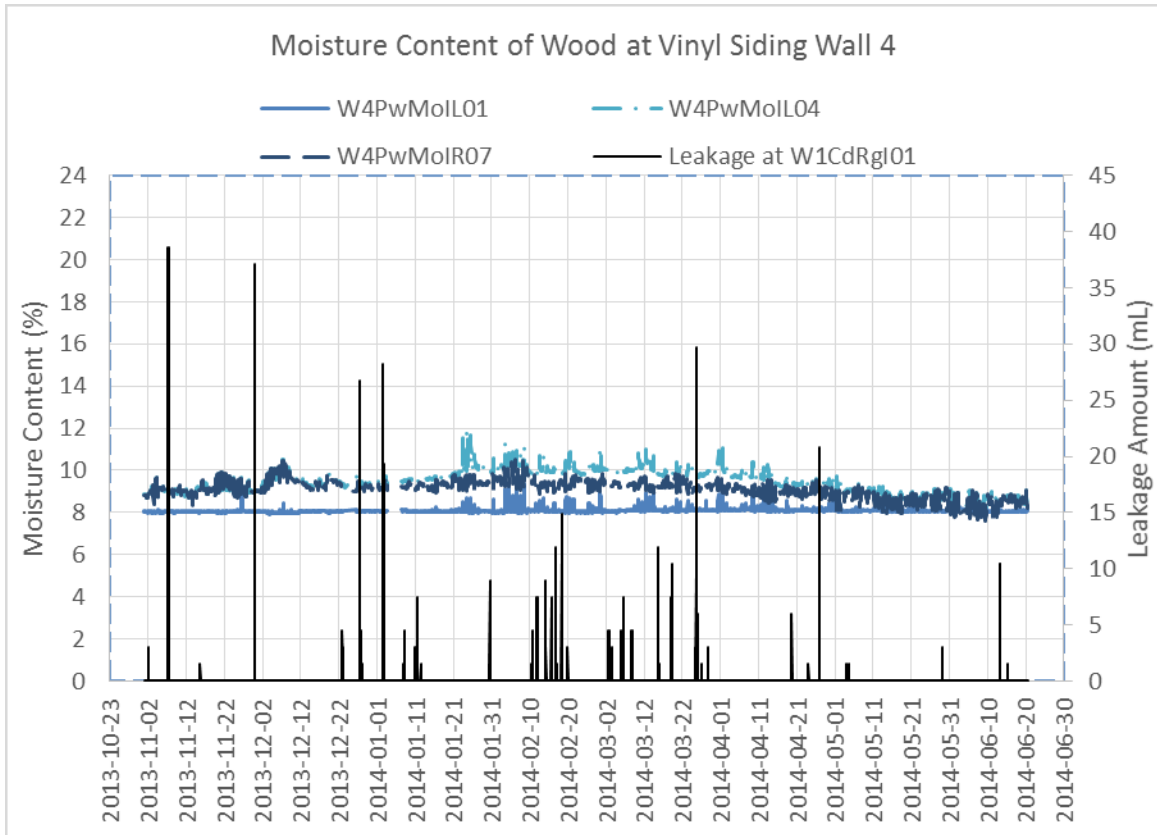
Figure 64. W4 Moisture content of plywood at upper moisture pin locations L01, L04, and R07, compared to the leakage amount at W1 as a reference to leakage events.

Figure 65 shows the trends of moisture content readings from the plywood of W5 at moisture pins locations L01, L03, L06, and R09. The moisture contents vary between 7% and 14%. Similar seasonal trends observed at W3 and W4 are also noted here. However, the moisture content levels from moisture pins L03 and R09 appear to reach the highest point earlier in the season, in mid-January.
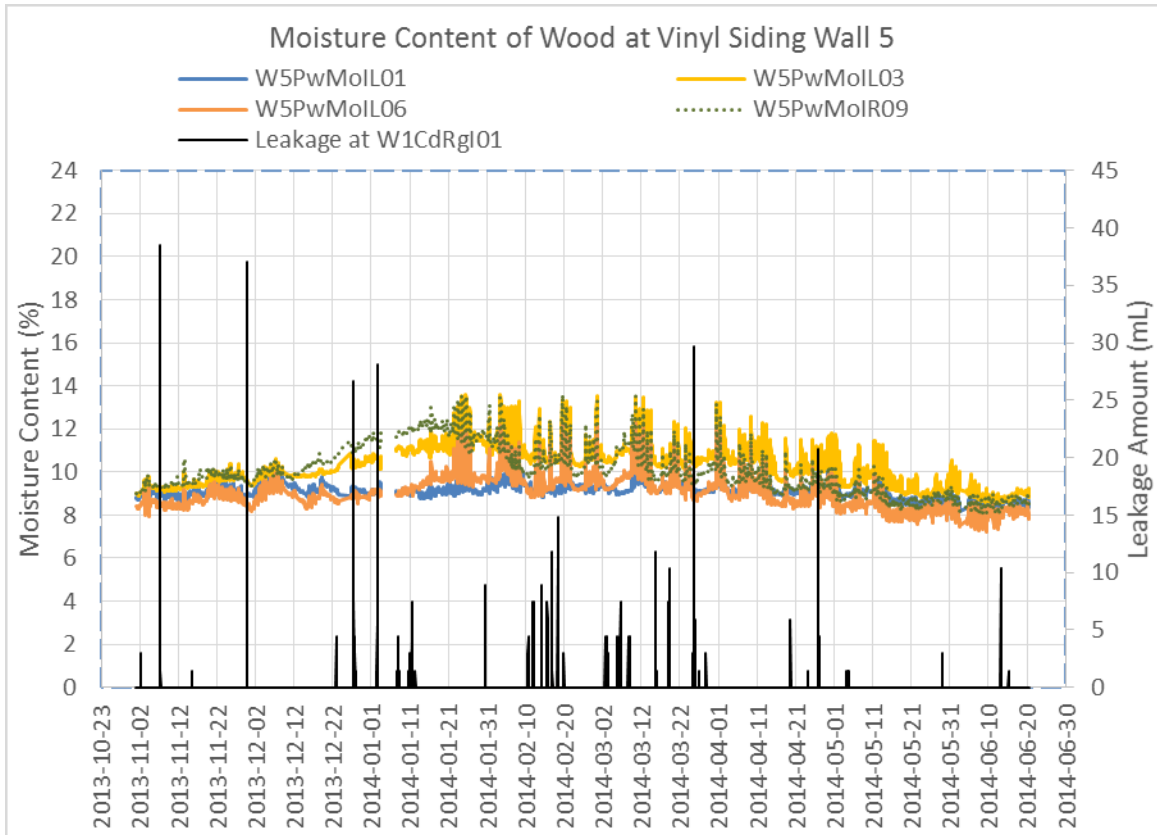
Figure 65. W5 Moisture content of plywood at moisture pin locations L01, L03, L06 and R09, compared to the leakage amount at W1 as a reference to leakage events.

5.6.3.3 Moisture Content Readings at Studs, Window Sill Plates and Bottom Plates

Figure 66 below shows the trends of moisture content at the window sill plates (location BMIL, BMIR) and the bottom sill plate of W3 (location TMIC). The moisture content readings average to approximately 10-12%, with no significant long-term increase or decrease.

Figure 66. W3 Moisture content of window sill plate (locations BMIL and BMIR) and bottom plate (location TMIC), compared to the leakage amount at W1 as a reference to leakage events.

Figure 67 shows the trends of moisture content at a trimmer stud supporting the rough opening for the window at W3. Locations UIC, MIC, and LIC were observed to vary closely together. The moisture content readings average to approximately 12%, with no significant long-term increase or decrease.

Figure 67. W3 Moisture content of stud next to wall cavity (locations UIC, MIC, and LIC), compared to the leakage amount at W1 as a reference to leakage events.

Figure 68 shows the trends of moisture content at the window sill plates (location BMIL, BMIR) and the bottom sill plate (location TMIC) of W4. Similar to W3, the moisture content readings average to approximately 10-12%, with no significant long-term increase or decrease.
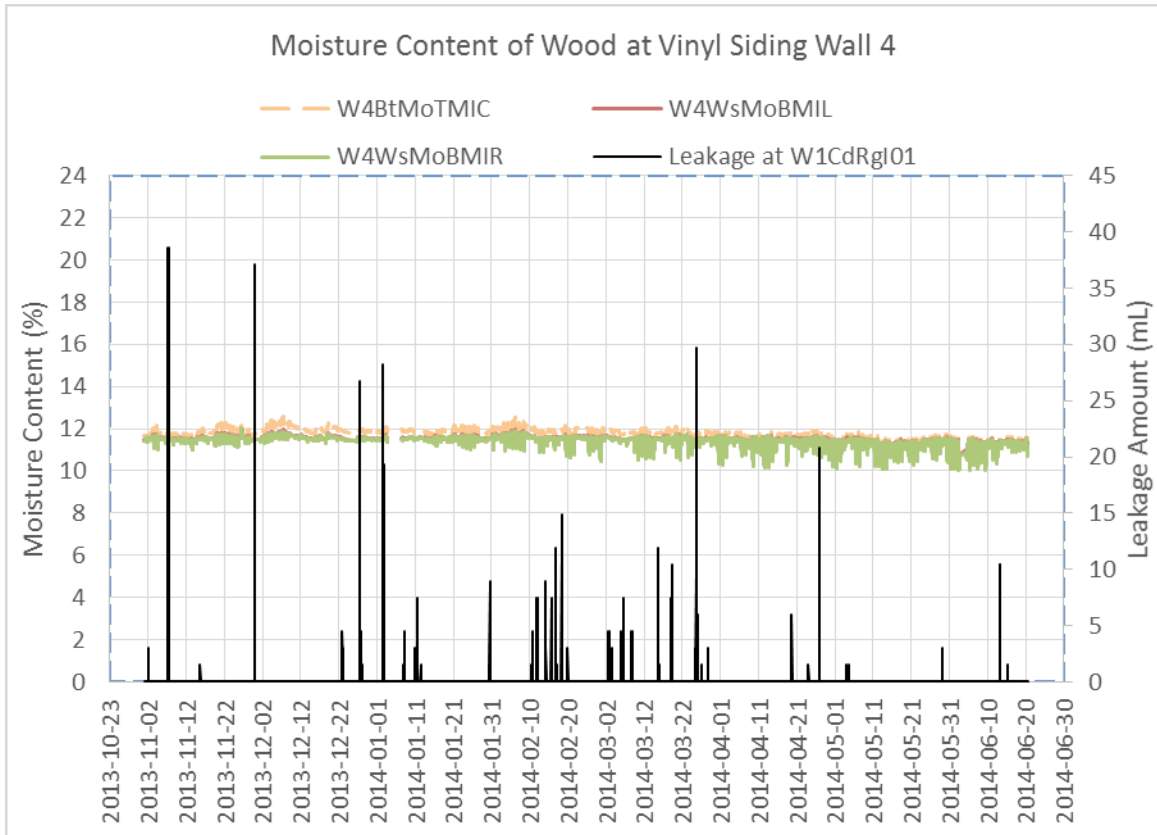
Figure 68. W4 Moisture content of window sill plate (locations BMIL and BMIR) and bottom plate (location TMIC), compared to the leakage amount at W1 as a reference to leakage events.

Figure 69 shows the trends of moisture content at a trimmer stud supporting the rough opening for the window at W4. Locations MIC and LIC are observed to vary closely together. Similar to W3, the moisture content readings at MIC and LIC average to approximately 12%, with no significant long-term increase or decrease. However, the pin at location UIC, the uppermost sensor on this trimmer stud, shows a gradual increase and decrease in moisture contents, with a trend that is more typically observed from the moisture pins at a plywood, rather than studs. The moisture contents at moisture pin W4TrMoUIC range between 12% and 16%. The highest moisture content base level is observed in mid-January. Regardless, the moisture content increase is within 4% and does not appear to be significantly caused by rain leakages into the wood framing.
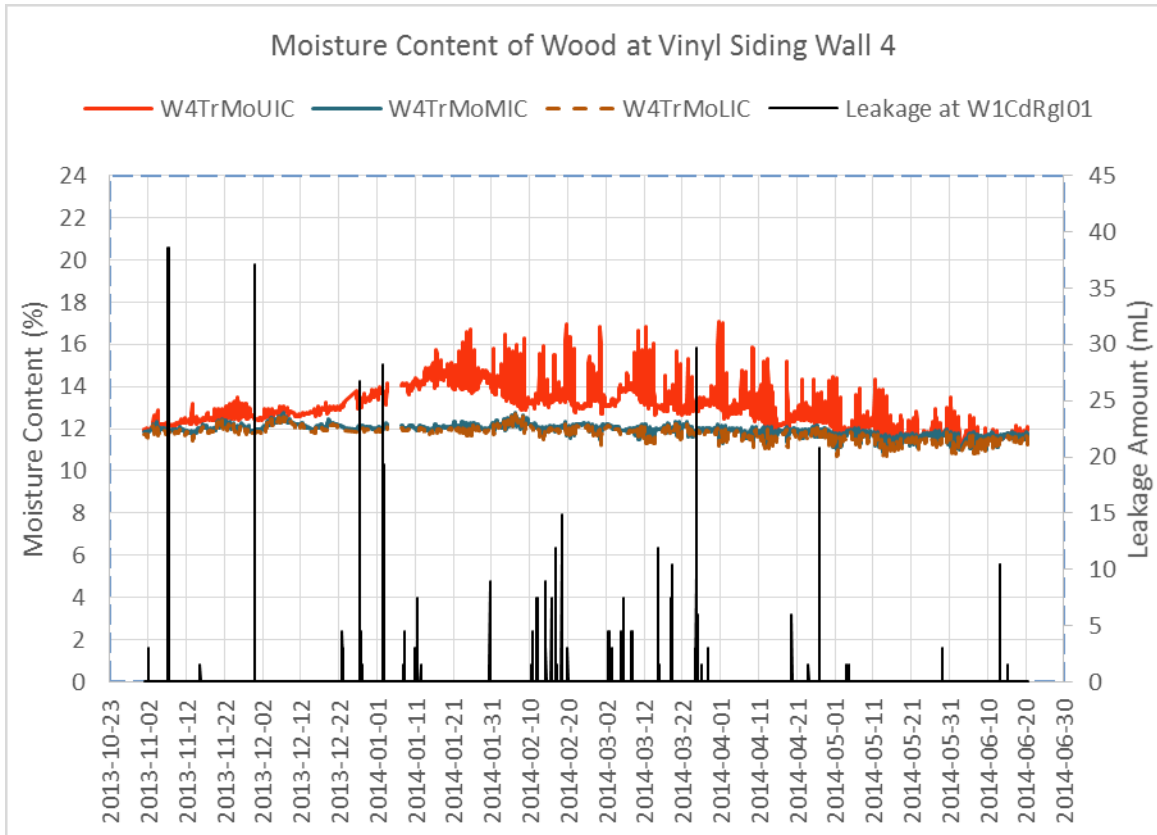
Figure 69. W4 Moisture content of stud next to wall cavity (locations UIC, MIC, and LIC), compared to the leakage amount at W1 as a reference to leakage events.

Figure 70 shows the trends of moisture content readings at the window sill plates (location BMIL, BMIR) and the bottom sill plate (location TMIC) of W5. Similar to at W3, the moisture content readings average to approximately 11-12% with no significant long-term increase or decrease in moisture content.
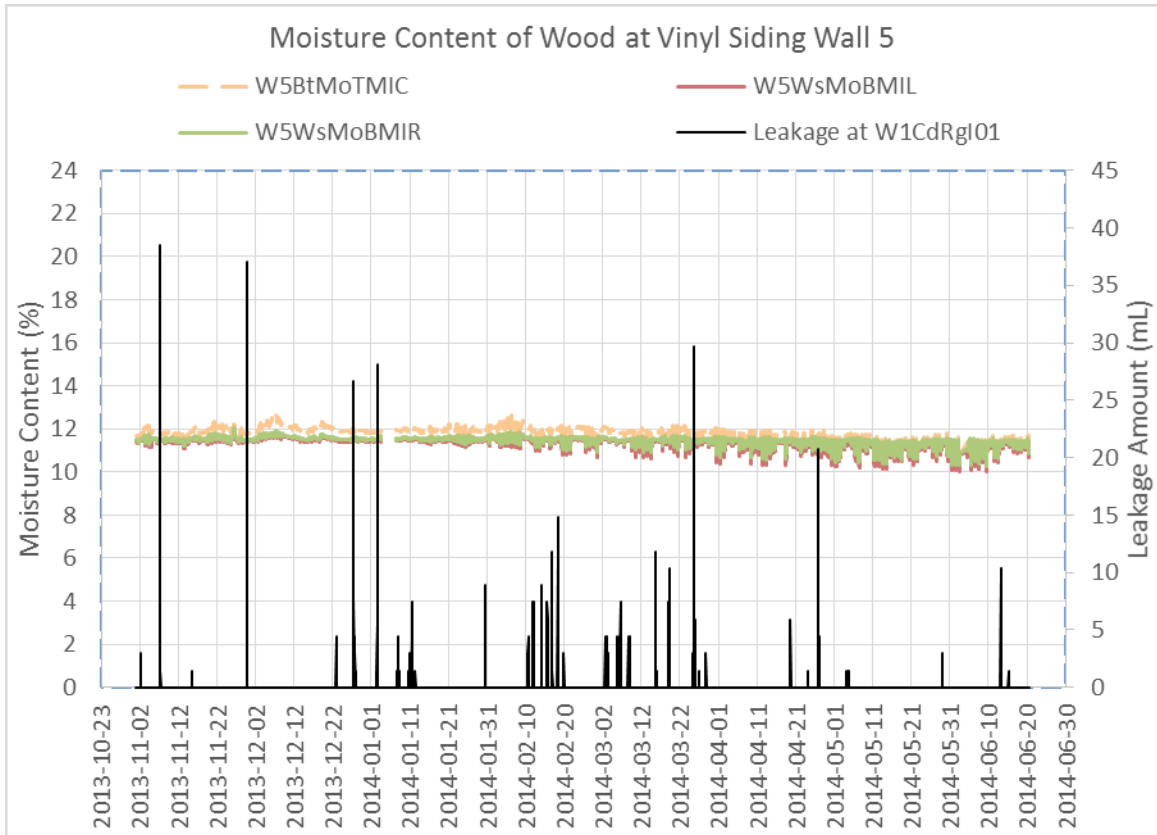
Figure 70. W5 Moisture content of window sill plate (locations BMIL and BMIR) and bottom plate (location TMIC), compared to the leakage amount at W1 as a reference to leakage events.

Figure 71 shows the trends of moisture content at a trimmer stud supporting the rough opening for the window at W5. The MC trends at locations UIC, MIC and LIC are observed to vary closely together. Similar to at W3, the moisture content readings average to approximately 12%, with no significant long-term increase or decrease. No leakages appear to have affected this trimmer stud.
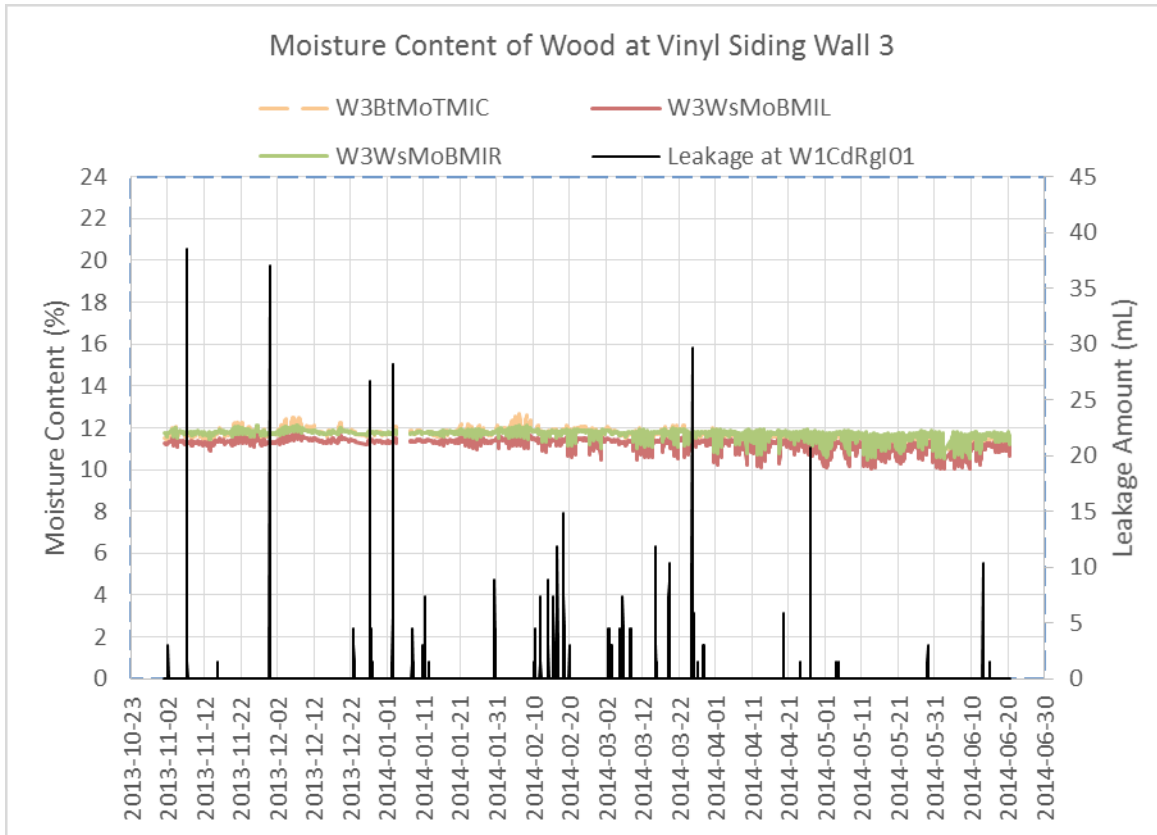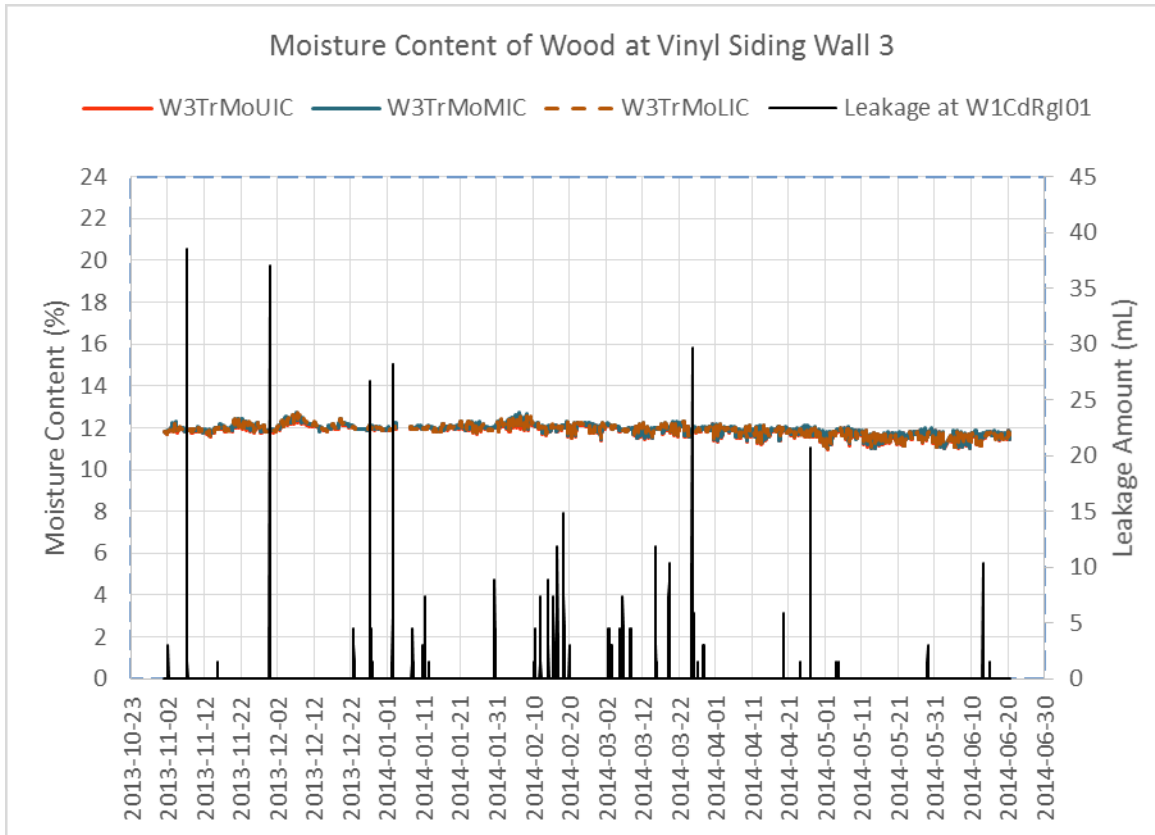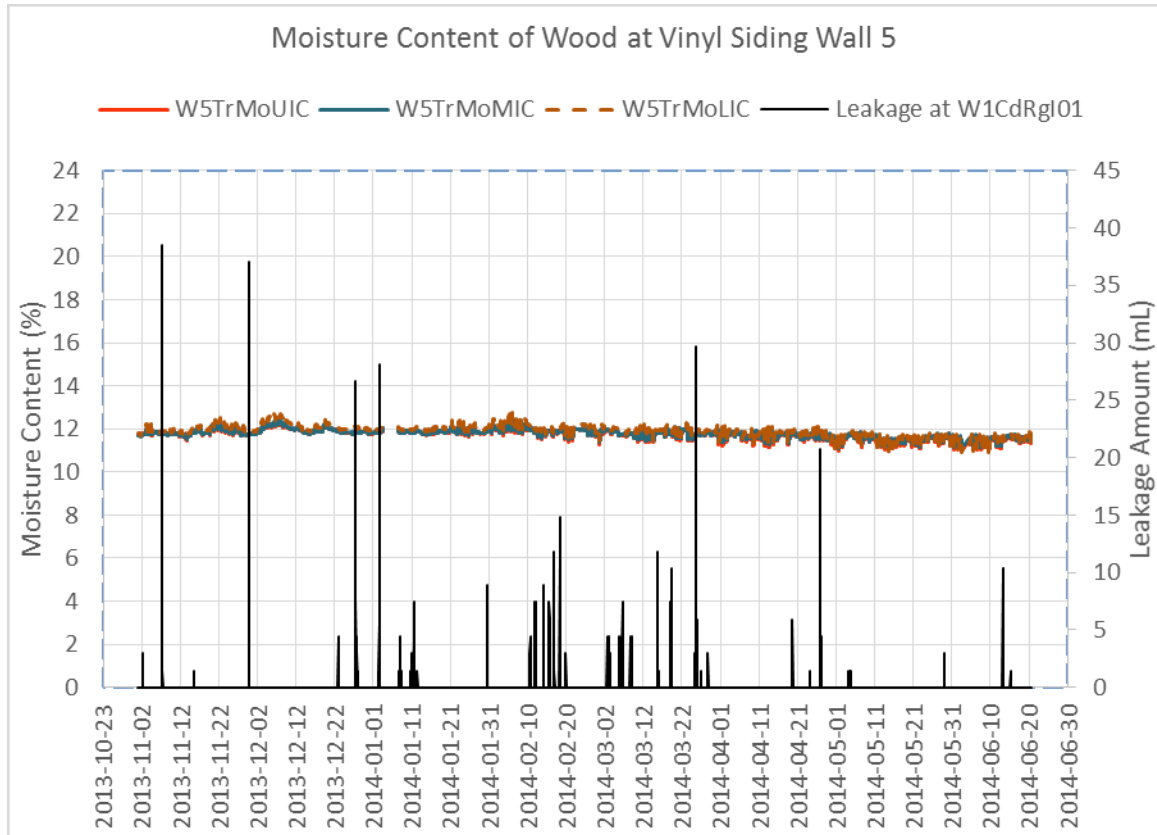
Figure 71. W5 Moisture content of stud next to wall cavity (locations UIC, MIC, and LIC), compared to the leakage amount at W1 as a reference to leakage events.

Overall, the moisture contents of the wood framing under the window sill of W3, W4, and W5 do not indicate any occurrence of leakage from rain penetration. The moisture content levels are within the range that is observed in Tariku, et al. (2015), which is between 6% to 13% overall. Two of the test panels in Tariku, et al. (2015) were built on the same SE façade of the BETF. The seasonal trends observed on these vinyl siding walls are also similar to the trends observed in the article.

5.6.3.4 Summary of Long Term Performance Observations at Vinyl Siding Walls

In the close-up view of the trends of moisture contents of W3 wood framing and sheathing over time during the month of March 2014 as shown in Figure 72, the moisture contents of the studs and plates are stable between 8% or 12%. The MC of the plywood typically fluctuates more,

approximately 1-1.5% more than the MC at the studs and plates. Over the rainy days, e.g. March 3rd to March 6th, the fluctuation range is less than the fluctuations during the sunny days.

This close-up view also shows that during a dry day's afternoon, the moisture content of the plywood increases to peaks, while the moisture content of the studs and plates decreases to the lowest point, or valleys, at approximately the same time. One hypothesis that may explain this observation is that as the outside temperature increases in the morning and reaches the highest in the afternoon, more evaporation happens from the plywood to the outside air behind the cladding, which draws the moisture vapour drive from the studs and plates into the wall cavity towards the plywood. Hence, the MC of the studs and plates decreases, while the MC of the plywood temporarily increases.
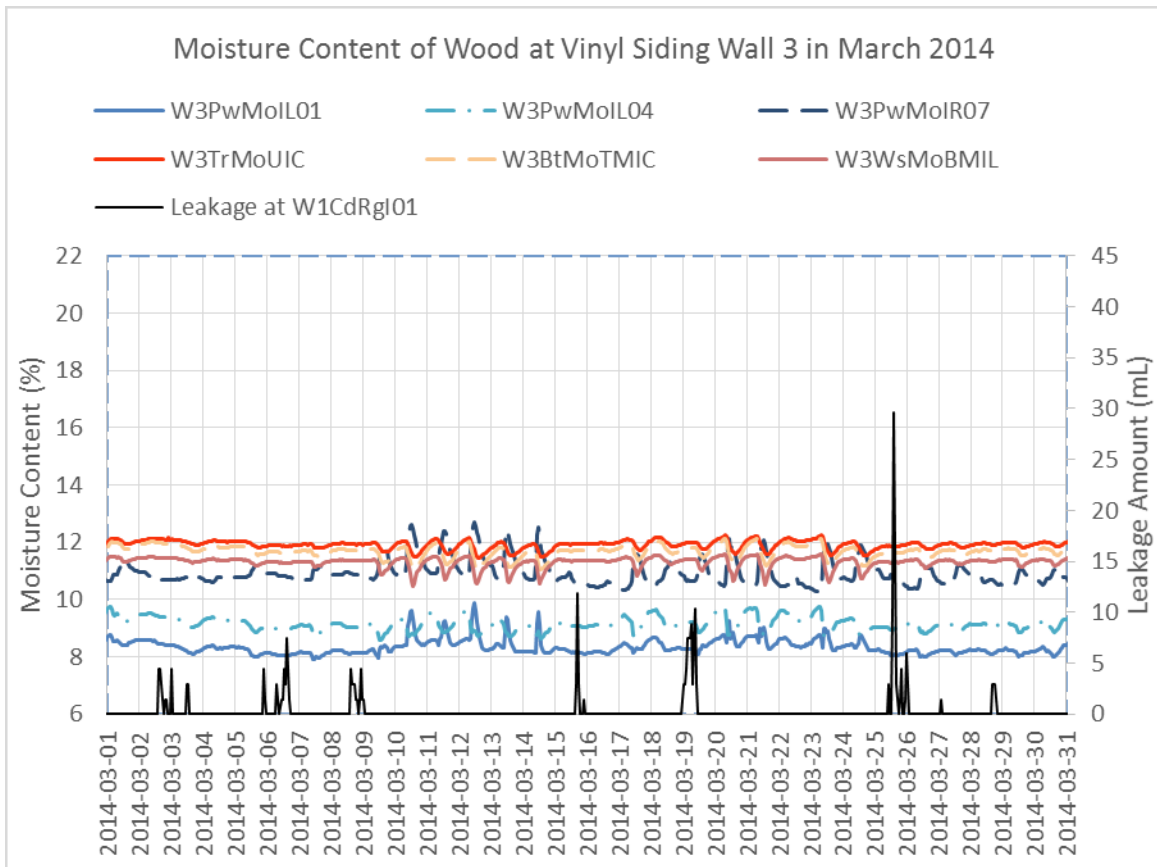
Figure 72. Close-up view of moisture content of plywood and wood framing at W3 in March 2014.

Although Figure 60 shows water draining through the moisture detection tapes below the sill corner of W3 (at locations 11, 14, and 16) frequently during several rain events and although Figure 58 shows that the draining water reaches the bottom trough collector, it appears that overall, the building paper at W3 wall managed to keep the water away from the plywood sheathing, as the moisture content of most of the plywood areas was steady.

Figure 73 shows the close-up view of trends of moisture contents of W4 wood framing and sheathing over time during the month of March 2014. The increasing trend of MC during one rain event (e.g. March 4th –March 8th) and the decreasing trend of MC during the following dry days (e.g. March 9th – March 14th) are well-defined here. The minimal amount of drainage water bottom wall trough collected from W4 shown in Figure 58, and the lack of significant moisture tape detection voltage reading above 0 V at W4 at all locations shown in Figure 61 indicates that rainwater seldom gets past the vinyl sidings at these locations.

The daily fluctuations of W4TrMoUIC also appear to be similar to the daily fluctuations at a pin located in the plywood, where towards the mid-day, the moisture content reaches the highest daily levels and decreases back to their base levels in the evening, following the solar radiation. As the wall panels have been demolished and there is no way to confirm the data from the moisture pin at W4TrMoUIC, this moisture pin will not be considered for further analysis.
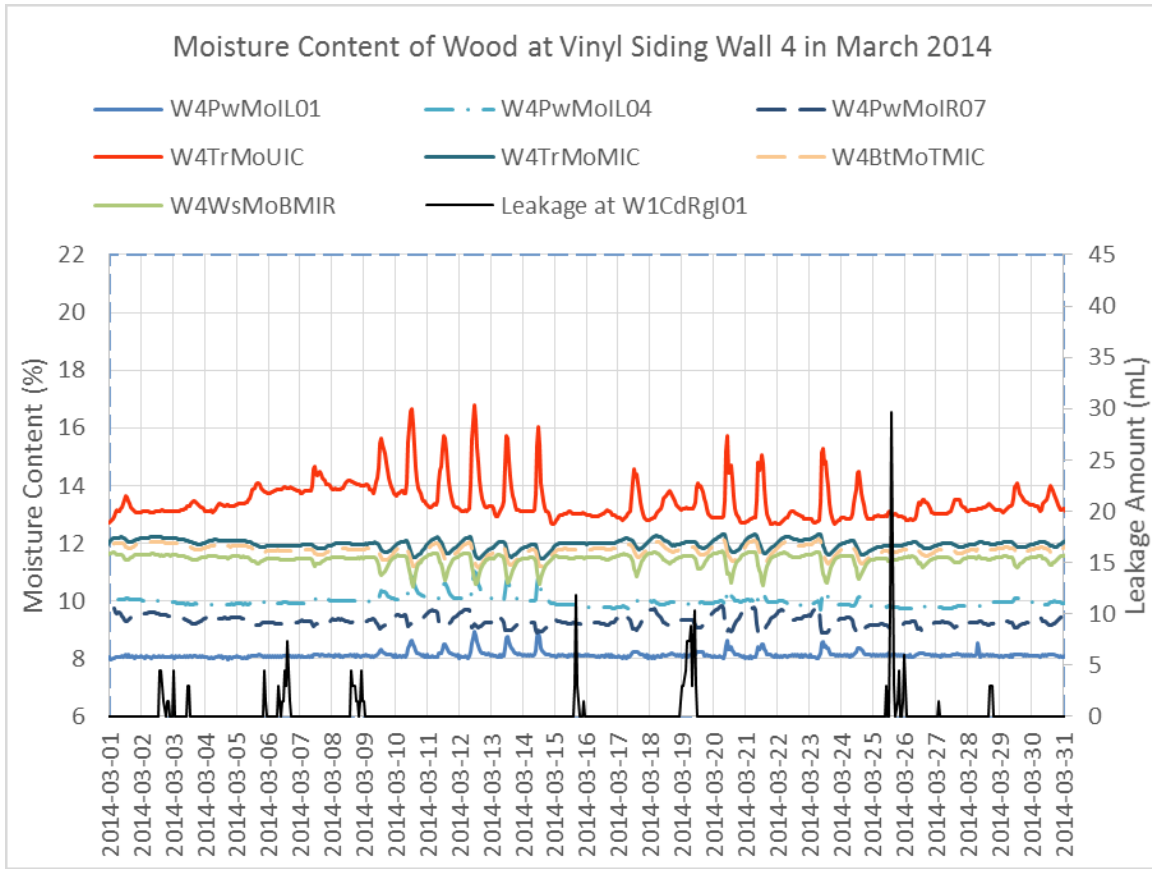
Figure 73. Close-up view of moisture content of plywood and wood framing at W4 in March 2014.

Compared to at W3, the moisture content trends at most moisture pins on the plywood of W4 are more stable than the trends at W3. This stability may be credited to the head flashing with drip edge above the window of W4 which appeared to have diverted most of the rainwater from above the flashing away from the window and the space behind the vinyl sidings below the window.

Figure 74 shows the close-up view of moisture content readings in W5 wood framing and sheathing over time during the month of March 2014. Instead of the upper moisture pins location L04 and L07, this chart shows the lower pin locations of L03, L06 and L09 as there are increasing and decreasing trends at these locations during rainy days, which are not observed in W3. The increasing trends of the moisture contents at the plywood return to the same initial moisture content – a similar daily fluctuation trends also observed in W3 and W4.
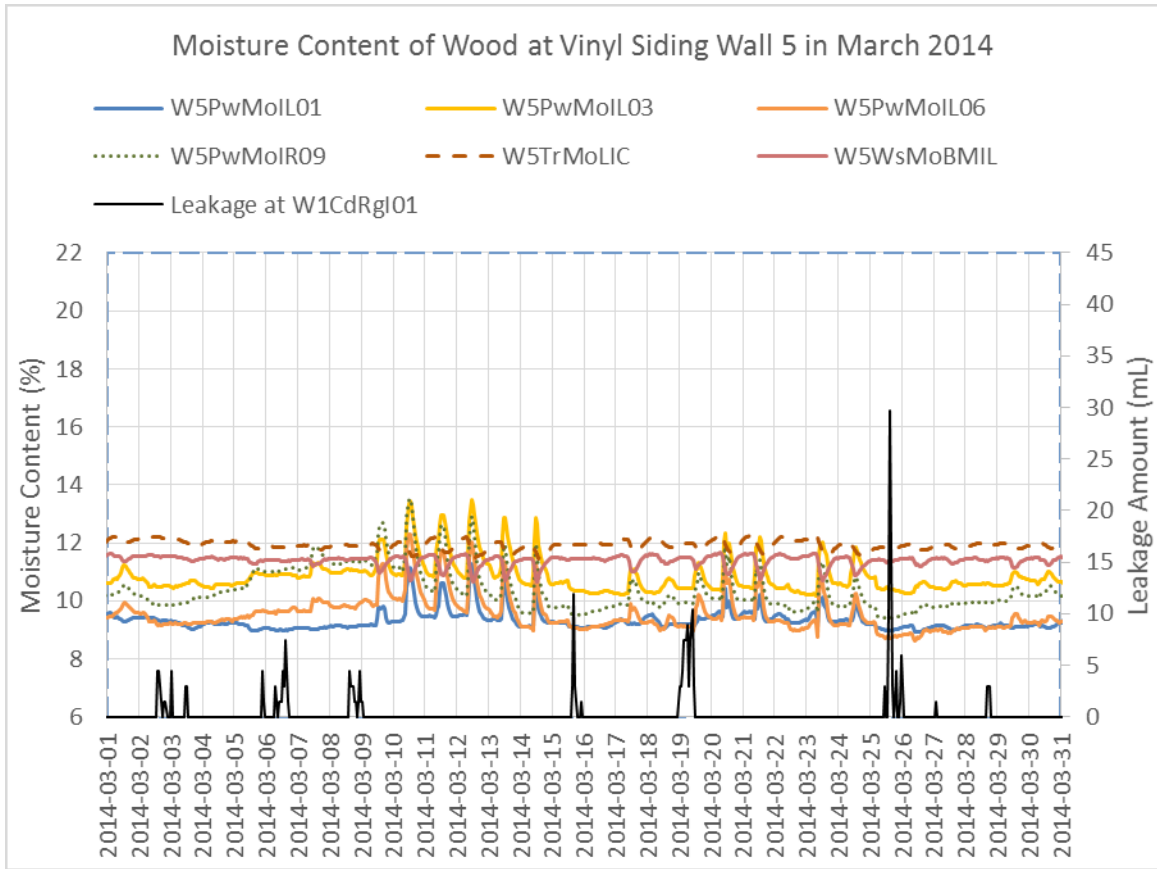
Figure 74. Close-up view of moisture content of plywood and wood framing at W5 in March 2014.

No rain penetration into the wood framing at W3, W4, and W5 appear to have affected the moisture content levels of their plywood sheathing boards, trimmer studs, window sill plates, and the bottom plates. In general, the moisture content range at the plywood is slightly larger than the moisture content range at the studs and plates, which is likely due to the fact that the plywood sheathing boards are closer to the outside air behind the vinyl sidings, and therefore, are affected by the humidity of the outside air and indirectly by the outside temperature fluctuations from the solar radiation.

The differences between the daily fluctuations of moisture contents in the plywood and those in the wood framing during the dry days are evident of vapour pressure gradient towards the outside. The low points of the moisture contents are observed from the moisture pins in the studs and plates,

while peaks are observed from the moisture pin in the plywood sheathing, indicating the movement of moisture from the stud and plates towards the plywood sheathing. The lack of these valleys and peaks during rainy days suggests that the vapour gradients were the effects of the solar radiation during the dry days.

5.6.4   Long Term Monitoring Sensors at Stucco Walls

5.6.4.1 Moisture Detection Tape Readings

The installation of the moisture detection tapes on the stucco walls is different from that on the vinyl siding walls. Small pieces of polyethylene film were installed to cover the MDT from being in contact with the stucco metal lath and the stucco itself as the presence of any electrical conductor other than the draining water is a source of error. Some slacks were allowed across the plastic film, i.e. the plastic film covers were not stretched tightly across the MDTs, to let potential draining water to pass in front of the MDTs. However, as shown in Figure 75, no significant voltage readings appear to be detected at W7, even though the bottom trough collector for W7 indicates that large amount of water drained through the stucco cladding, as shown previously in Figure 58. Therefore, it is concluded that the MDTs at W7 did not work as intended.
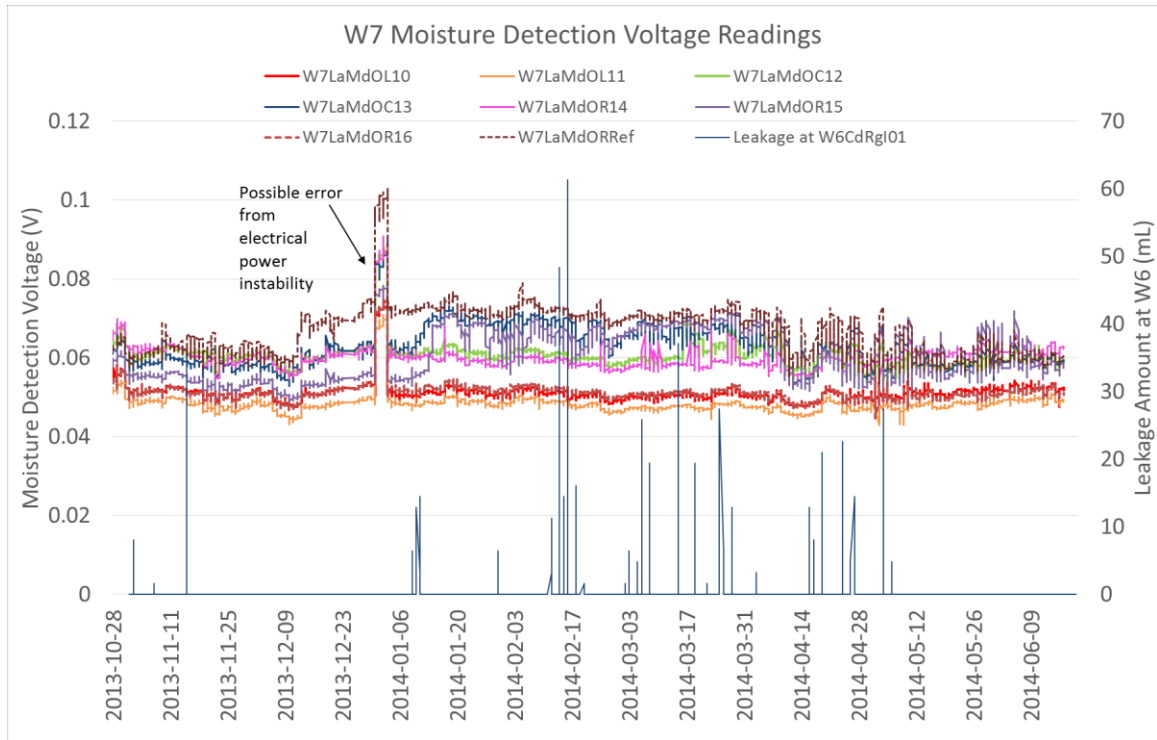
Figure 75. W7 moisture detection tape voltage readings from November 2013 – mid June 2014.

In contrast, at W8, two moisture detection tapes, W8SmMdOR13 and W8SmMdOR16, showed significant voltage readings, ranging from 1 V to 6V, starting from the beginning of the monitoring period, as shown in Figure 76. The high voltage readings were recorded both during rainy and dry days. These readings only decreased to 0 V during the spring season towards the summer.
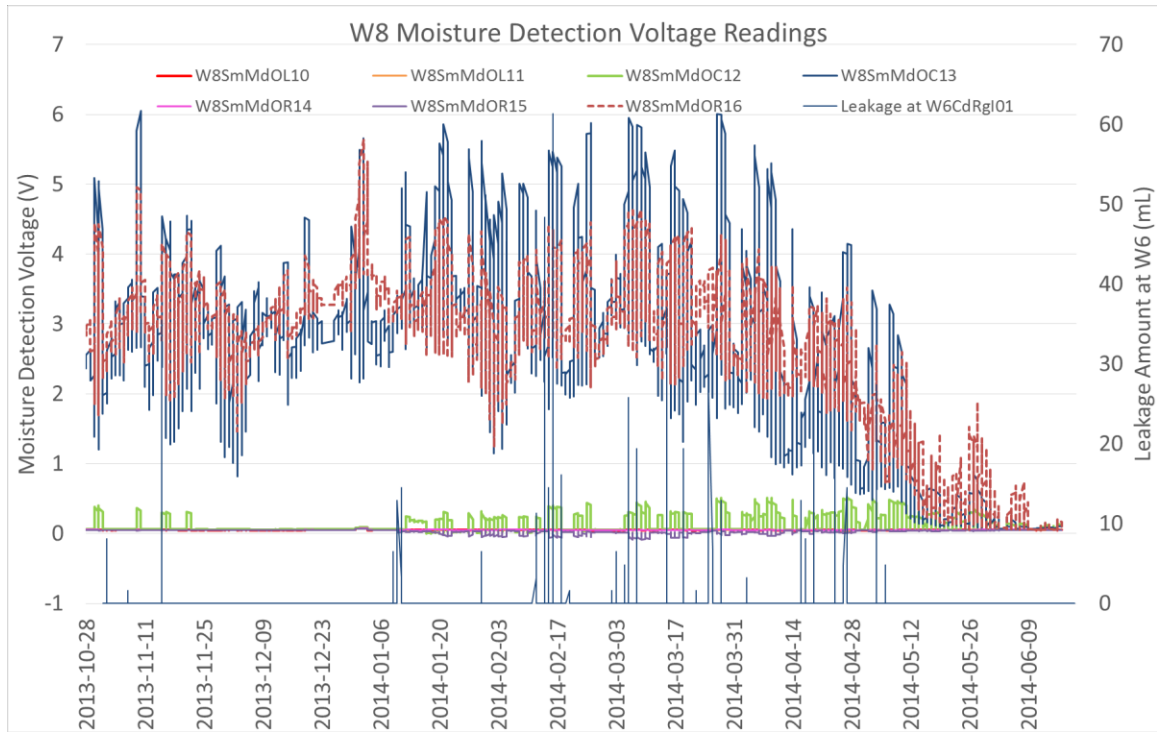
Figure 76. W8 moisture detection tape voltage readings from November 2013 – mid June 2014. Only W8SmMdOR13 and W8SmMdOR16 showed significant voltage readings.

5.6.4.2 Moisture Content Readings at Plywood Sheathing Boards

Figure 77 shows that the overall trends of the moisture contents (MC) at stucco wall W7 are similar to the MC trends at the vinyl siding walls, where fluctuations are observed during dry days and more stable readings are observed during rainy days. The moisture content levels in the plywood of stucco wall W7 vary between 8%-18% for pins at locations L01 and L04, while the moisture content of the pin at location L06 reaches as high as 22% in April 2014 with the daily fluctuations. The MC levels at the plywood of W7 only started to decrease after the end of the rain events in mid-May towards the beginning of summer.
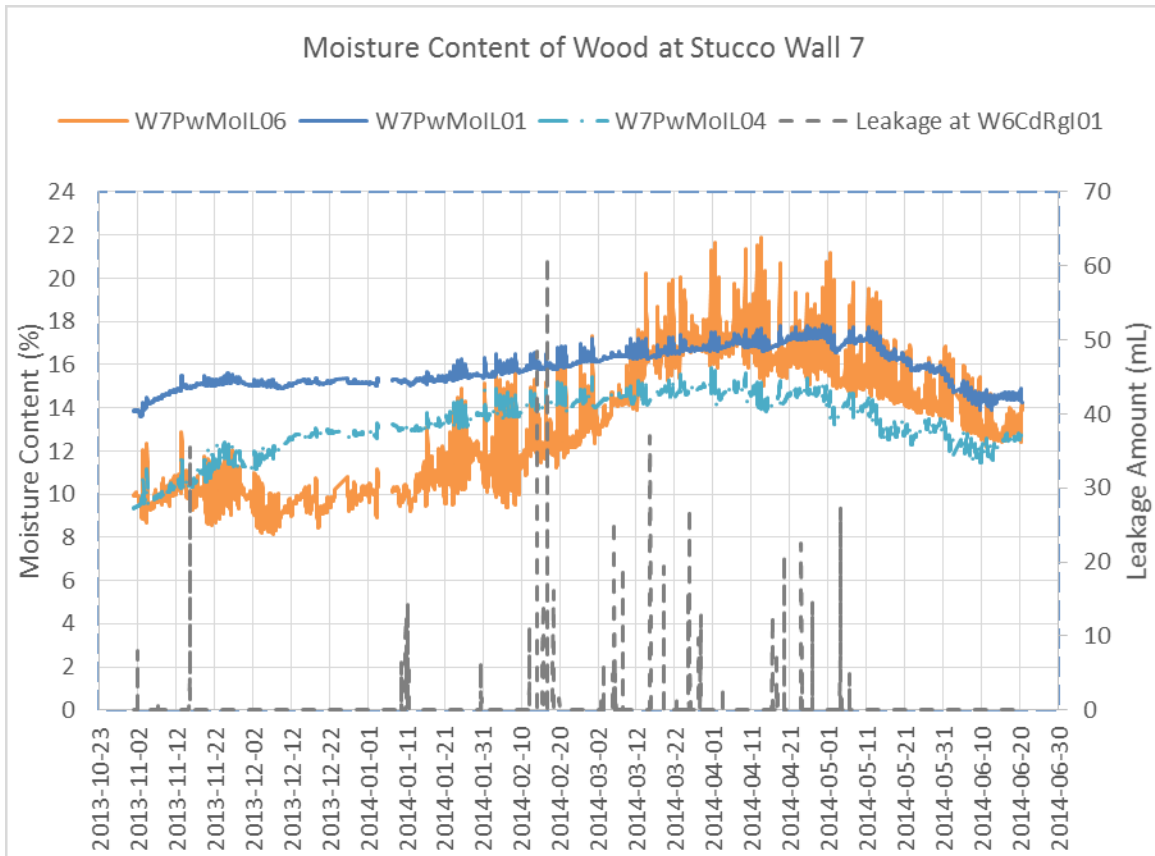
Figure 77. Moisture content of W7 plywood at moisture pin locations L01, L04, and L06, compared to the leakage amount at W6 as a reference to leakage events.

Valid W8 moisture pin sensor readings are only available starting from March 7, 2014 evening due to issues with the power and the data acquisition system. As shown in Figure 78, the moisture contents at the plywood are also higher than at the studs and plates, ranging from 13% to 18%, with a small increase towards mid-day. Comparing the moisture content levels at location 07, 08, and 09, it appears that, as the moisture pins are located higher up in the wall cavity, the moisture content levels decrease. The MC at location 09 is also similar to the MC at location 06, which is at approximately similar height. It appears that there is a vapor pressure gradient along the height of the wall cavity. In comparison with the vinyl siding walls, the moisture content fluctuations throughout a dry day are smaller in range.
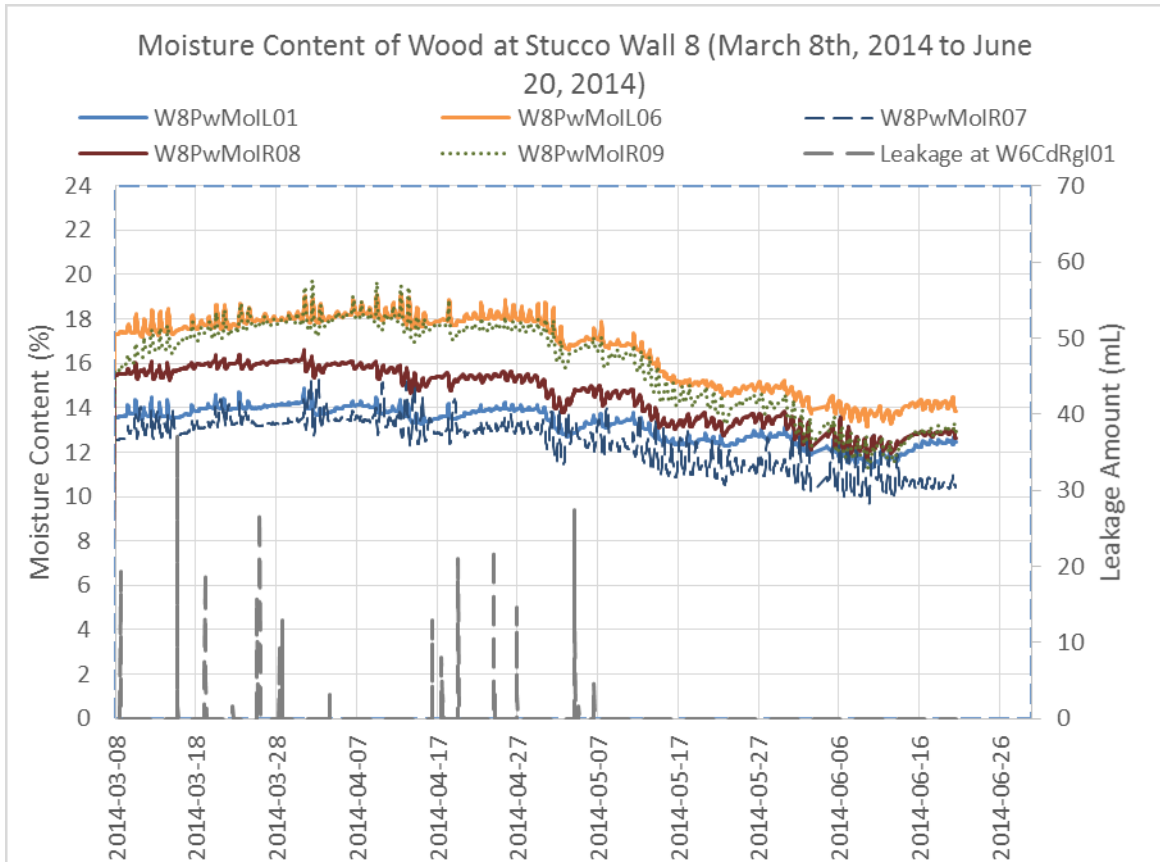
Figure 78. Moisture content of W8 plywood at upper moisture pin locations L01, L06, and L07, compared to the leakage amount at W6 as a reference to leakage events.

5.6.4.3 Moisture Content Readings at Studs, Window Sill Plates and Bottom Plates

Figure 79 shows the moisture content readings at the window sill plates (location BMIR) and the bottom sill plate of W7 (location TMIC). The moisture content readings at location TMIC average to approximately 11-12%, with no significant long-term variations. This level of MC is similar to those observed typically in vinyl siding walls. It appears that no leakage has affected the moisture content of this bottom plate. However, starting from April 1, 2014, the base line of the moisture content readings at window sill plate location BMIR increases gradually with larger fluctuations reaching the moisture content of 16%. Considering that this is the start of the drying period, these larger fluctuations and gradual increase are likely the effects from the daily temperature variations due to the outdoor air and solar radiation.
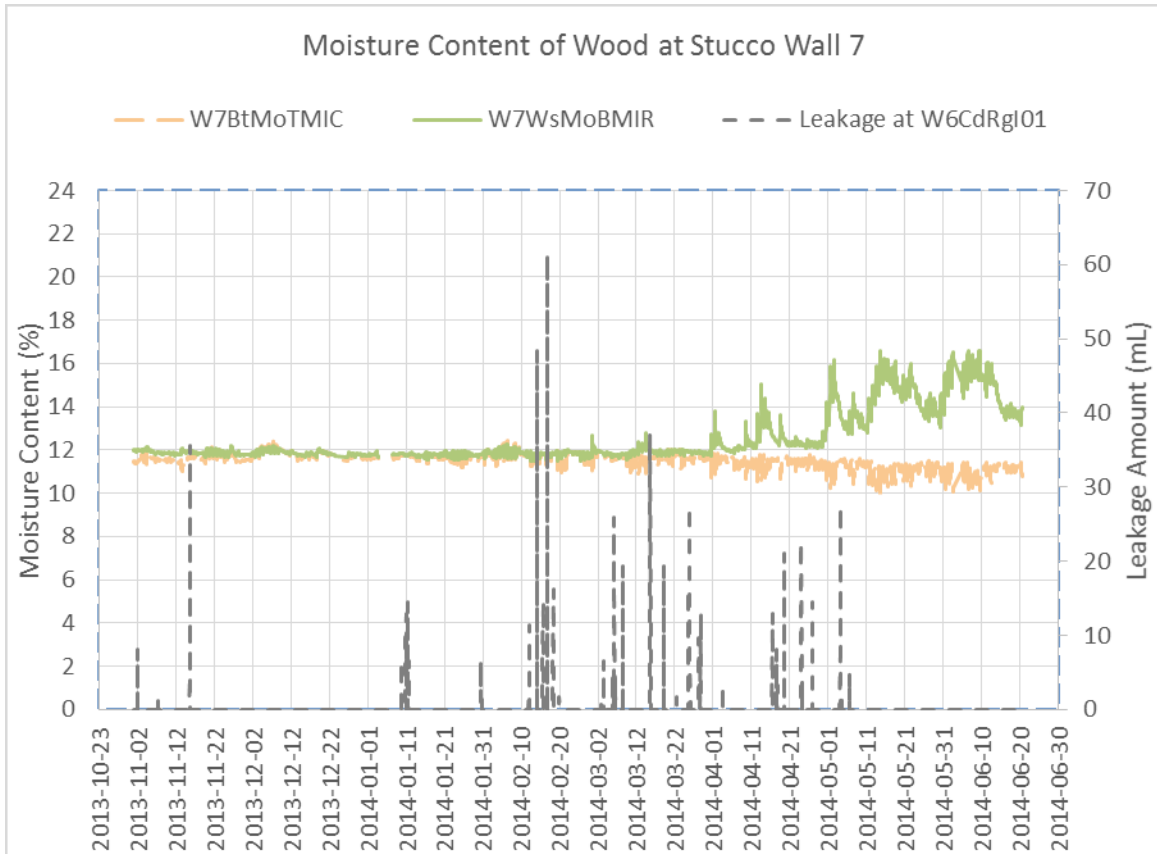
Figure 79. Moisture content of W7 window sill plate (location BMIR) and bottom plate (location TMIC), compared to the leakage amount at W6 as a reference to leakage events.

Figure 80 shows the trends of moisture content at a stud supporting the rough opening for the window around the monitored wall cavity at W7. Locations MIC and LIC are observed to initially vary closely together around 12% MC, similar to the level of MC observed at vinyl siding walls. However, starting from April 1, 2014, the moisture content at location MIC gradually increases and fluctuates at larger range, reaching to 16%. The trend at MIC is similar to the trend at the window sill plate location BMIR. Unfortunately, the moisture pin sensor readings at location UIC above the MIC are not available to help explain the cause of this observation, as the sensor is faulty.
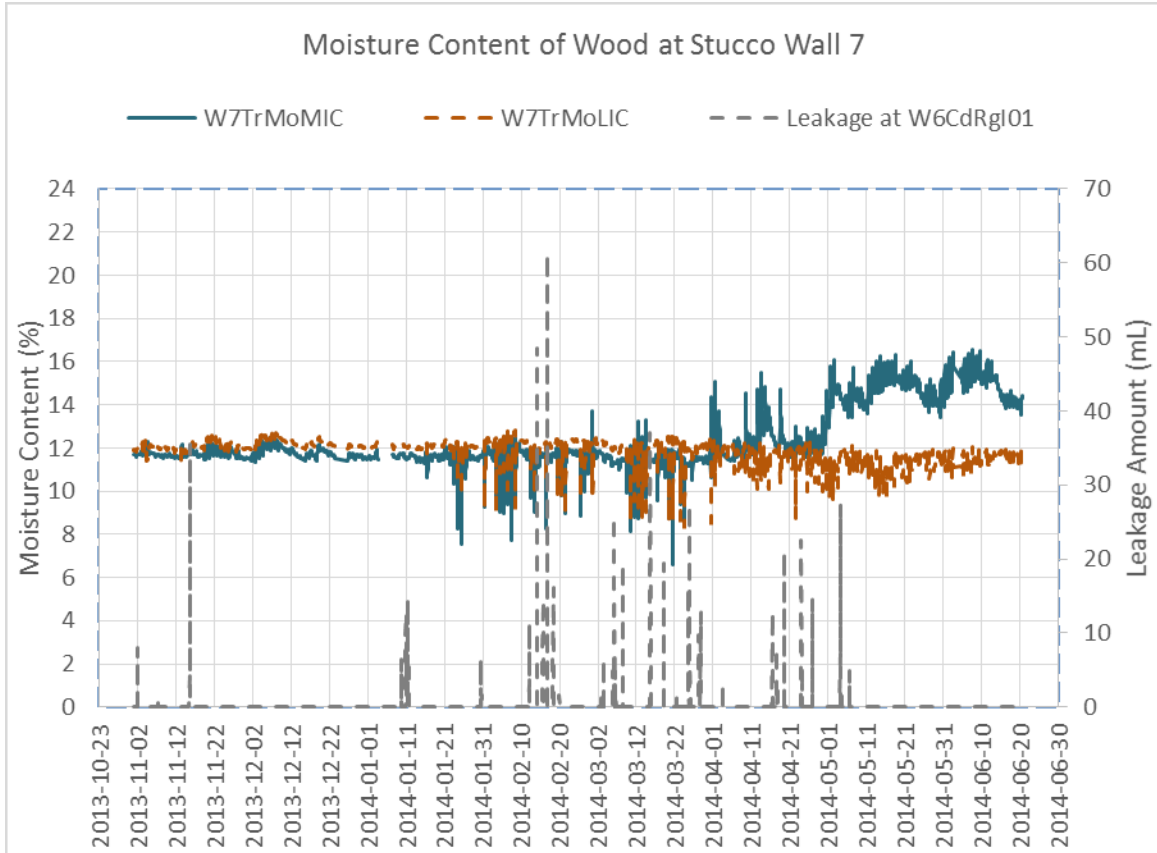
Figure 80. Moisture content of the W7 stud next to wall cavity (locations MIC and LIC), compared to the leakage amount at W6 as a reference to leakage events.

Figure 81 shows the trends of the moisture content readings at plate locations TMIC and BMIL at W8. The moisture contents of the studs and plates at W8 are generally similar as observed in W7, averaging at 12%. No gradual increase in MC is observed; therefore, it appears that no rainwater leakage has affected the window sill plate and bottom plate at W8 during this period of time.
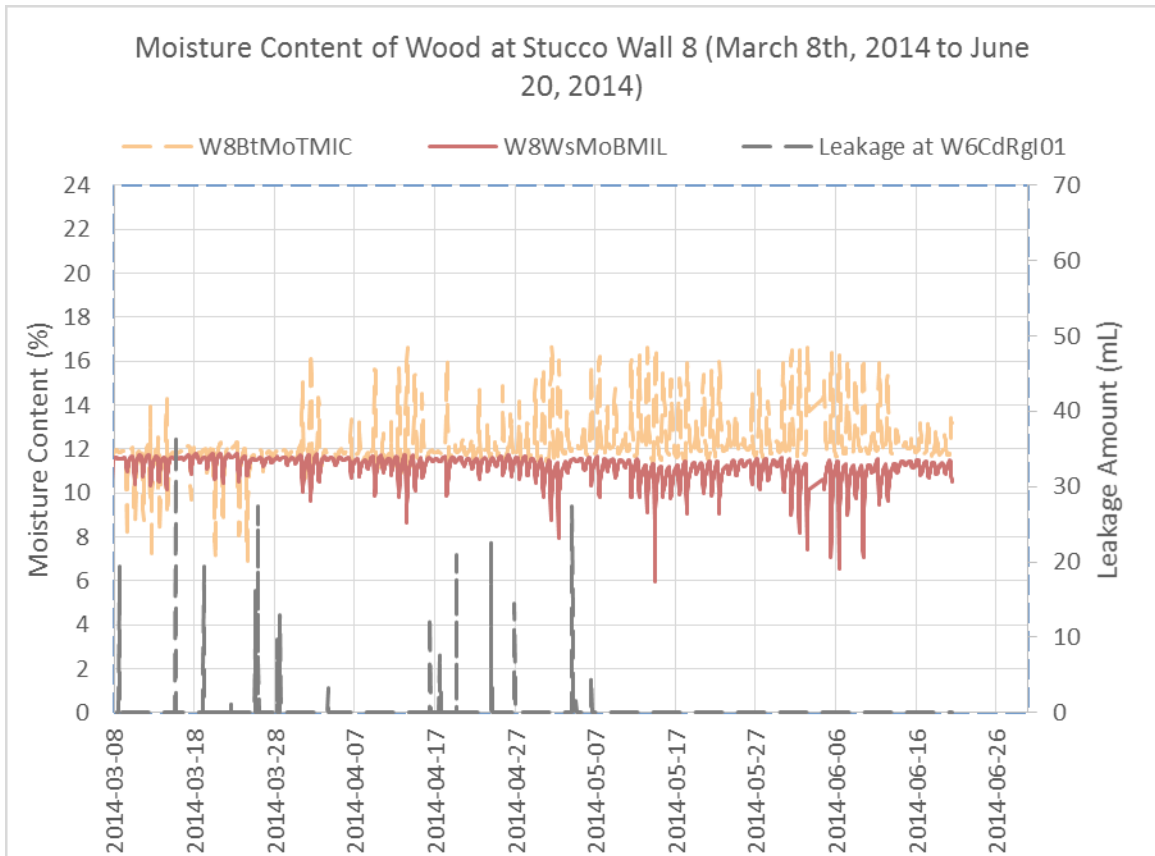
Figure 81. Moisture content of W8 window sill plate (locations BMIL) and bottom plate (location TMIC), compared to the leakage amount at W6 as a reference to leakage events.

Figure 82 shows the trends of moisture content at one of the stud that supports the rough opening for the window at W8. Locations UIC and MIC are observed to vary closely together. Similar to at W7, the moisture content readings at these two locations average to approximately 12%, with no significant long-term increase or decrease, indicating that this stud was not affected by any rainwater leakage. Towards the dry summer season, the moisture content levels at these pins fluctuate at larger range.
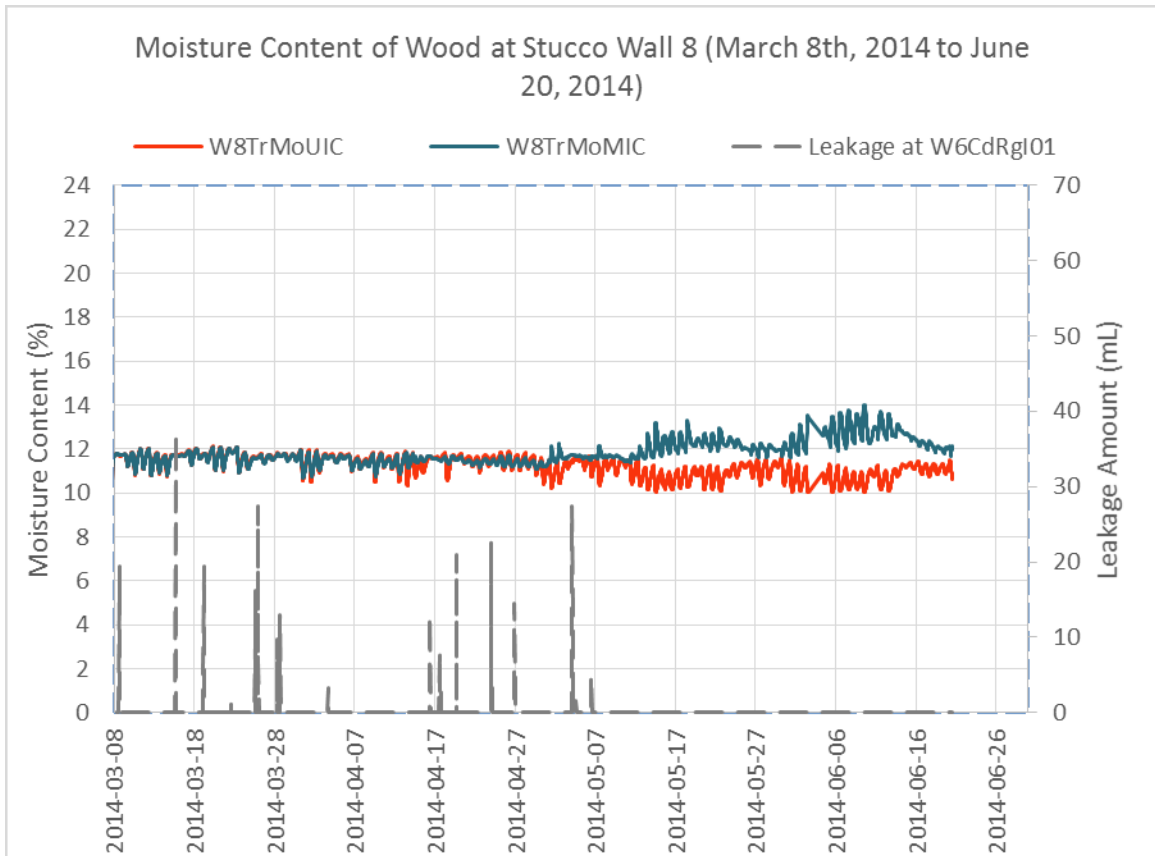
Figure 82. Moisture content of W8 stud next to wall cavity (locations UIC and MIC), compared to the leakage amount at W6 as a reference to leakage events.

5.6.4.4 Summary of Long Term Performance Observations at Stucco Walls

Figure 83 compares the close-up view of the moisture contents of W7 studs, plates and plywood sheathing during the month of March 2014. The daily fluctuations of MC during dry days are similar to the fluctuations observed in the vinyl siding walls. However, compared to the MC at vinyl sidings walls, the moisture content levels of the plywood sheathing at W7 are higher than the MC levels at studs and plates. Intuitively, the higher MC level at the plywood sheathing is likely due to the proximity of the building paper and the plywood to the moisture-retaining stucco mass, in contrast to the air space available between the vinyl sidings to the building paper. Overall, the average MC of the plywood at W7 is approximately 4% higher than the MC of the studs and plates.

133
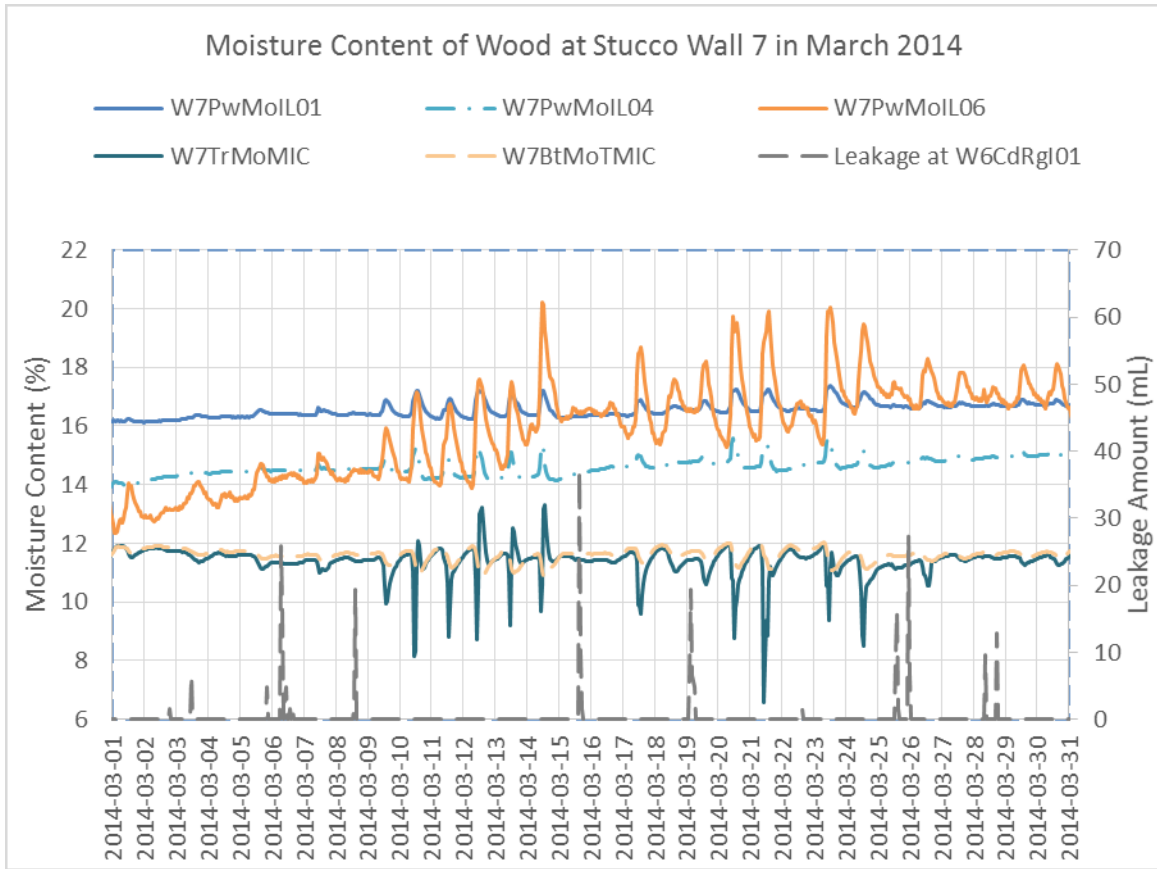
Figure 83. Close-up view of moisture content of plywood and wood framing at W7 in March 2014.

Figure 84 shows the close-up view of the moisture contents of W8 wood framing and plywood during March 2014. Again, similar to the daily fluctuations observed in W7 during dry days, these fluctuations are also observed in W8.
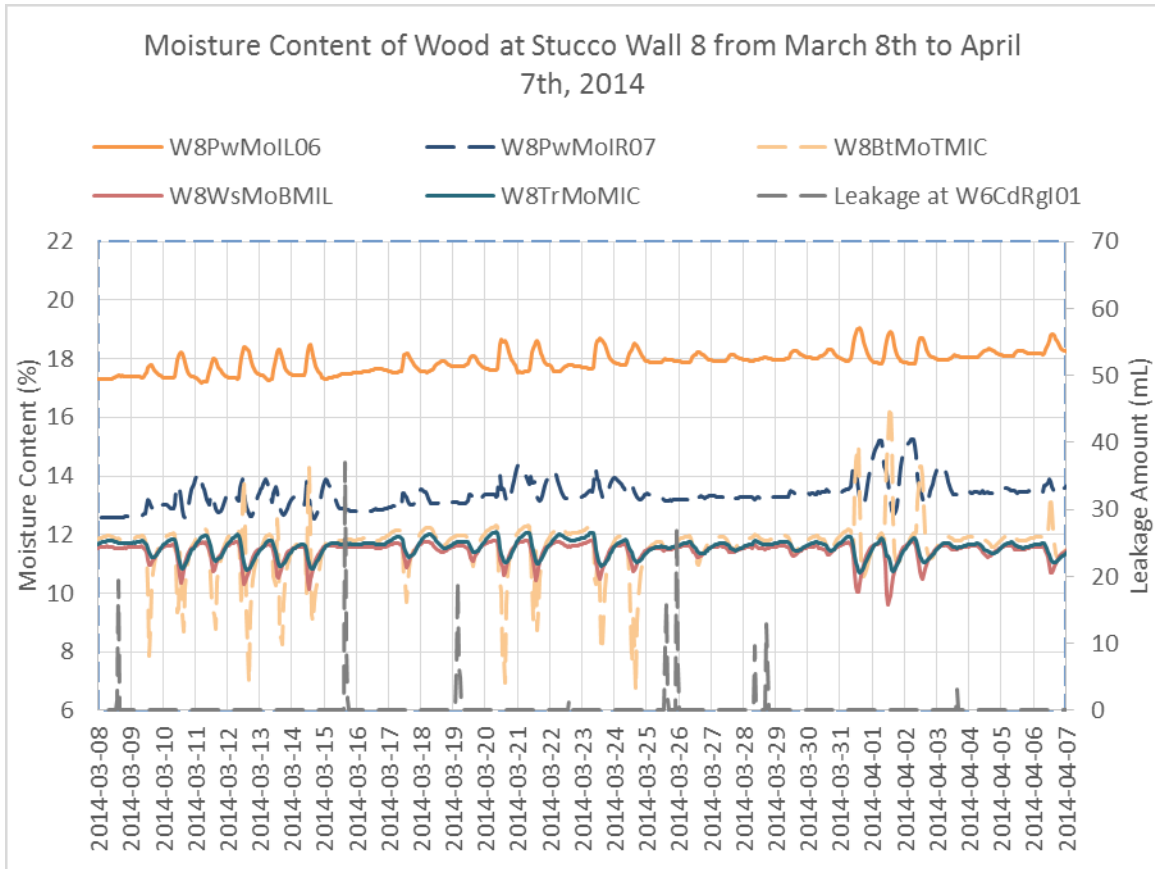
Figure 84. Close-up view of moisture content of plywood and wood framing at W8 in March 2014.

In spite of the higher plywood MC levels observed at the stucco walls here, the seasonal trends and the range of the moisture content levels are still comparable to the results published by Tariku, et al. (2015) for the test panel with no capillary break, which ranged from 5% to 20% overall.

The overall observations of the moisture content readings in the five walls are as following:

- The magnitude of the fifteen moisture content sensor readings at each wall could be grouped into two groups: the sensors on plywood sheathing and the sensors on studs and plates.

- In general, the moisture contents at the stud and plates moisture pins of all walls were around 11%-12%. The moisture content at the plywood moisture pins varied between 7%-14% at vinyl sidings walls and between 8%-22% at stucco walls.

- The moisture content of the plywood at the stucco walls was generally higher than the moisture content of the plywood at the vinyl siding walls. At stucco walls, the wet stucco cladding was in contact with the building paper on the outside of the plywood; the effect of rain as the moisture load on the moisture content in the plywood was evident. On the other hand, at vinyl siding walls, air spaces created by the profile of the vinyl sidings in front of the building paper contributed to the observed lower moisture content by providing a capillary break that reduces moisture transfer via direct contact of liquid water to the building paper.

- Where there was no leakage, it appeared that the plywood in vinyl siding walls was affected by the indoor and outdoor air humidity, in contrast to the plywood in stucco walls which seemed to be affected by the direct moisture transfer from the rain load to the plywood and by the solar radiation-driven vapour pressure gradients.

- For the most part, the daily fluctuations observed in the moisture contents of the wood framing and sheathing board showed uniform moisture distribution in the stud cavities of both vinyl siding walls and stucco walls. However, during the drying periods, in the stucco walls, the increase of the moisture content at the plywood was lagged (in several instances, by approximately 3 hours) from the time that the moisture content at the studs & plates decreased.

5.6.5   Relative Humidity in Wall Cavity of Long Term Performance Walls

The Relative Humidity (RH) inside the monitored wall cavities under each window sill was measured to observe the effect of the wetting and drying of the wood framing around the wall cavities. The overall relative humidity sensor readings in the wall cavities of the five walls are presented in Figure 85. The leakage amounts measured in W1 and W6 are included in the graph to indicate the occurrence of the rain events that may have contributed to the changes in relative humidity sensor readings, if any. Figure 85 shows that the RH inside the wall cavities of all of the

long term walls generally increases from winter to summer period. However, the rise in RH in the stucco walls is much higher than the increase in the RH of vinyl siding walls.
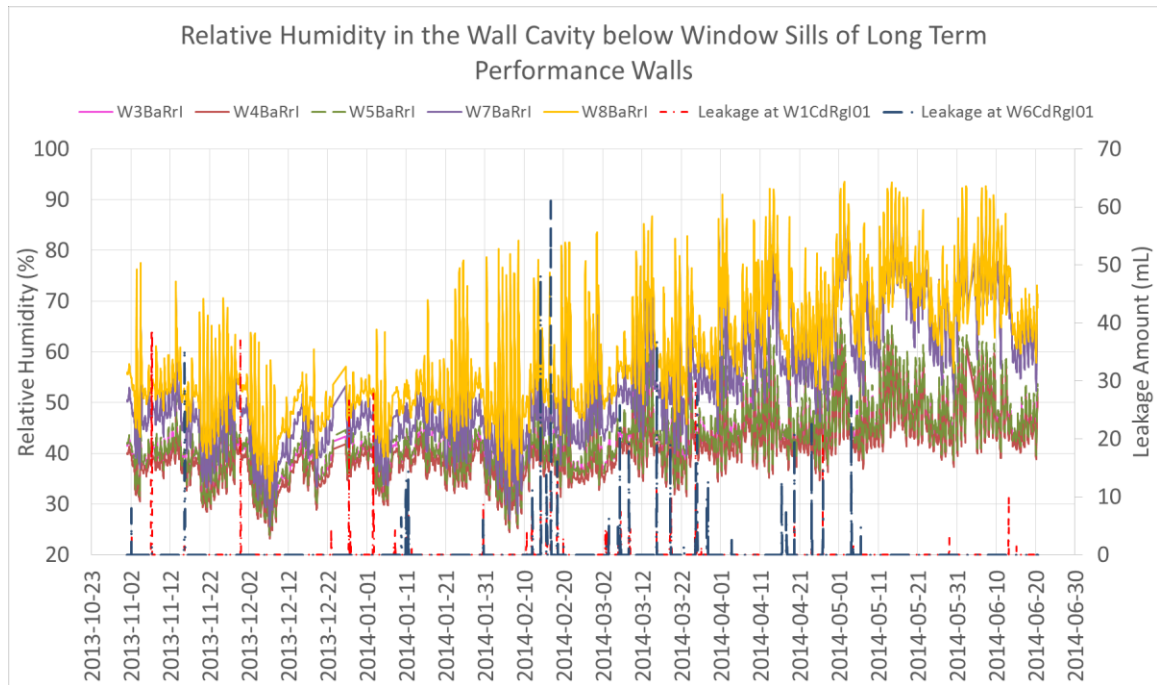
Figure 85. Relative humidity in the wall cavities of long term performance walls from November 2013 – mid June 2014.

A close-up view of the relative humidity sensor readings during the month of March 2014 is shown in Figure 86 to better compare the trends observed for vinyl siding walls and stucco walls. Where the leakage events occur in W1 and/or W6, as indicators of rainy days and low solar radiation, the RH levels only fluctuates within approximately 10% range. Overall, the RH levels in the stucco walls start at approximately 10% higher than the RH levels in the vinyl sidings. The RH levels in the stucco walls also fluctuate over a larger range. For example, as shown in Figure 86, on March 21, 2014, the RH change in the stucco wall is approximately 36%, compared to the RH change in the vinyl sidings walls of approximately 24%.
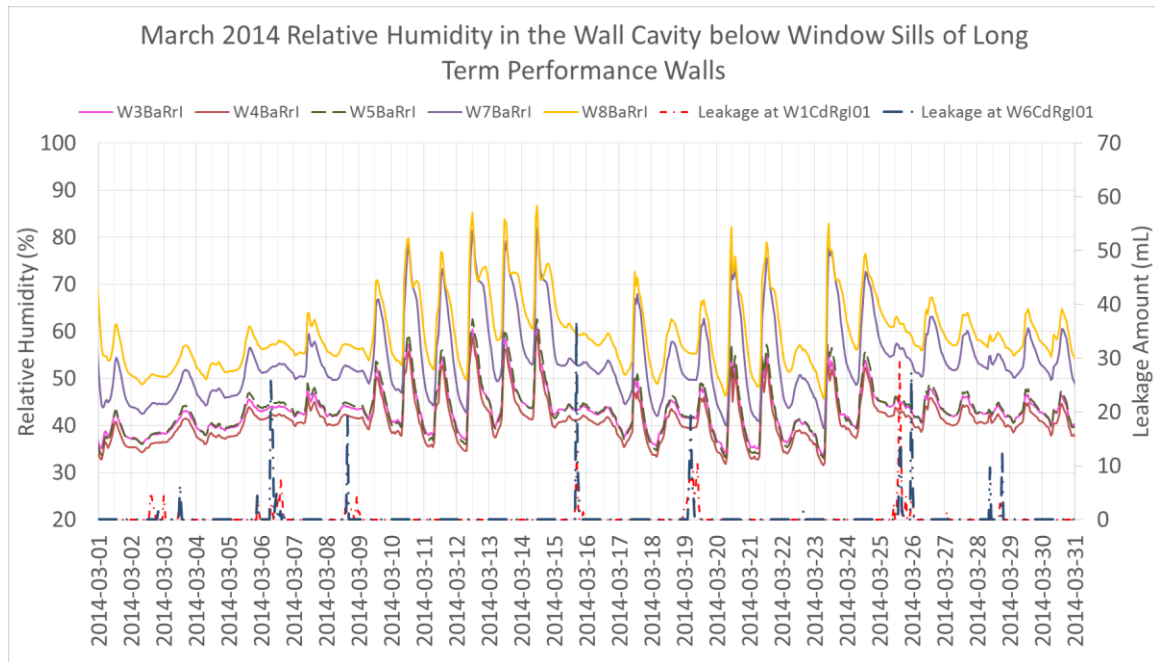
Figure 86. Close-up view of relative humidity in the wall cavities of long term performance walls in March 2014.

This difference in fluctuation range may be attributed to the difference in heat transfer mechanism at stucco walls and vinyl siding walls. In the stucco walls, the solar heat gain was directly conducted through the stucco to the plywood, whereas in the vinyl siding walls, the heat transfer was influenced by the air gap between the vinyl sidings and the sheathing membrane. Due to this latter mechanism, the heat gain by the sheathing board of the vinyl sidings walls was lower than that in stucco walls. Therefore, the large fluctuations observed in the stucco walls were mainly due to the heating and cooling cycle of the sheathing board by solar radiation. The daily fluctuation in RH during the dry days and rainy days further showed the effect of solar radiation on the uniform moisture distribution inside the wall cavities, with the plywood sheathing as the main moisture buffer and later followed by the studs and plates.

As a conclusion to the discussion on the long-term performance monitoring walls, a holistic view of the moisture and solar heat load on W7 is reviewed. Figure 87 is a plot that compares the moisture content at selected locations on W7, the amount of water draining over the building paper at W7,

and the leakage amount at W6 corner defect location over time to indicate the effect of the WDR on the stucco wall W7 with similar replicated corner sealant defect. In this graph, the slight increases in the moisture content levels of the plywood appeared to coincide with the higher amounts of water draining on the building paper and collected by the bottom trough, in particular from early January to early May 2014. The seasonal increase of moisture content levels in this plywood was therefore likely due to the increased rain load on the stucco walls.

The moisture content levels at plywood location 06 also increased starting early January 2014. However, the trend was different compared to the moisture content at the other plywood locations. The highest increase was in February 2014, coinciding with the frequent full collections of drainage water by the bottom trough. Reviewing Figure 22 and Figure 25, moisture pin location 06 was very close to the aluminum bottom trough. It is likely that the high moisture content readings at location 06 was due to this close vicinity of the moisture pin to the full bottom trough. In addition, the bottom trough was made of aluminum metal, which would increase the heat conduction from the solar radiation on the stucco cladding to the plywood, causing the large daily fluctuation range of the moisture content level.
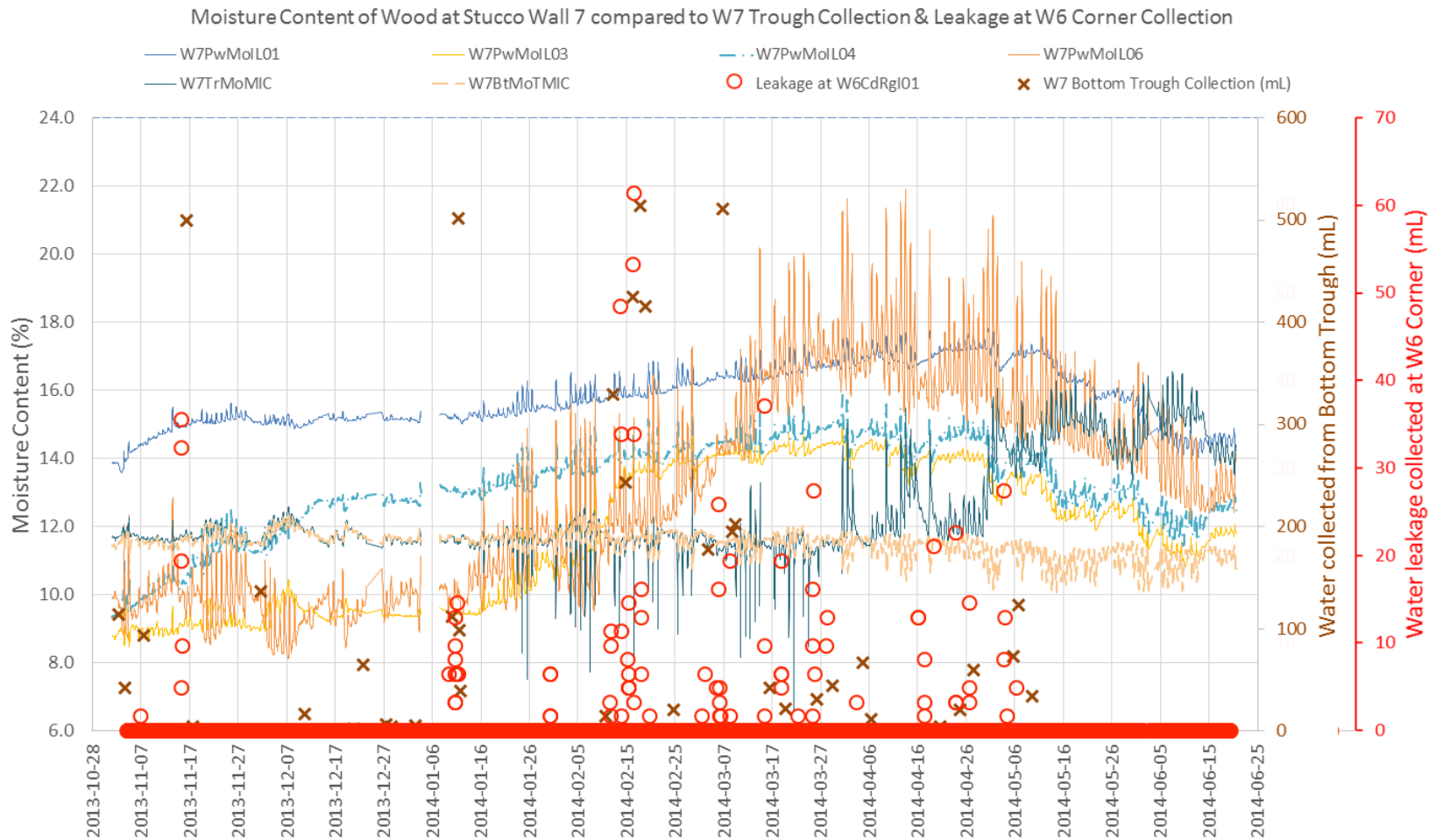
Figure 87. Comparison of the moisture content of wood framing around W7 wall cavity below corner window sill defect to the bottom trough water collection at W7, and to leakage amount at W6 Corner collection.

At the start of the drying period, i.e. in this case starting mid-May 2014, the moisture content level of the plywood decreased. However, the moisture content of the trimmer stud increased with fluctuations at W7TrMoMIC. This has also been shown previously in Figure 80. A similar trend was observed at the window sill plate location W7WsMoBMIR. Figure 88 was plotted to examine the possible cause of the increase in moisture contents at locations MIC and BMIR, which were on the middle of the trimmer stud and on the right side of the window sill plate, respectively.

The relative humidity in the stud cavity of stucco wall W7 and the temperature on the outside surface of the stucco cladding of W7 were plotted together with the readings from these two moisture pins. The temperature of the exterior of the stucco reached above 40°C in May 2014. In addition, the trends of the temperature at the surface of the stucco appeared to coincide with the relative humidity in the stud cavity. The increase in the moisture content levels of these two moisture pins also coincided with the trends in relative humidity levels in the wall cavities. The possibility of vapour pressure gradient along the height of the wall cavity was observed for W8 and was shown in Figure 78. It is likely that the higher moisture content levels at the upper wood framing components were due to this vapour pressure gradient and the movement of the moisture upwards towards the window sill plate carried by the hotter air during sunny days.
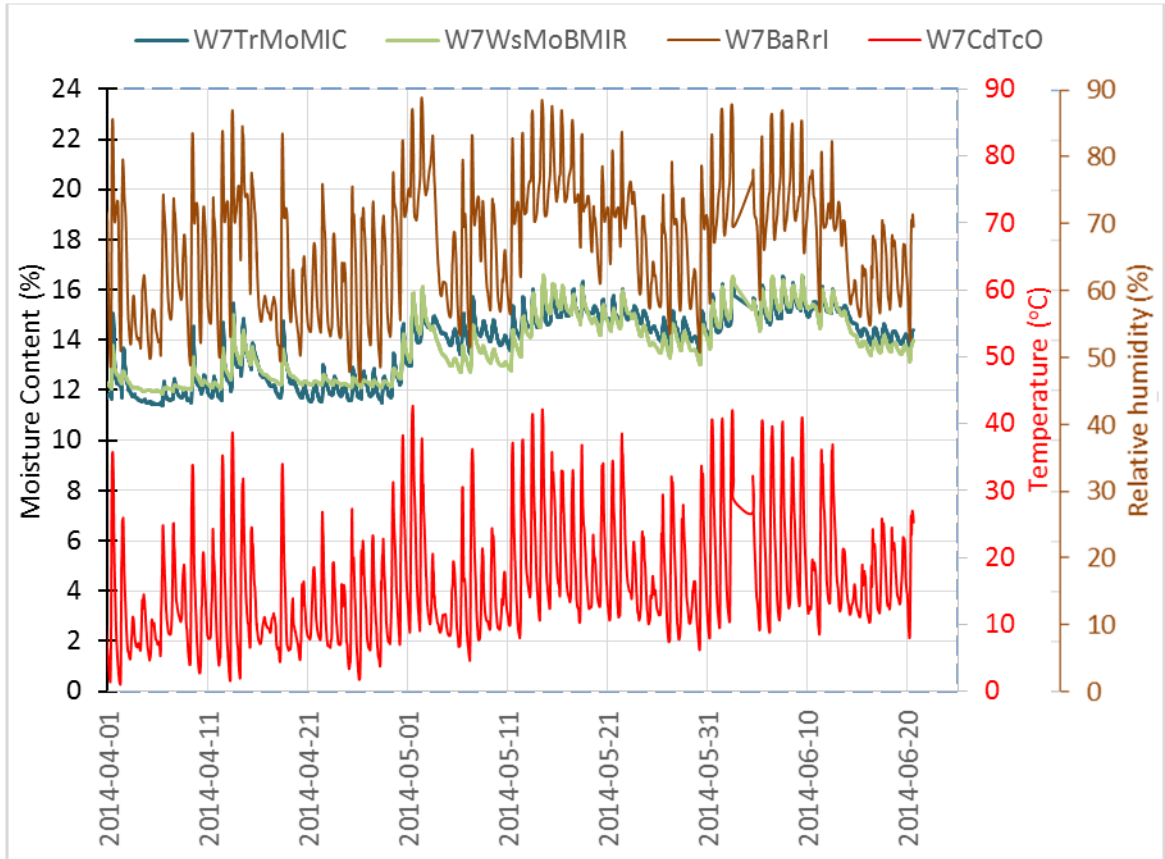
Figure 88. Moisture contents of trimmer studs at middle location MIC and window sill plate location BMIR, relative humidity in the stud cavity of stucco wall W7 by sensor W7BaRrI, and outside temperature measured at thermocouple W7CdTcO located on the exterior surface of stucco from April 1st, 2014 to June 21, 2014.

CHAPTER 7: CONCLUSIONS AND FUTURE WORK

The primary focus of this field experimental study was to estimate the potential moisture rain load that may contribute to a leakage into a wall assembly. The most vulnerable location of entry for rain penetration is confirmed to be at the sill corner of windows, rather than along the mid-lengths of the sill. By common sense, this may also apply to the sill corner of doors and other polygon-shaped wall penetration requiring J-trim or casing beads or other channel-like geometry. At these sill corner locations, the installation of extra moisture barrier protection is recommended.

Predicting potential moisture rain load contributing to leakages into a wall assembly is complicated and appears to depend on rain runoff in addition to the wind driven rain. At sill corner location of vinyl sidings wall, the leakage amount appears to depend largely on the wind-driven rain and the duration of the wind-driven rain. On the other hand, as the absorptive stucco cladding retains much of the WDR and the statistical model indicates dependence on horizontal rain amount and on the wind speed normal to the wall, rain run-off effect is suspected to be a factor. However, the wind-driven rain amount seems to be the primary predictors for both the W1 and W6 corner leakage amounts.

Using the simple plot of the leakage amount to the WDR amount, the leakage amount at W1 is approximately estimated to be 0.55% of WDR, while at W6 corner, the leakage amount is approximately 1.5% of WDR. Compared to the maximum limit set in ASHRAE 160 Standard, the leakage amount estimated at this particular stucco wall sill corner detail is one and a half times higher than the limit.

The moisture load and path of the leakage at the sill corner of W1 can be estimated to be primarily by the WDR above the window, with the WDR eventually runs off and is captured by the head J-trim and directed down the jamb J-trim towards the sill corner location. This moisture load only affects the wood components of the wall assembly if a leakage entry point through the wall sheathing membrane has existed along the moisture load path down the wall and around the sill corner locations. This is because the moisture load is generally not retained by vinyl sidings

cladding, unless a construction defect creates a container that can hold this moisture load next to the sheathing membrane for a longer period of time.

On the other hand, the path of the moisture load on the stucco wall to the sill corner location appears to be more complex. Any WDR and horizontal rain running off the surface of the stucco above the window are likely retained and are suspected to travel within the mass of stucco and behind the stucco cladding, until these moisture loads enter the sill corner collection location with the pressure from the wind speed normal to the wall.

The collected drainage water behind the cladding provides further knowledge on the relative amount of rainwater that the different types of wall cladding have to manage. Large amount of water goes past the acrylic-finished stucco cladding, compared to the minimal amount that is experienced behind the vinyl siding panels. In this manner, the design intent of the vinyl siding panels geometry of shedding surface runoff away from the wall assembly appears to function as intended. However, it fails at the interface around windows. The comparison between the collected drainage water at the vinyl sidings wall panels with head drip cap vs no head flashing emphasize again the importance of the principle of rainwater deflection. The channel-like J-trim accessories at the head flashing acts like a trough and the jamb J-trims further direct the rainwater to the vulnerable sill corners. Where the gap between the window frames and the J-trims are blocked by the sealants, the exit path of rainwater is further blocked and the water may be directed on to the water resistive barrier instead, which ultimately add to the moisture load source for potential rain penetration.

On the long term performance walls, the moisture contents of the wood sheathing are kept wetter longer at the stucco walls than at the vinyl sidings walls. This is likely due to the presence of air gap channels behind the vinyl sidings that may accelerate the evaporation of the moisture on the sheathing membrane and the sheathing board; while at the stucco walls, the stucco mass retains the higher moisture close to the sheathing membrane and board, keeping the plywood wetter for longer

period of time. This highlights the benefits of having an air gap or capillary break between the back of the cladding and the sheathing membrane.

At stucco walls, despite the high leakage amount of just below 1000 mL, the high solar exposure on the South East façade helps accelerating the drying process. However, stucco walls on North facing façade would be in higher risk of deterioration.

Overall, the daily solar radiation and air temperature fluctuations typically lead to a cycle of moisture content rise and fall during the dry days. The high humidity during rainy days reduces the diurnal fluctuations and raises the moisture content. At areas exposed to higher moisture load, the moisture content levels remain high during long periods of rain, and only decreases after long period of dry days.

The results from the bottom trough water collection under the stucco walls W7 and W8 and the results from the leakage gauge at the stucco wall W6 corner location show that the concealed barrier design of the stucco wall itself may be the more critical issue compared to the focus on a missing sealant defect issue near the high moisture load-exposed sill corner area. Further testing is needed to validate this important finding.

The data from the bottom trough water collectors have shown that the sheathing membrane experience large amount of moisture load. In addition, solar-driven vapour diffusion drive towards the stud cavity occurs during the drying of the retained moisture load in these acrylic-finished stucco walls. Combined with the large numbers of nails creating additional water entry paths into the wood framing through the sheathing membrane and the wind pressure on the wall, leakages due to rain penetration are likely to occur at concealed barrier stucco walls, not only at window interfaces, but also on the field of the walls. A future study on this likelihood would be beneficial.

Although rain runoff on the surface of the cladding was not quantified in this study, how much the rain runoff contributes to the leakage will likely depends on the material of the cladding, the geometry around the window or other wall penetration. Typically, rain runoff can be captured by a horizontal length of trough across the cladding. However, this method of quantifying the runoff

would have compromised the amount of potential moisture rain load measured by at the leakage gauge. Future studies on quantifying the runoff amount have been planned on the same SE façade of the BETF. Finally, validations of the leakage models will be done by analyzing the new sets of data that have been collected over the fall of 2014 and the winter of 2015.

REFERENCES

Abuku, M., Blocken, B., & Roels, S. (2009a). Moisture response of building facades to wind-driven rain: field measurements compared with numerical simulations. *Journal of Wind Engineering and Industrial Aerodynamics, 97*(5), 197-207.

Abuku, M., Janssen, H., Poesen, J., & Roels, S. (2009b). Impact, absorption and evaporation of raindrops on building facades. *Building and Environment, 44*(1), 113-124. doi: 10.1016/j.buildenv.2008.02.001

Alberta Municipal Affairs & City of Calgary. (2008). Building Envelope Survey. Alberta.

ASHRAE Standard. (2009). ASHRAE Standard 160-2009: Criteria for Moisture Control Design Analysis in Buildings " *American Society of Heating, Refrigerating and Air-Conditioning Engineers, Atlanta*.

ASTM. (2006). ASTM D4756-06 *Standard Practice for Installation of Rigid Poly(Vinyl Chloride) (PVC) Siding and Soffit*. West Conshohocken, PA: ASTM International.

ASTM. (2007). ASTM E2112-07 *Standard Practice for Installation of Exterior Windows, Doors and Skylights*. West Conshohocken, PA: ASTM International.

ASTM. (2014). ASTM C1063-14 *Standard Specification for Installation of Lathing and Furring to Receive Interior and Exterior Portland Cement-Based Plaster*. West Conshohocken, PA: ASTM International.

ASTM. (2015). ASTM C926-15 *Standard Specification for Application of Portland Cement-Based Plaster*. West Conshohocken, PA: ASTM International.

Beijer, O. (1977). *Concrete walls and weathering*. Paper presented at the RILEM/ASTM/CIB symposium on evaluation of the performance of external vertical surfaces of buildings, pp. 67-76.

Best, A. (1950a). The size distribution of raindrops. *Quarterly Journal of the Royal Meteorological Society, 76*(327), 16-36.

Best, A. C. (1950b). Empirical formulae for the terminal velocity of water drops falling through the atmosphere. *Quarterly Journal of the Royal Meteorological Society, 76*(329), 302-311.

Blocken, B., & Carmeliet, J. (2007). *Wind-Driven Rain Assessment on Buildings Using Climatic Data Sets : What Time Resolution is Needed ?* Paper presented at the Thermal Performance of Exterior Envelopes of Whole Buildings X International Conference, Florida, U.S.A.

Blocken, B., & Carmeliet, J. (2010). Overview of three state-of-the-art wind-driven rain assessment models and comparison based on model theory. *Building and Environment, 45*(3), 691-703. doi: http://dx.doi.org/10.1016/j.buildenv.2009.08.007

Blocken, B., & Carmeliet, J. (2012). A simplified numerical model for rainwater runoff on building facades: Possibilities and limitations. *Building and Environment, 53*, 59-73. doi: 10.1016/j.buildenv.2012.01.010

Blocken, B., & Carmeliet, J. (2015). Impact, runoff and drying of wind-driven rain on a window glass surface: Numerical modelling based on experimental validation. *Building and Environment, 84*, 170-180.

Blocken, B., Derome, D., & Carmeliet, J. (2013). Rainwater runoff from building facades: A review. *Building and Environment, 60*(0), 339-361. doi: http://dx.doi.org/10.1016/j.buildenv.2012.10.008

Blocken, B., Desadeleer, W., & Carmeliet, J. (2003). *Numerical study of façade disfigurement by driving rain*. Paper presented at the Proceedings of the Second International Building Physics Conference.

Bomberg, M., Rousseau, M., Desmarais, G., Nicholls, M., & Lacasse, M. A. (2002). Report from Task 2 of MEWS Project-Description of 17 Large Scale Wall Specimens Built for Water Entry Investigation in IRC Dynamic Wall Testing Facility.

Carmeliet, J., & Blocken, B. (2004). *Driving Rain, Rain Absorption, and Rainwater Runoff for Evaluating Water Leakage Risks in Building Envelopes*. Paper presented at the

Performance of Exterior Envelopes of Whole Buildings IX, Conference Proceedings, pp. 5-10.

Carmeliet, J., Rychtarikova, M., & Blocken, B. (2006, August 27 - 31, 2006). *Numerical modelling of impact, runoff and drying of wind driven rain on a window glass surface.* Paper presented at the Third International Building Physics Conference, Montreal, Quebec, pp. 905-912.

CEN. (1997). Hygrothermal performance of buildings - Climatic data - Part 3: Calculation of a driving rain index for vertical surfaces from hourly wind and rain data. *Draft prEN 13013-3*.

Choi, E. (1994a). Determination of wind-driven-rain intensity on building faces. *Journal of Wind Engineering and Industrial Aerodynamics, 51*(1), 55-69.

Choi, E. C. (1994b). Characteristics of the co-occurrence of wind and rain and the driving-rain index. *Journal of Wind Engineering and Industrial Aerodynamics, 53*(1), 49-62.

Choi, E. C. (1994c). Parameters affecting the intensity of wind-driven rain on the front face of a building. *Journal of Wind Engineering and Industrial Aerodynamics, 53*(1), 1-17.

Choi, E. C. (1998). Criteria for water penetration testing. In R. Kudder & J. Erdly (Eds.), *Water leakage through building facades* (Vol. 1314, pp. 3-16): American Society of

Choi, E. C. (1999). Wind-driven rain on building faces and the driving-rain index. *Journal of Wind Engineering and Industrial Aerodynamics, 79*(1), 105-122.

Choi, E. C. (2000). Variation of wind-driven rain intensity with building orientation. *Journal of Architectural Engineering, 6*(4), 122-128.

City of Woodbury Building Inspection Division. (2011). Stucco in New Residential Construction: A Position Paper Includes Updates to Original Information. Woodbury, Minnesota.

Cope, L., & Horst, M. (2014). *Common sources of distress in stucco facades.* Paper presented at the 29th RCI International Convention, Anaheim, CA.

Couper, R. (1972). *Drainage from vertical faces.* Paper presented at the Symposium on Wind-Driven Rain and the Multi-Storey Building.

CSA. (2007). CSA A440.4-07 *Window, door, and skylight installation* (Vol. CSA A440.4-07): Canadian Standards Association.

Dalgliesh, W., Cornick, S., Maref, W., & Mukhopadhyaya, P. (2005). *Hygrothermal performance of building envelopes: Uses for 2D and 1D simulation.* Paper presented at the Proc., 10th Conf. on Building Science and Technology.

Dingle, N., & Lee, Y. (1972). Terminal fallspeeds of raindrops. *Journal of Applied Meteorology, 11*(5), 877-879.

El-Shimi, M., White, R., & Fazio, P. (1980). Influence of facade geometry on weathering. *Canadian Journal of Civil Engineering, 7*(4), 597-613.

Erkal, A., D'Ayala, D., & Sequeira, L. (2012). Assessment of wind-driven rain impact, related surface erosion and surface strength reduction of historic building materials. *Building and Environment, 57*(0), 336-348. doi: http://dx.doi.org/10.1016/j.buildenv.2012.05.004

Garden, G. K. (1963). Rain penetration and its control *Canadian building digest 40* (pp. 4): National research council of canada.

Google Maps (Cartographer). (2015). British Columbia Institute of Technology, Burnaby Campus [Satellite Map]. Retrieved from https://www.google.ca/maps/place/BCIT/@49.2424357,-123.0002577,162m/data=!3m1!1e3!4m2!3m1!1s0x548676e1f29254bb:0x1bca2f3260d1a28c!6m1!1e1

Hall, C., & Hoff, W. D. (2011). *Water transport in brick, stone and concrete*: CRC Press.

Johansson, P., Svensson, T., & Ekstrand-Tobin, A. (2013). Validation of critical moisture conditions for mould growth on building materials. *Building and Environment, 62*(0), 201-209. doi: http://dx.doi.org/10.1016/j.buildenv.2013.01.012

Krpan, R. (2013). *Wind-driven Rain on Buildings in Metro Vancouver: Parameters for Rain Penetration Testing of Window Assemblies.* (MASc.), Concordia University, Montreal, QC, Canada.

Krus, M., Michael, S., & Sedlbauer, K. (2010). *Comparative Evaluation of the Predictions of Two Established Mold Growth Models.* Paper presented at the Thermal Performance of the Exterior Envelopes of Whole Buildings XI International Conference.

Lacy, R. E. (1965). Driving-rain maps and the onslaught of rain on buildings: Building Research Station.

Lawton, M. D. (Ed.). (1999). *Reacting to Durability Problems with Vancouver Buildings*. Ottawa: Institute for Research in Construction, National Research Council Canada.

Leslie, N. P. (2007). *Evaluation of Water-Resistive Barrier Performance in Stucco Walls.* Paper presented at the Thermal Performance of Exterior Envelopes of Whole Buildings X International Conference, Florida, U.S.A.

Mao, Q., Fazio, P., & Rao, J. (2011). A limit state design (LSD) approach for comparing relative drying performance of wood-frame envelope systems with full-scale lab testing. *Building and Environment, 46*(3), 797-806. doi: http://dx.doi.org/10.1016/j.buildenv.2010.10.015

McClanaghan, D., & Copas, J. (2007). Assessment of Future Demand for the HPO Reconstruction Program. British Columbia: Homeowner Protection Office.

Morrison Hershfield. (1996). Survey of building envelope failures in the coastal climate of British Columbia. *Morrison Hershfield Ltd. Report for Canada Mortgage and Housing Corporation, Ottawa, Ontario*.

Morse, R. G., & Haas, P. E. (2010). *Stucco Failures and Remediation.* Paper presented at the Building Enclosure Science & Technology Conference (BEST2), Portland, OR.

Nelson, C., & Norris, R. E. (2009, October 26-27, 2009). *Mock-up Water Test Results of Sample Flashing Systems for Storefront Windows in Stucco Walls.* Paper presented at the Building Envelope Technology Symposium, San Diego, CA.

Ngudjiharto, E., Tariku, F., & Fazio, P. (2014, October 28-30, 2014). *Preliminary results from field experimental study of rain load and penetration into wood-frame wall systems at window sill defects.* Paper presented at the 14th Canadian Conference on Building Science and Technology, Toronto, ON, Canada.

Parsons, A. (2004). *An analysis of residential window waterproofing systems.* Massachusetts Institute of Technology.

Pazera, M., & Bomberg, M. (2010). *Applying Lessons from Clay-Brick Veneer to Design a Stucco Mix.* Paper presented at the Building Enclosure Science & Technology Conference (BEST2), Portland, OR.

Penner, D. (2014, May 25). Leaky Condo Crisis Rears its Head again in B.C., *Vancouver Sun*.

RDH Building Engineering Ltd. (2001). Study of High-Rise Envelope Performance in the Coastal Climate of British Columbia. Available from Home Owner Protection Office, Branch of BC Housing   http://www.hpo.bc.ca/building-science-research-projects#envelope

RDH Building Engineering Ltd. (2003). *Water Penetration Resistance of Windows – Study of Manufacturing, Building Design, Installation and Maintenance Factors*. Ottawa: for Canada Mortgage and Housing Corporation.

Sahal, N., & Lacasse, M. A. (2008). Proposed method for calculating water penetration test parameters of wall assemblies as applied to Istanbul, Turkey. *Building and Environment, 43*(7), 1250-1260. doi: 10.1016/j.buildenv.2007.03.009

Spagna, F. J., & Ruggiero, S. S. (2003). Stucco Cladding-Lessons Learned from Problematic Facades. *ASTM Special Technical Publication, 1422*, 214-230.

Straube, J. F. (1998). *Moisture control and enclosure wall systems.* (Doctor of Philosophy), University of Waterloo, Waterloo, Ontario.

Straube, J. F., & Burnett, E. F. (1998). Driving rain and masonry veneer. In R. Kudder & J. Erdly (Eds.), *Water leakage through building facades* (Vol. 1314, pp. 73-90).

Straube, J. F., & Burnett, E. F. P. (2000, 18-21 September 2000). *Simplified Prediction of Driving Rain on Buildings.* Paper presented at the International Building Physics Conference, Eindhoven, The Netherlands, pp. 375-382.

Straube, J. F., & Burnett, E. F. P. (2005). *Building Science for Building Enclosures*. Massachusetts: Building Science Press Inc.

Tariku, F., Cornick, S. M., & Lacasse, M. A. (2007). *Simulation of Wind-Driven Rain Penetration Effects on the Performance of a Stucco-Clad Wall.* Paper presented at the Thermal Performance of Exterior Envelopes of Whole Buildings X International Conference, Florida, U.S.A.

Tariku, F., Simpson, Y., & Iffa, E. (2015). Experimental investigation of the wetting and drying potentials of wood frame walls subjected to vapor diffusion and wind-driven rain loads. *Building and Environment, 92*, 368-379. doi: http://dx.doi.org/10.1016/j.buildenv.2015.05.013

TenWolde, A. (2008). ASHRAE 160P-- Criteria for Moisture Control Design Analysis in Buildings. *ASHRAE Transactions, 114*(1), 167.

TenWolde, A. (2011). A Review of ASHRAE Standard 160—Criteria for Moisture Control Design Analysis in Buildings. *Journal of Testing and Evaluation, 39*(1). doi: 10.1520/JTE102896

Timber Frame Housing 2002 Consortium. (2002). Appendix 3: International and National Case Studies *Study on Timber Frame Housing in Ireland for the Department of Environment, Heritage and Local Government*. Ireland.

Tom, R. (2001). Wall Moisture Problems in Alberta Dwellings. *Canada Mortgage and Housing Corporation (CMHC)*.

Van Goethem, S. (2014). *Rainwater runoff on building facades: numerical simulations and analysis of wetting patterns.* (Master of Science), Ghent University.

Vereecken, E., & Roels, S. (2012). Review of mould prediction models and their influence on mould risk evaluation. *Building and Environment, 51*(0), 296-310. doi: http://dx.doi.org/10.1016/j.buildenv.2011.11.003

Weston, T. A., Minnich, L. C., Smegal, J., Mullekom, J. V., Schumacher, C., & Conlon, J. S. (2010). *Evaluation of Cladding and Water-Resistive Barrier Performance in Hot-Humid Climates Using a Real-Weather, Real-Time Test Facility.* Paper presented at the Thermal Performance of the Exterior Envelopes of Whole Buildings XI International Conference.

Wu, W. K. (2011). *The effects of microclimate and time resolution of meteorological data on hygrothermal analysis of wood frame building facades.* (MASc), Ryerson University, Toronto, ON, Canada.

APPENDIX A: CALIBRATION AND TESTING OF SENSORS AND GAUGES

A.1   CALIBRATION OF WALL RAIN GAUGES

The wall rain gauges were calibrated to 2.0 ± 0.1 grams or mL of water/tip by first leveling the gauge, dripping a pre-measured amount of water through the funnel until the bucket tips one time and then measuring the amount of water that was left in that same container to determine the amount of water needed to tip that side of the bucket. The height of the screws supporting the buckets after they tip were adjusted and these steps of calibration were repeated several times until both sides tip after collecting 2.0 ± 0.1 grams or mL of water. Finally, the steps of calibration were repeated for a minimum of 5 times per each buckets.

Initially, the water were dripped into the funnel using an eyedropper. However, once a peristaltic pump (Figure A. 1) was available in the lab, drips of water were introduced automatically through a tubing into the funnel, and the pump was simply stopped once the bucket tips, as the pump records the amount of water that it was discharged.

Figure A. 1. Cole-Parmer Masterflex® L/S® peristaltic pump and a water container used to calibrate the wall rain gauges and leakage gauges.

A.2   CALIBRATION OF LEAKAGE GAUGES

The leakage gauges were calibrated to the lowest amount of water that the bucket must collect for it to tips, but without causing the bucket to bounce back, which would have caused multiple counts of tipping being recorded. The leakage gauges were calibrated following the same steps in the procedure to calibrate the wall rain gauges. Initially, the manual dripping was used to calibrate the gauges in the lab during the adjustments of the buckets and screws. After the leakage gauges were installed within the wall cavities of the water collecting walls and they were levelled, the gauges were re-calibrated again using the peristaltic pump shown in Figure A. 1 and were tested to ensure that the buckets do not bounce. On average, the gauges were calibrated to 1.5 ± 0.1 mL of water/tip. The following Table A. 1 summarizes the sensitivity of each leakage gauges used.

Table A. 1. Calibrated amount of leakage gauges at water collection walls.

Location of Leakage Collection	Calibrated amount mL/tip
W1	1.482
W2	1.336
W6 Corner	1.613
W6 Middle	1.511

A.3   CALIBRATION OF THERMOCOUPLES

The thermocouples were calibrated by inserting the sensing ends into a water bath controlled at $5 \,^{\circ}C$ and $24 \,^{\circ}C$, as shown in Figure A. 2. The readings were recorded for a minimum of two hours.
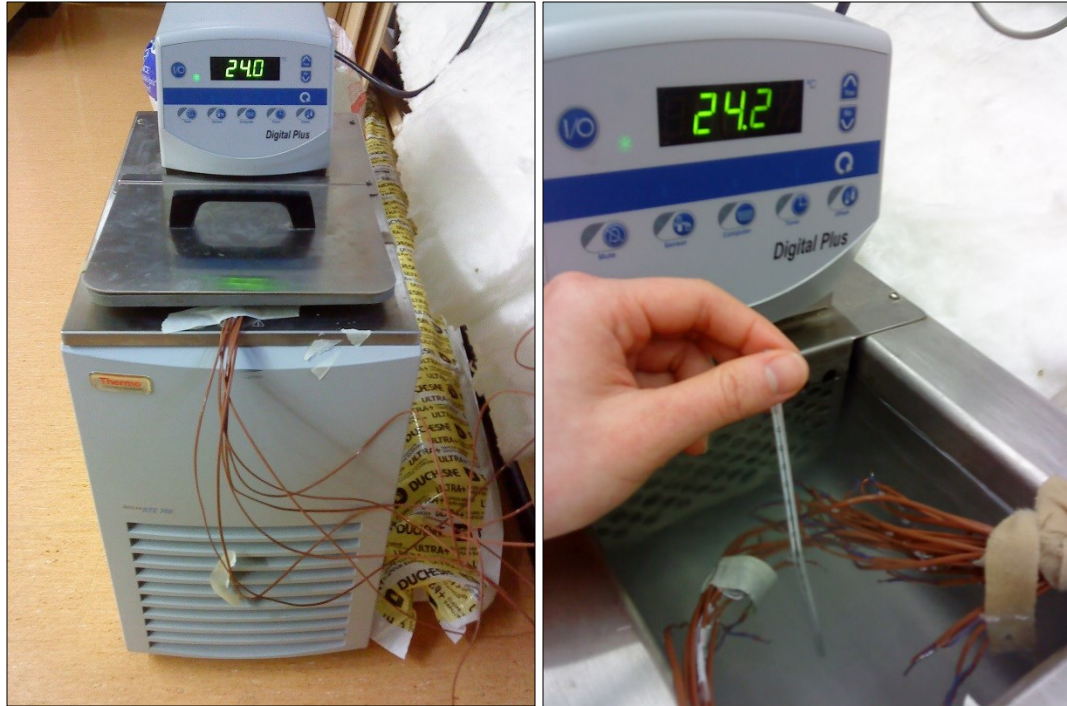
Figure A. 2. Calibration set up for thermocouples on the left photo and close up view of the controlled water bath on the right photo.

Figure A. 3 shows the typical calibration curve of the thermocouples at 5°C. All thermocouples calibrated are within ±0.4°C accuracy.
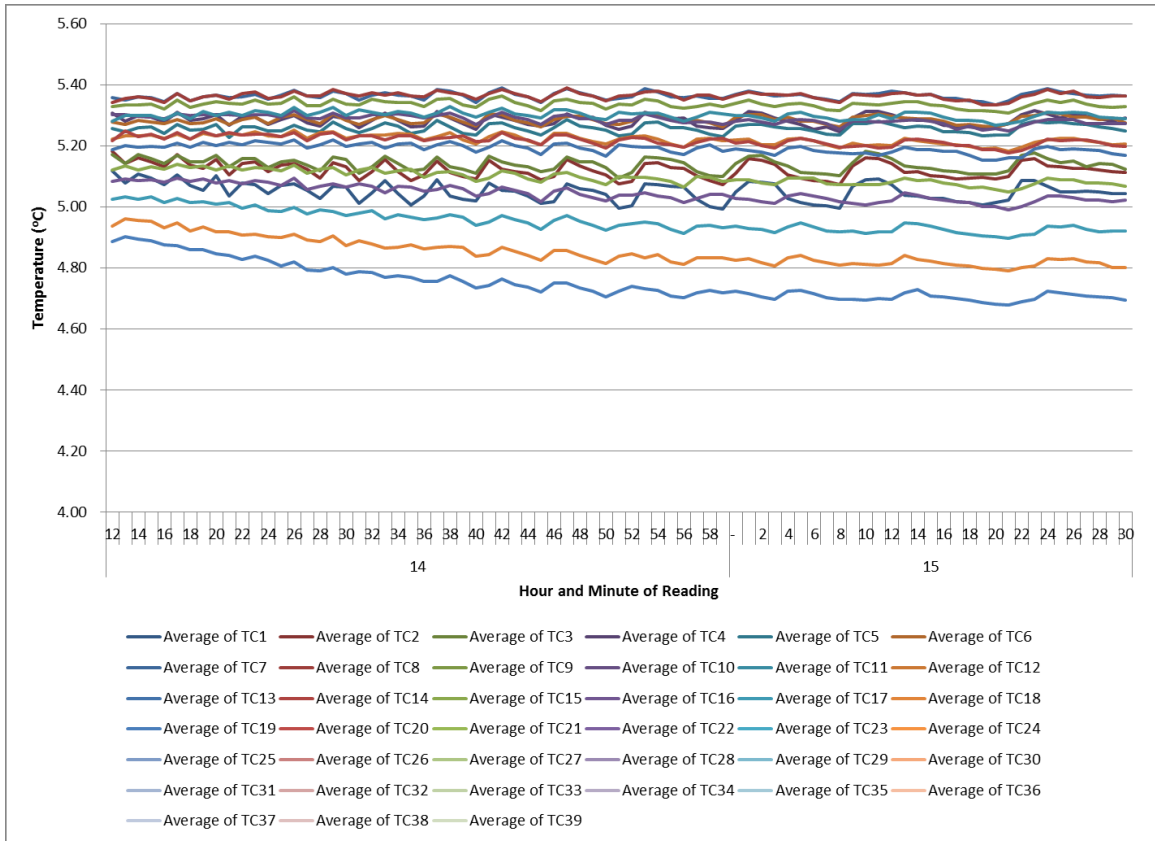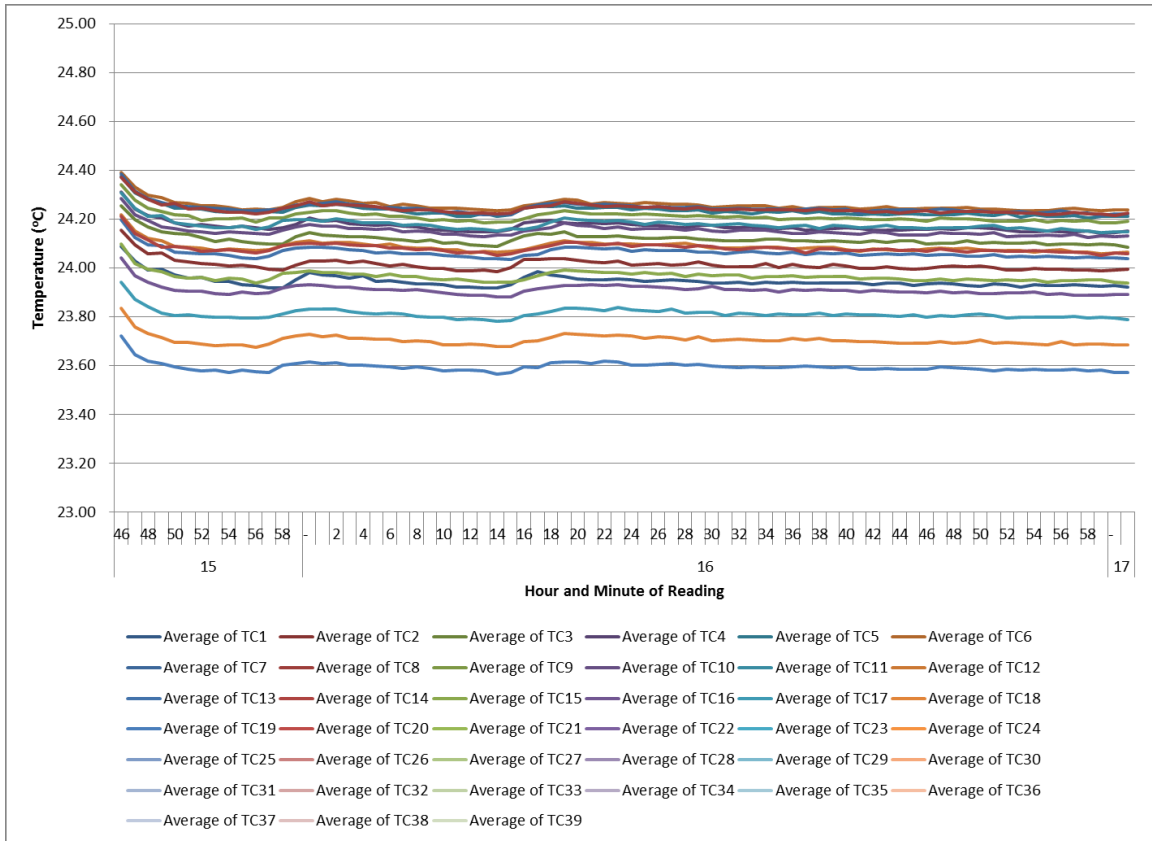
Figure A. 3. Calibration curve of thermocouples sensors at 5ºC.

Figure A. 4 shows the typical calibration curve of the thermocouples at 24ºC. All thermocouples calibrated are within ±0.4ºC accuracy.

Figure A. 4. Calibration curve of thermocouples sensors at 24ºC.

A.4 TESTING OF WIRED MOISTURE PINS

After 24-gauge wires were soldered to the moisture pins, the pins were tested by connecting the moisture pins to a resistor of known resistance value and connecting the end of the 24-gauge wires to a digital circuit tester for a measurement of the resistance, as shown in Figure A. 5.
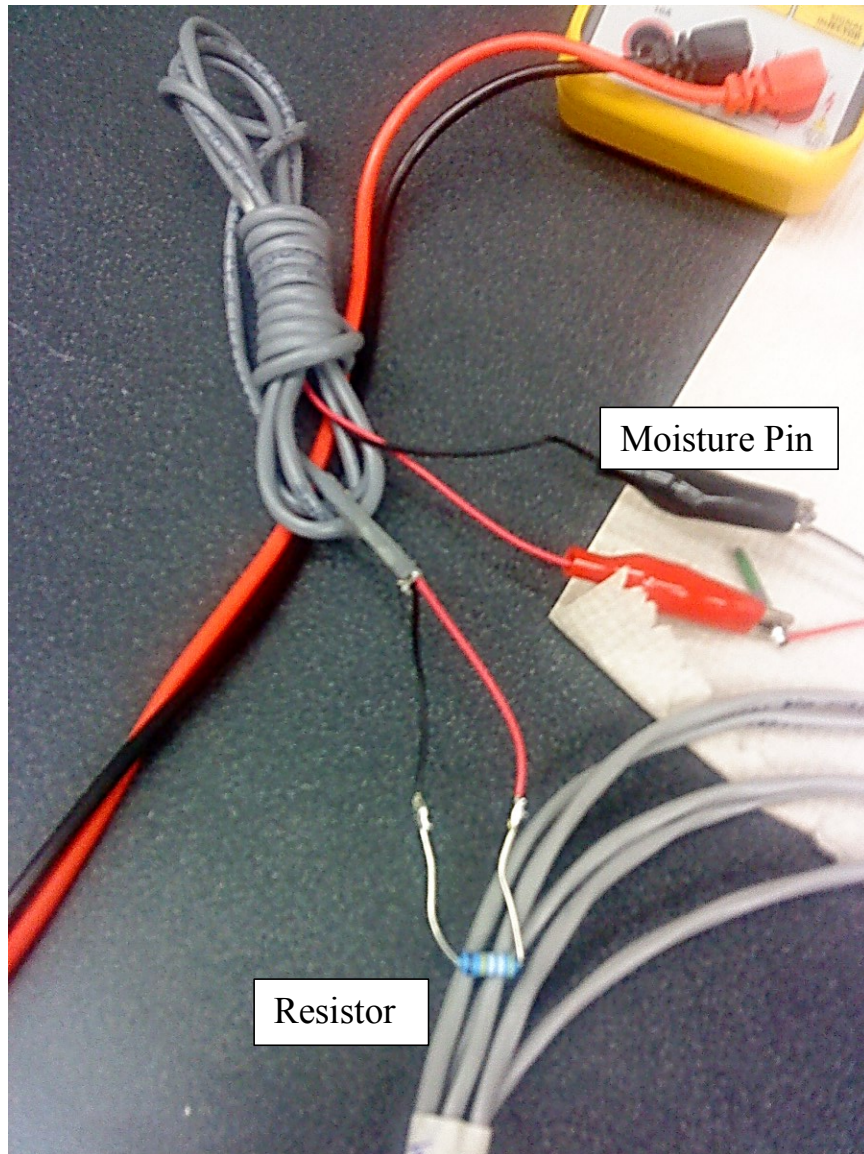
Figure A. 5. Testing of moisture pins using a resistor and digital circuit tester.

A.5   TESTING OF WIRED MOISTURE DETECTION TAPES

Similar to the testing of the moisture pins, after 24-gauge wires were soldered to the moisture pins, the moisture detection tapes were tested by connecting the tapes to a resistor of known resistance value and measuring the resistance using a digital circuit tester from the other end of the 24-gauge wires (Figure A. 6).

Figure A. 6. Testing setup for moisture detection tapes.

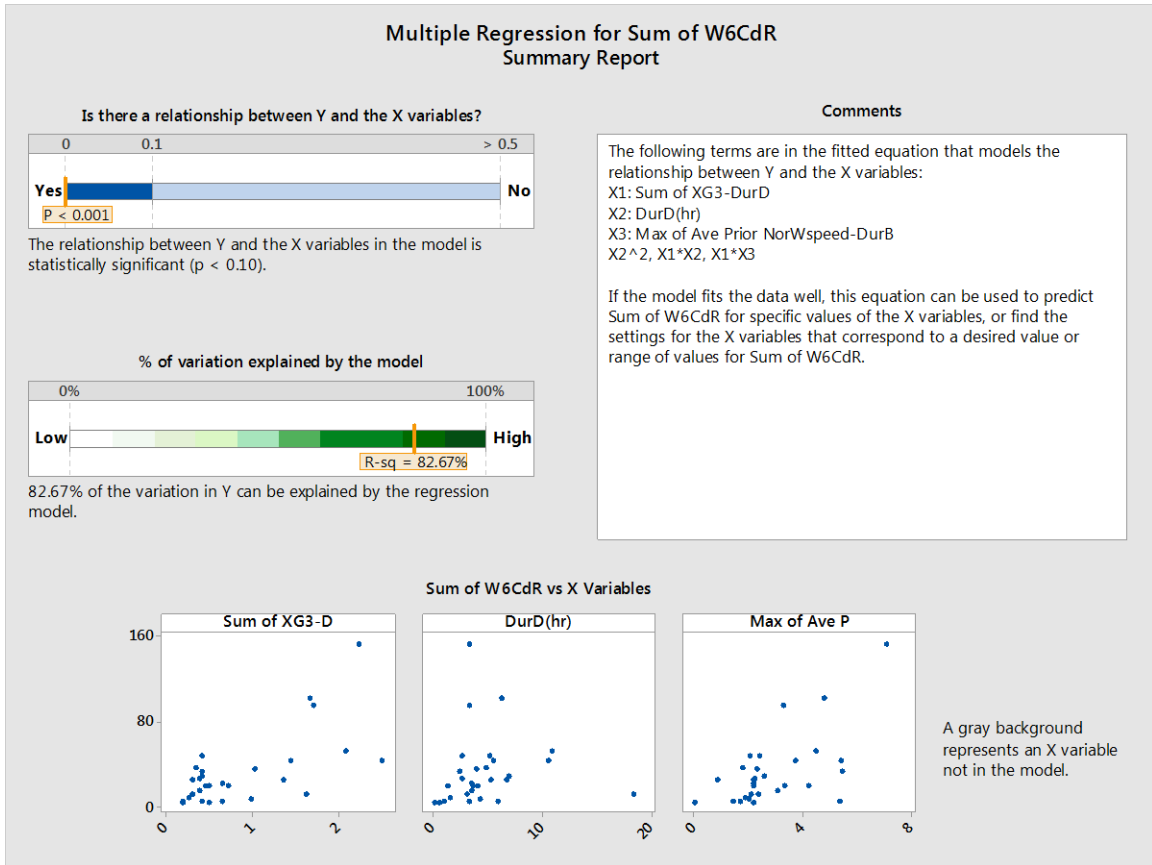# APPENDIX B: SELECTION OF STATISTICAL REGRESSION MODELS

As an example of how the statistical regression models were selected, the statistical analysis output from Minitab17 software used to analyze the leakage event at W6 corner are discussed below. Several statistics were used to evaluate the models:

- S statistics is the distance that data values fall from the regression line in the units of leakage amount (ml). Therefore, models with lower S statistics are better models.

- R-Sq statistics is based on the Analysis of Variance method and indicates the percentage proportion of how well each response, i.e. the Y-values are explained by the predictors or the X-variables. The higher the R-sq value, the better fitting the model is.

- R-Sq (adj) or Adjusted R-Sq statistics modifies R-Sq to adjust for the number of terms in the model. When additional predictors are included as terms in the model, the R-Sq statistics increases as well; however, Adjusted R-Sq decreases as more terms are added to the model, and is therefore used when comparing models with different numbers of predictors.

- PRESS and R-Sq (pred) or Predicted R-Sq statistics predict how well new observations fit in the model. A good fitting model has R-Sq (pred) that is not too different from the R-Sq and R-Sq (adj) values.

The following are the Minitab17 statistics reports on the four regression models considered for the leakage amount at W6 corner.

B.1   MODEL 1
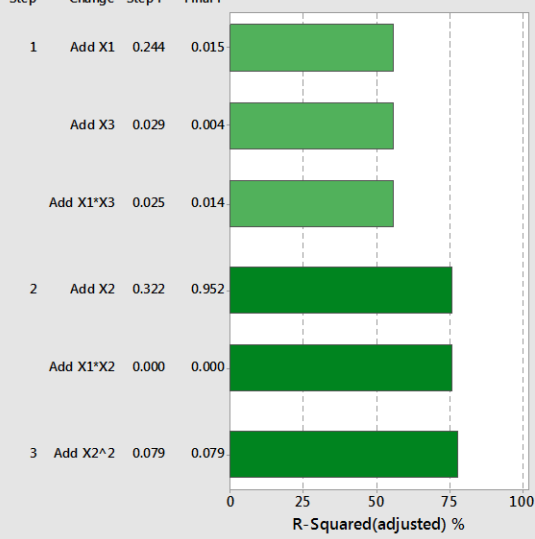

Multiple Regression for Sum of W6CdR
Summary Report

Is there a relationship between Y and the X variables?

The relationship between Y and the X variables in the model is statistically significant (p < 0.10).

% of variation explained by the model

R-sq = 82.67%

82.67% of the variation in Y can be explained by the regression model.

Comments

The following terms are in the fitted equation that models the relationship between Y and the X variables:
X1: Sum of XG3-DurD
X2: DurD(hr)
X3: Max of Ave Prior NorWspeed-DurB
X2^2, X1*X2, X1*X3

If the model fits the data well, this equation can be used to predict Sum of W6CdR for specific values of the X variables, or find the settings for the X variables that correspond to a desired value or range of values for Sum of W6CdR.

Sum of W6CdR vs X Variables

A gray background represents an X variable not in the model.

Multiple Regression for Sum of W6CdR
Model Building Report

X1: Sum of XG3-D   X2: DurD(hr)   X3: Max of Ave P

Final Model Equation

Sum of W6Cd = -11.4 + 38.0 X1 + 4.29 X2 + 1.14 X3 + 0.302 X2^2 - 8.23 X1*X2 + 7.74 X1*X3

Model Building Sequence
Displays the order in which terms were added or removed.

| Step	Change	Step P	Final P
1	Add X1	0.244	0.015
	Add X3	0.029	0.004
	Add X1*X3	0.025	0.014
2	Add X2	0.322	0.952
	Add X1*X2	0.000	0.000
3	Add X2^2	0.079	0.079

R-Squared(adjusted) %

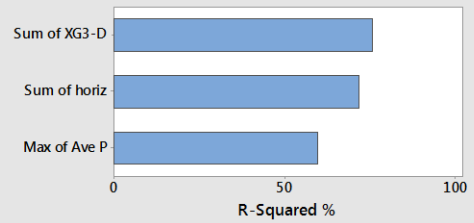**Incremental Impact of X Variables**
Long bars represent Xs that contribute the most new information to the model.
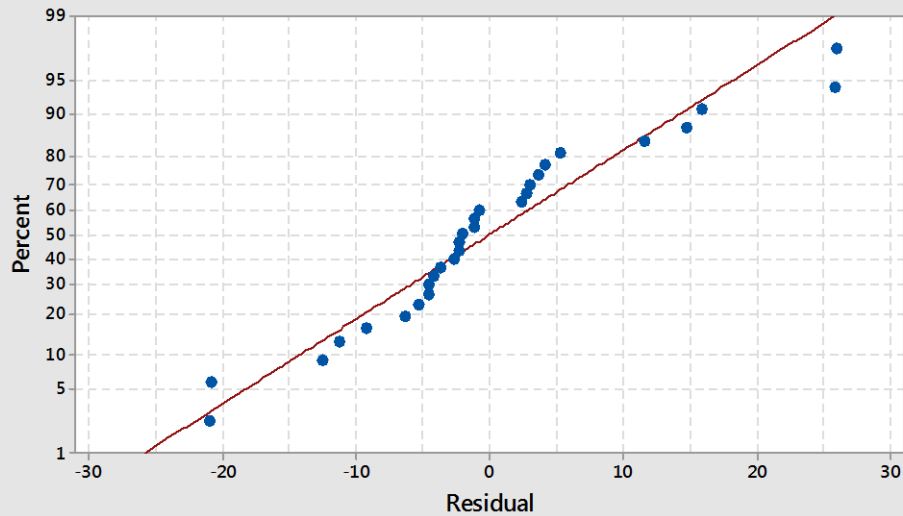
Increase in R-Squared %

Each X Regressed on All Other Terms
Gray bars represent Xs that do not help explain additional variation in Y.

R-Squared %
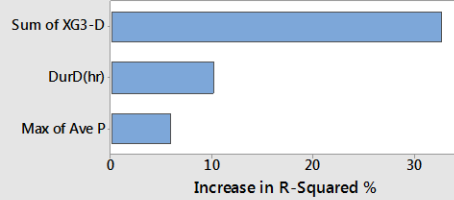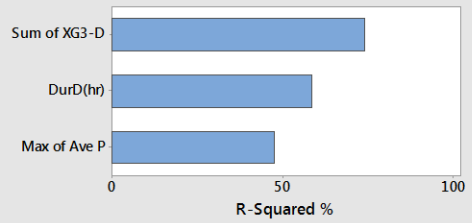
A gray bar represents an X variable not in the model.

Normal Probability Plot
(response is Sum of W6CdRgI01-DurB)
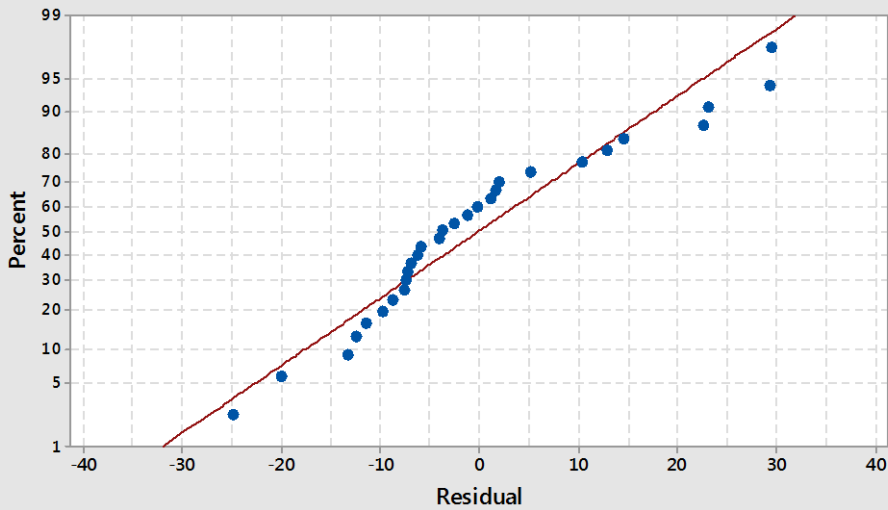
Model 1 Summary

```
     S    R-sq  R-sq(adj)     PRESS  R-sq(pred)
15.4776  82.67%     77.95%  18557.7      38.99%
```

```
Sum    of    W6CdRgI01-DurB    =    -11.4    +    38.0    Sum    of    XG3-DurD
+ 1.14 Max of Ave Prior NorWspeed-DurB
                    + 4.29 DurD(hr) + 0.302 DurD(hr)*DurD(hr)
                    + 7.74 Sum of XG3-DurD*Max of Ave Prior NorWspeed-DurB
                    - 8.23 Sum of XG3-DurD*DurD(hr)
```

B.2   MODEL 2
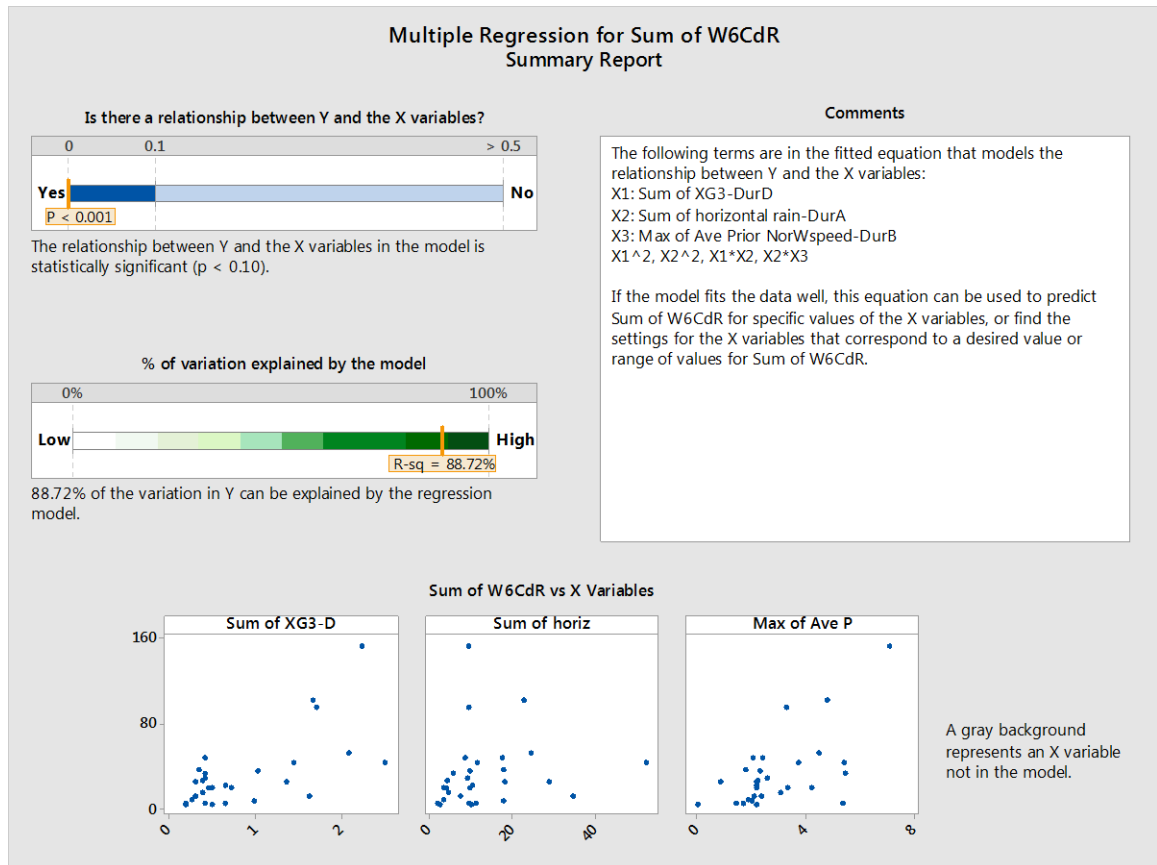
Multiple Regression for Sum of W6CdR
Model Building Report

X1: Sum of XG3-D   X2: Sum of horiz   X3: Max of Ave P

Final Model Equation

Sum of W6Cd = -14.0 + 45.1 X1 + 0.72 X2 + 0.94 X3 + 19.68 X1^2 + 0.0877 X2^2 - 5.48 X1*X2 + 0.931 X2*X3
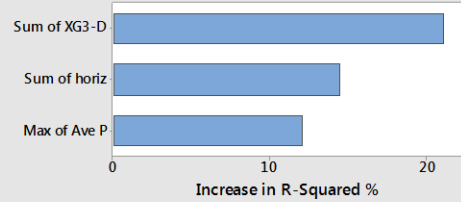
Normal Probability Plot
(response is Sum of W6CdRgI01-DurB)

Model 2 Summary

```
       S    R-sq   R-sq(adj)    PRESS   R-sq(pred)
12.7847   88.72%     84.95%   69368.8       0.00%
```

```
Sum of W6CdRgI01-DurB = -14.0 + 45.1 Sum of XG3-DurD + 0.72 Sum of horizontal rain-
DurA
                        + 0.94 Max of Ave Prior NorWspeed-DurB
                        + 19.68 Sum of XG3-DurD*Sum of XG3-DurD
                        +     0.0877    Sum     of     horizontal     rain-
DurA*Sum of horizontal rain-DurA
                        - 5.48 Sum of XG3-DurD*Sum of horizontal rain-DurA
                        +     0.931    Sum     of     horizontal     rain-
DurA*Max of Ave Prior NorWspeed-DurB
```

B.3   MODEL 3
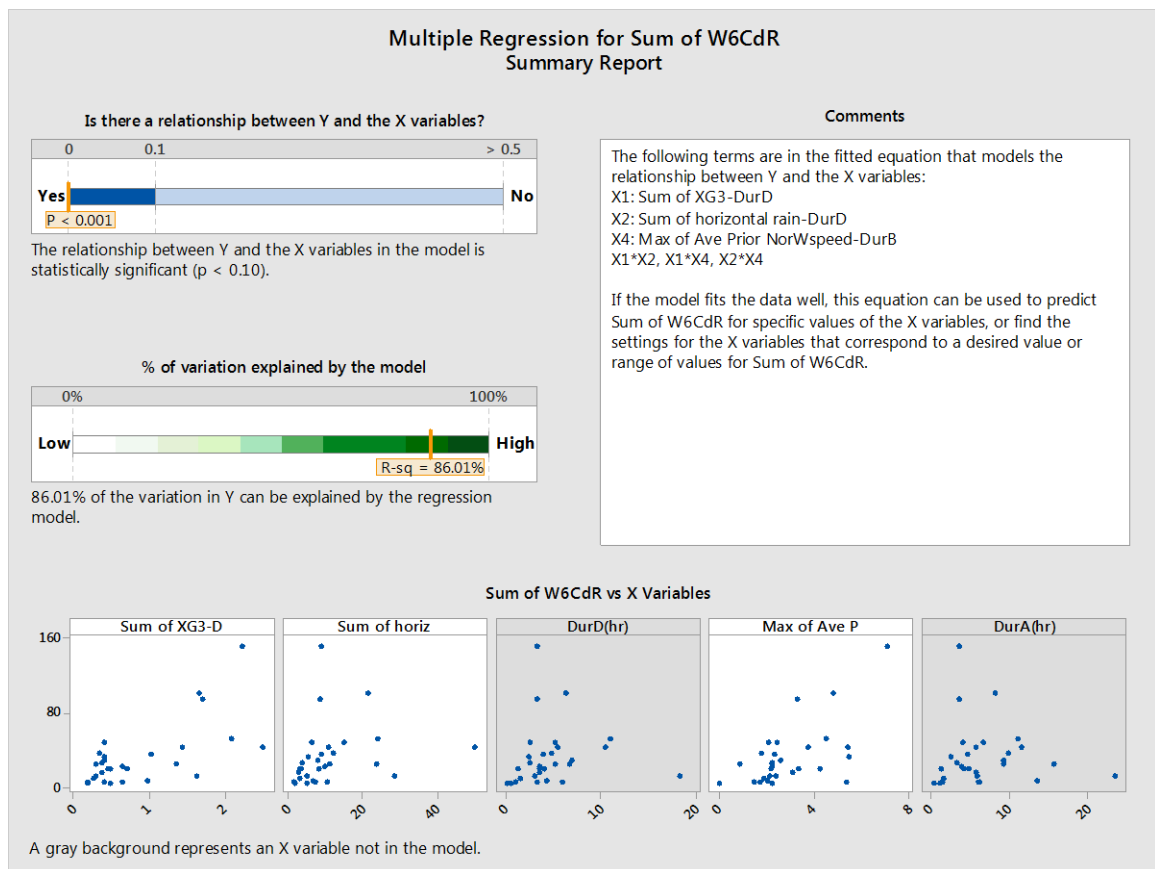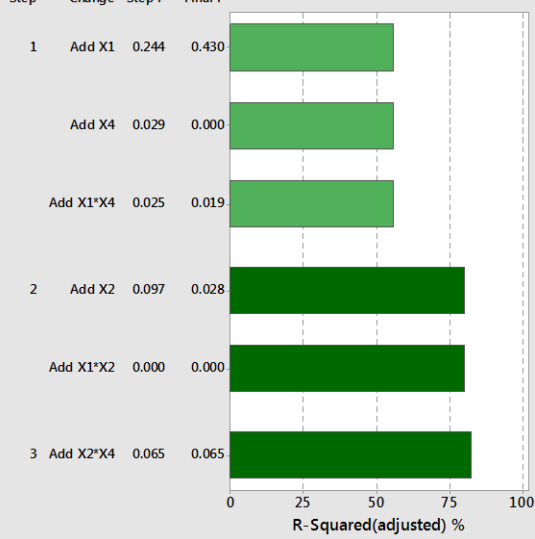
Multiple Regression for Sum of W6CdR
Model Building Report

X1: Sum of XG3-D   X2: Sum of horiz   X3: DurD(hr)   X4: Max of Ave P   X5: DurA(hr)

Final Model Equation
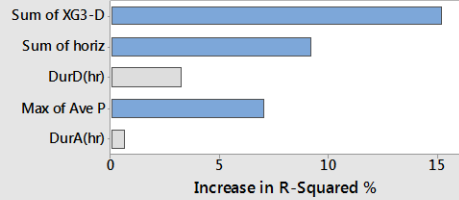Sum of W6Cd = -8.4 + 20.2 X1 + 2.37 X2 - 1.06 X4 - 3.253 X1*X2 + 7.79 X1*X4 + 0.704 X2*X4

Normal Probability Plot
(response is Sum of W6CdRgI01-DurB)
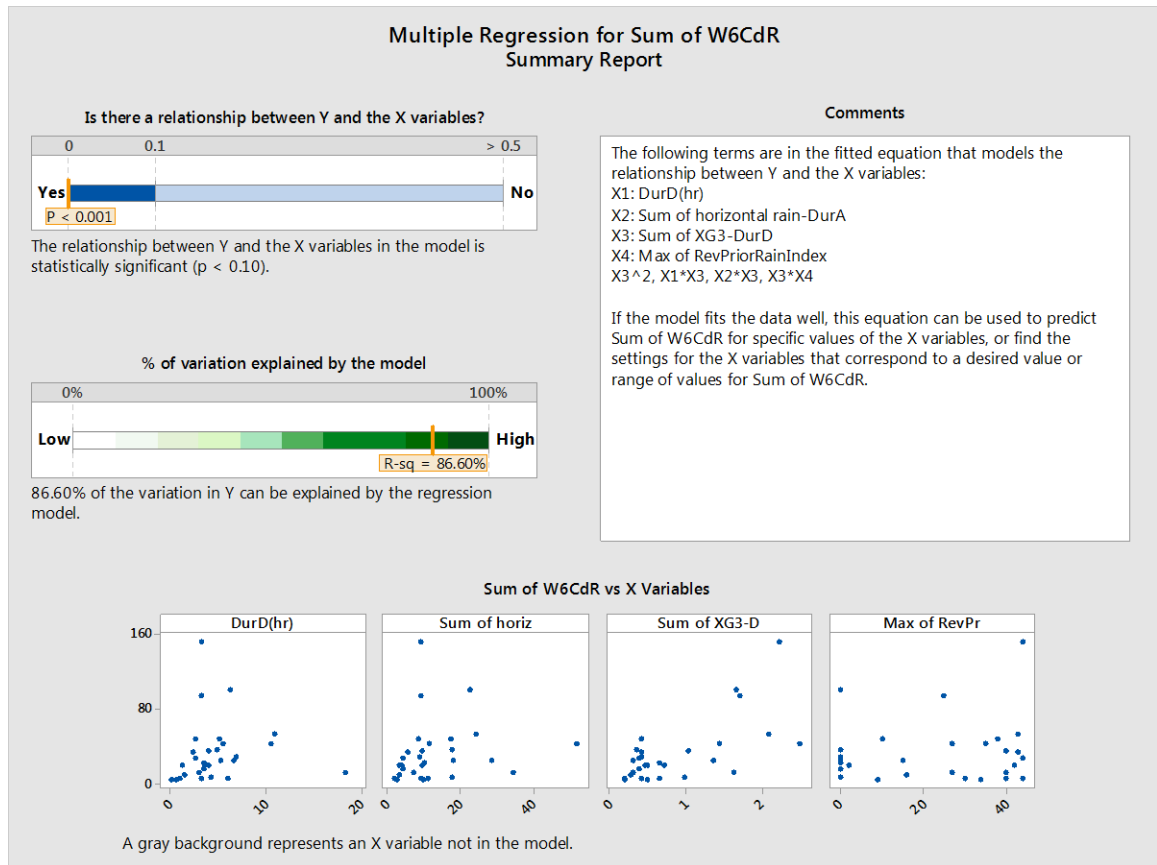
Model 3 Summary

```
      S     R-sq   R-sq(adj)     PRESS   R-sq(pred)
13.9102   86.01%     82.19%   8195.99       73.05%
```

```
Sum of W6CdRgI01-DurB = -8.4 + 20.2 Sum of XG3-DurD + 2.37 Sum of horizontal rain-
DurD
                         - 1.06 Max of Ave Prior NorWspeed-DurB
                         - 3.253 Sum of XG3-DurD*Sum of horizontal rain-DurD
                         + 7.79 Sum of XG3-DurD*Max of Ave Prior NorWspeed-DurB
                         +    0.704    Sum    of    horizontal    rain-
DurD*Max of Ave Prior NorWspeed-DurB
```

B.4   MODEL 4

Note that X4 – Max of RevPriorRainIndex is the PRI$_{48}$.

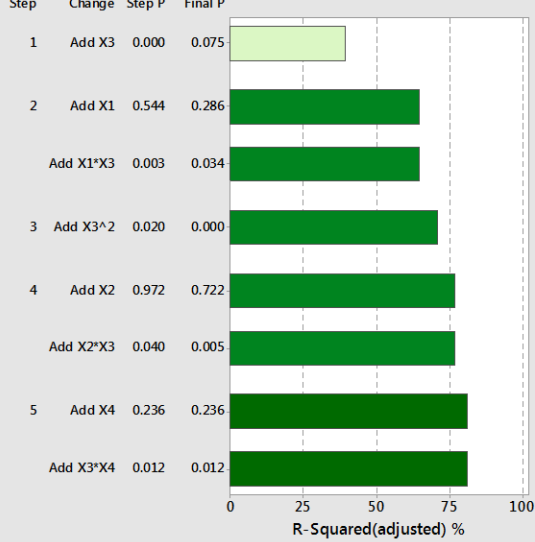## Multiple Regression for Sum of W6CdR
Model Building Report

X1: DurD(hr)   X2: Sum of horiz   X3: Sum of XG3-D   X4: Max of RevPr

Final Model Equation

Sum of W6Cd = -3.4 + 6.02 X1 + 1.308 X2 - 24.5 X3 + 0.638 X4 + 65.5 X3^2 - 4.85 X1*X3 - 1.816 X2*X3 - 1.063 X3*X4

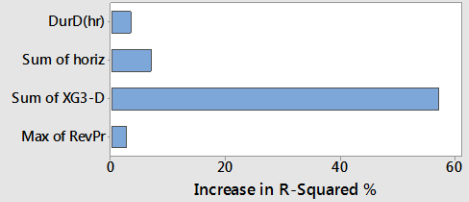### Model Building Sequence
Displays the order in which terms were added or removed.

| Step	Change	Step P	Final P
1	Add X3	0.000	0.075
2	Add X1	0.544	0.286
	Add X1*X3	0.003	0.034
3	Add X3^2	0.020	0.000
4	Add X2	0.972	0.722
	Add X2*X3	0.040	0.005
5	Add X4	0.236	0.236
	Add X3*X4	0.012	0.012

Incremental Impact of X Variables
Long bars represent Xs that contribute the most new information to the model.
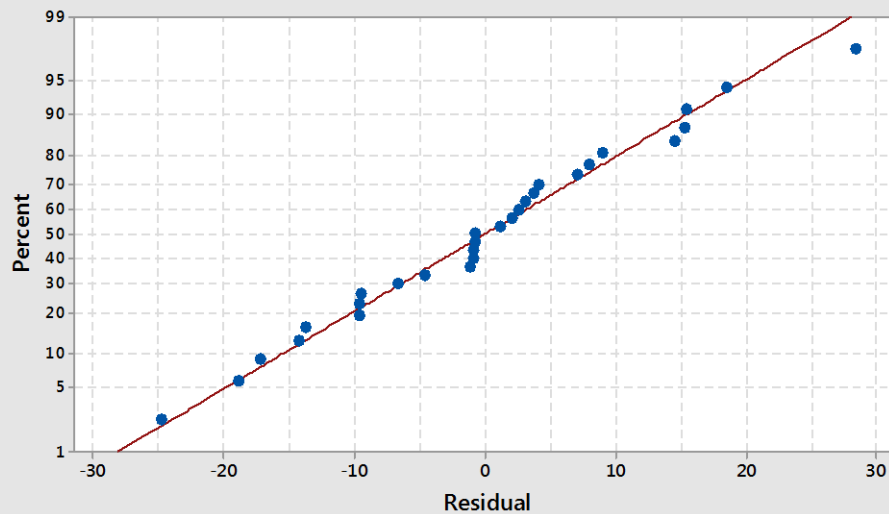
Each X Regressed on All Other Terms
Gray bars represent Xs that do not help explain additional variation in Y.
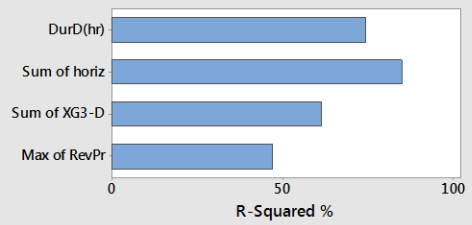
A gray bar represents an X variable not in the model.

Normal Probability Plot
(response is Sum of W6CdRgI01-DurB)


```
Model 4 Summary

     S     R-sq  R-sq(adj)    PRESS  R-sq(pred)
14.2757  86.60%    81.24%   10032.1     67.02%
```

```
Sum of W6CdRgI01-DurB = -3.4 - 24.5 Sum of XG3-DurD + 1.308 Sum of horizontal rain-
DurA
                        + 6.02 DurD(hr) + 0.638 Max of RevPriorRainIndex
                        + 65.5 Sum of XG3-DurD*Sum of XG3-DurD
                        - 1.816 Sum of XG3-DurD*Sum of horizontal rain-DurA
                        - 4.85 Sum of XG3-DurD*DurD(hr)
                        - 1.063 Sum of XG3-DurD*Max of RevPriorRainIndex
```

B.5   DETERMINATION OF BEST-FITTING MODEL FOR W6 CORNER

To compare the four models describe above, the following table summarizes the statistics for each

models:

Statistics / Criteria	Model 1	Model 2	Model 3	Model 4
Number of predictors	3	3	3	4
S	15.48 mL	12.78 mL	13.91 mL	14.28 mL
R-Sq	82.67%	88.72%	86.01%	86.60%
R-Sq(adj)	77.95%	84.95%	82.19%	81.24%
R-Sq(pred)	38.99%	0%	73.05%	67.02%

Model 2 has the highest R-Sq and R-Sq(adj), and the lowest S, the R-Sq(pred) is zero, and is thus

eliminated. Model 1 has the lowest R-Sq value among the four models and is therefore also

eliminated. Model 3 and Model 4 have similar statistics. However, Model 4 has slightly higher S

and slightly lower R-Sq(pred). Moreover, as the two models have different number of predictors,

the R-Sq(adj) is the better criteria to be used. Model 3 is therefore chosen as the best-fitting model

for W6 corner.